

ASSESSING THE POTENTIAL AND LIMITATIONS OF HEAVY OIL
UPGRADING BY ELECTRON BEAM IRRADIATION

A Thesis

by

DANIYAR ZHUSSUPOV

Submitted to the Office of Graduate Studies of
Texas A&M University
in partial fulfillment of the requirements for the degree of

MASTER OF SCIENCE

December 2006

Major Subject: Chemical Engineering

ASSESSING THE POTENTIAL AND LIMITATIONS OF HEAVY OIL
UPGRADING BY ELECTRON BEAM IRRADIATION

A Thesis

by

DANIYAR ZHUSSUPOV

Submitted to the Office of Graduate Studies of
Texas A&M University
in partial fulfillment of the requirements for the degree of

MASTER OF SCIENCE

Approved by:

Chair of Committee, Maria A. Barrufet
Committee Members, Rosana Moreira
Mahmoud El-Halwagi
Head of Department, N.K. Anand

December 2006

Major Subject: Chemical Engineering

ABSTRACT

Assessing the Potential and Limitations of Heavy Oil Upgrading by Electron Beam
Irradiation. (December 2006)

Daniyar Zhussupov, B.S., Kazakh State University, Kazakhstan

Chair of Advisory Committee: Dr. Maria A. Barrufet

Radiation technology can economically overcome principal problems of heavy oil processing arising from heavy oil's unfavorable physical and chemical properties. This technology promises to increase considerably yields of valuable and environmentally satisfying products of thermal cracking; to simplify complexity of refinery configuration; and to reduce energy expenses of thermal cracking.

Objectives of the present study are:

- Evaluate heavy oil viscosities with respect to absorbed dose and effect of different solvents on the viscosity of irradiated crude oil by comparing selected physical properties of irradiated samples to a non-irradiated control group;
- Investigate effect of e-beam radiation on the yields of light fractions comparing yields of radiation-thermal cracking to yields of conventional thermal cracking.

The viscosity was used as an indicator of the change in the molecular structure of hydrocarbons upon irradiation. We found that the irradiation of pure oil leads to the increase of the molecular weight calculated from the Riazi-Daubert correlation. Thus, irradiation up to 10 kGy resulted in a 1.64% increase in the molecular weight, 20 kGy — 4.35% and 30 kGy — 3.28%.

It was found that if irradiated oil was stored for 17 days, its viscosity increased by 14% on average. The irradiation of samples with added organic solvent in the following weight percentages 10, 5, 2.5wt.% resulted in the increase in the viscosity by 3.3, 3.6 and 14.5%, respectively. The irradiation of the sample with added distilled water

also resulted in an increase in the viscosity. This increase mainly happened because the thermal component was absent in the activation energy and hydrogen, produced from radiolysis of solvent and water molecules in mixture with crude oil, and was not consumed by hydrocarbon molecules and no reduction in molecular size occurred.

Implementation of radiation to the thermal cracking increased yields of light fractions by 35wt.% on average compared to the process where no radiation was present.

The last chapter of this thesis discusses a profitability of installation the hypothetical radiation-thermal visbreaking unit. The calculation of profitability was performed by a rate of return on investment (ROI) method. It showed that implementation of radiation-thermal processing resulted in an increase of ROI from 16 to 60%.

ACKNOWLEDGMENTS

I would like to take this opportunity to thank all those who have contributed to the successful completion of this thesis. The most appreciation is given to Dr. Maria A. Barrufet, advisor and chair of my committee, for guiding and encouraging me towards completion of my graduate studies.

I would like to extend gratitude to Dr. Moreira for providing access to the Van de Graaff facility, a valuable contribution to the successful completion of the project. I would like to thank Dr. El-Halwagi for serving on my committee and for providing his valuable time. I would like to express my appreciation to my colleagues, Jongsoon Kim, Paulo Fortes Da Silva, Jerry George, Bilal Akin and Renat Shaykhutdinov for valuable discussions, exchange of ideas, and friendship.

Finally, I would like to thank my parents, Alfiya and Magaiya, my brother, Arslan, and my sister, Diana, for lighting my path with love and support.

TABLE OF CONTENTS

	Page
ABSTRACT.....	iii
ACKNOWLEDGMENTS.....	v
TABLE OF CONTENTS.....	vi
LIST OF FIGURES.....	viii
LIST OF TABLES.....	x
CHAPTER	
I INTRODUCTION.....	1
II LITERATURE REVIEW.....	3
2.1 Heavy oil resources, composition, properties.....	3
2.2 Upgrading methods for heavy oil and chemistry of thermal cracking.....	9
2.3 Radiation background.....	16
2.3.1 Interaction of fast electrons with matter.....	16
2.3.2. Dosimetry methods for electrons.....	19
2.4 Radiation-thermal processing.....	24
2.4.1 Industrial radiation processing.....	24
2.4.2. Radiation chemistry of hydrocarbons.....	26
2.4.3 Radiation-thermal cracking.....	28
III EXPERIMENTAL METHODOLOGY AND MATERIALS.....	34
3.1 Facility for irradiation.....	34
3.2 Van de Graaff accelerator.....	36
3.4 Preparation of Hamaca oil sample.....	40
3.5 Irradiation of crude oil sample by electron beam.....	44
3.7 Radiation-thermal cracking experiment layout.....	51
3.7.1 Estimation of absorbed dose for Pyrex glass and aluminum can.....	52
3.7.2 Design of setup with aluminum can.....	56

CHAPTER	Page
IV	RESULTS AND DISCUSSION.....63
	4.1. Viscosities of oil and mixtures before and after irradiation.....63
	4.2. Yields from RTC experiment.....77
	4.2.1 Dose measurement.....78
	4.2.2 Material balance of radiation-thermal cracking in aluminum can.....80
V	ECONOMIC ANALYSIS OF RADIATION THERMAL PROCESS.....87
VI	CONCLUSIONS AND FUTURE WORK RECOMMENDATIONS.....99
	6.1 Conclusions.....99
	6.2 Recommendations for future work.....101
	REFERENCES.....102
	APPENDIX A: CALIBRATION OF THE VISCOMETER.....109
	APPENDIX B: DESCRIPTION OF THERMOCOUPLE.....112
	APPENDIX C: ELECTRONIC BALANCE SETTINGS.....113
	APPENDIX D: GAS CHROMATOGRAPHY ANALYSIS RESULTS.....114
	VITA.....123

LIST OF FIGURES

	Page
Fig. 1 Simplified composition diagram for crude oils [13].....	9
Fig. 2. Thermal cracking unit [11]	10
Fig. 3 Major thermal upgrading processes distribution [20].....	13
Fig. 4 Ring opening reaction of decalin molecule	14
Fig. 5 Thermal decomposition of hydrocarbon components.....	16
Fig. 6 Electron range-energy curve for materials composed of hydrocarbons [21].....	19
Fig. 7 Ionization chamber [30].....	22
Fig. 8 Saturation curve [30].....	23
Fig. 9 Design model of facility at the Biological and Agricultural Engineering Department.....	35
Fig. 10 General view of VDG facility at the Biological and Agricultural Engineering Department.....	35
Fig. 11 Control room equipment	35
Fig. 12 Schematics of Van de Graaff accelerator [53].....	36
Fig. 13 Acceleration of charged particle between two parallel plates.....	37
Fig. 14 General view of Van de Graaff machine	39
Fig. 15 E-beam exit window with parallel plate transmission ion chamber and sample of crude oil placed in front of it (left). E-beam bending magnets (right).....	39
Fig. 16 System of vacuum pumps (left). Pressurized tank, where, in the atmosphere of inert gas, the accelerating column is placed (right).....	39
Fig. 17 Depth-dose curve at 5 mm Hamaca crude oil.....	41
Fig. 18 Sample preparation	42
Fig. 19 Sample of Hamaca crude oil ready for irradiation.....	43
Fig. 20 Lateral view of irradiation point <i>P</i> positioned in front of exit window	44
Fig. 21 Front panel of charge counter from transmission ion chamber	45
Fig. 22 Dose distribution and histogram in sample №1-front side	49
Fig. 23 Dose distribution and histogram in sample №1-back side.....	49

	Page
Fig. 24 Dose distribution and histogram in sample №2-front side	50
Fig. 25 Dose distribution and histogram in sample №2-back side.....	50
Fig. 26 Schematics of radiochromic films and crude oil.....	51
Fig. 27 VDG tank and attached tube with aluminum foil inside.....	52
Fig. 28 General view of radiation-thermal cracking in can.....	58
Fig. 29 Configuration for thermal cracking experiment	59
Fig. 30 Temperature profile of the heater	60
Fig. 31 Aluminum can design	61
Fig. 32 Predicted and measured viscosities for XYZ oil, Walther's correlation.....	65
Fig. 33 Predicted and measured viscosities for XYZ oil, Arrhenius equation.....	65
Fig. 34 Error distribution.....	66
Fig. 35 Shear rate and viscosity dependence of Hamaca heavy oil	67
Fig. 36 Results of power-law correlation	72
Fig. 37 Results of Shu's correlation	73
Fig. 38 Changes in viscosity with wt.% DW at 50°C	76
Fig. 39 Changes in viscosity with wt.% DW at 70°C	76
Fig. 40 Simulation of radiation thermal cracking in the can.....	79
Fig. 41 Dose-yield relation.....	82
Fig. 42 Overlapped graphs of mass of distillate vs temperature profile for thermal cracking	84
Fig. 43 Overlapped graphs of time vs mass of distillate for thermal cracking	84
Fig. 44 Overlapped graphs of time vs temperature of outcoming fumes for thermal cracking	85
Fig. 45 Overlapped graphs of mass of distillate vs temperature of outcoming fumes for radiation-thermal cracking.....	85
Fig. 46 Overlapped graphs of time vs mass of distillate for radiation-thermal cracking	86
Fig. 47 Overlapped graphs of time vs temperature of outcoming fumes for radiation-thermal cracking	86
Fig. 48 Combined VB and RTC unit.....	88

LIST OF TABLES

	Page
Table 1 Comparison of heavy oil and light oil properties.....	5
Table 2 Common distillation fractions of petroleum [13].....	8
Table 3 Hamaca hydrocarbon fluid composition and properties [56].....	40
Table 4 Average dose and percentage in the interval of 0.8 – 1.2 kGy	48
Table 5 Electron energy losses in accelerator tube	53
Table 6 Theoretical calculations of absorbed dose and optimum distance from exit beam window.....	55
Table 7 Viscosity values of XYZ heavy crude oil	64
Table 8 Results of the viscosity measurements and molecular weight estimates	69
Table 9 Effect of aging in the irradiated oil	70
Table 10 Results of power-law correlation	72
Table 11 Results of Shu’s correlation	73
Table 12 Viscosity test report for oil and PD samples at 50 °C	74
Table 13 Viscosity of 10wt.% DW sample before and after irradiation up to 10 kGy.....	76
Table 14 Viscosity of 5wt.% DW sample before and after irradiation up to 10 kGy.....	77
Table 15 Results of experimental calculation of the absorbed dose	79
Table 16 RTC simulation results.....	80
Table 17 Results of experiment.....	81
Table 18 Baseline capital cost for a high-power accelerator facility	88
Table 19 Visbreaker annual operating requirements and cost	90
Table 20 RTC annual operating requirements and cost	91
Table 21 Current prices of crude oil and petroleum products.....	91
Table 22 Annual cost of raw material, labor and value for products for VB.....	92
Table 23 Annual cost of raw material, labor and value for products of RTC	94
Table 24 Annual total product cost at 100% capacity for VB	95

	Page
Table 25 Annual total product cost at 100% capacity for RTC	96
Table 26 Suggested values for risk and m_{ar}	98

CHAPTER I

INTRODUCTION

Current global statistical data shows that the share of heavy crude oil deposits exceeds light oil deposits by two orders of magnitude; furthermore, worldwide light crude oil fractions have been depleting for the last two decades. The rapid depletion of lighter crude oil reserves is accompanied by growing demand for various kinds of petrochemical products. This forces the refining and petrochemical industries to shift to more efficient and profitable processing of heavy crude oil. It is obvious that future supply of petroleum products directly depends on heavy crude oil deposits.

One solution to the problem of efficient heavy oil processing may be electron irradiation technology. Irradiation processing may provide efficient control of a great variety of radiation-induced reactions in hydrocarbons without the use of catalysts or similar chemical agents.

According to the literature [1-3], the main advantages of radiation thermal cracking (RTC) over conventional thermal cracking in heavy crude oil are high yield of gasoline and other light oil fractions, elimination of catalysts, and the possibility of low-temperature cracking.

The main goal of this project is to investigate the effect of e-beam irradiation on the transformation of heavy oil and/or bitumen into light fluids. The specific objectives of this study are:

- Evaluate change of heavy oil viscosities with respect to irradiation dose
- Evaluate the effect of different solvents on the viscosity of irradiated crude oil
- Determine how electron beam radiation affects yields of radiation-thermal cracking compared to yields from conventional thermal cracking
- Perform economic feasibility analysis of RTC on industrial scale

Some of the possible economic benefits of developing this technology include reduction of expensive catalyst waste, lower energy consumption (30% to 40% savings) [4, 5], and simpler and more compact facilities. We compared effects of e-beam radiolysis by comparing selected physical properties of irradiated samples to a non-irradiated control group. These tests included viscosity-temperature profiles and monitoring temperature-time yields.

The Van de Graaff (VDG) accelerator facility of the Biological and Agricultural Department of Texas A&M University was used to irradiate crude oil samples and conduct thermal cracking experiments. A container to hold the oil samples was designed to efficiently and uniformly irradiate heavy oil at room temperature and pressure. A cone-and-plate viscometer was used to compare viscosities before and after irradiation.

Application of radiation in petroleum processing is a new area of research, and the following section (Chapter II) documents and reviews all pertinent literature. Chapter III describes equipment and procedures used to evaluate viscosity, and a laboratory-scale experimental layout to conduct research on the thermal cracking of heavy crude oil under a beam of fast electrons. Chapter IV develops simple and efficient techniques to detect changes in the molecular structure of crude oil after irradiation and presents analysis of radiation-thermal cracking experiments. Chapter V is a description of economic feasibility analysis of the radiation-thermal process on an industrial scale. Chapter VI summarizes this thesis with conclusions and recommendations for future work.

CHAPTER II

LITERATURE REVIEW

2.1 Heavy oil resources, composition, properties

Recent studies show that the extracted crude oil density in the last ten years increased by 30-40%. It will be a logical prediction to say that the production of heavier oils will continue to increase because reserves of heavy oil in our planet are more than 6 trillion or 6×10^{12} barrels. These reserves exceed light oil deposits by two orders of magnitude. Large amounts of heavy oil are located in Canada (1.7 trillion barrels), Russia (200 billion barrels) and Venezuela (1.2 trillion barrels). Other heavy oil reserves (about 2.9 trillion barrels) are spread all over the world, particularly in Alaska, Saudi Arabia, Mexico and Madagascar [6]. According to Meyer [7], the amount of oil in place in the Alberta oil sands of Canada and in the Orinoco Oil Belt of Venezuela is estimated to be as much as 4 trillion barrels.

It is also predicted that in near future these nonconventional reserves promptly will replace those that have been produced in the form of conventional oil [8].

There is no consistent definition of heavy oil, and based on density, it varies. According to World Energy Council, oil is classified as heavy if its density is less than 22.3°API [9]. API gravity can be calculated from the following equation:

$$^{\circ}API = \frac{141.5}{\gamma_o} - 131.5 \quad (1)$$

where γ_o is the oil specific gravity defined as the ratio of oil to water density at 15.6°C.

A common definition for heavy oil relates to a density less than 20 ° API. Oil of density less than 10°API is classified as extra-heavy [7]. However, for refineries, crude is considered heavy if its density corresponds or is below 28°API [10].

By definition, viscosity is the measure of the internal resistance of a fluid to motion because of the forces of cohesion between molecules. Heavy oils are usually very viscous, which is very critical for transportation and exploration.

Generally, viscosity increases with density of crude oil at a constant temperature. However, viscosity is not perfectly correlated with API gravity and therefore heavy oil can not be defined in terms of viscosity as the sole indicator [6].

The effect of temperature on viscosity of crude oil is generally estimated by Walther's correlation [11]:

$$\log[\log(\mu + c)] = A + B \log T \quad (2)$$

where μ is absolute viscosity, T is temperature, and A and B are constants, which vary widely with different oils, whereas c is equal to 0.6 for heavy oils. Equation 1 has been found to be applicable for a variety of liquid hydrocarbons, from light to very heavy crude oils, of paraffinic as well as naphthenic and/or aromatic nature in 75-600°F temperature range. It was shown to be suitable for the dynamic viscosity of heavy oils and their fractions, with viscosities ranging from 1 to 800000 mPa-s. Coefficient c was introduced to avoid undefined double logarithm at viscosities 1 cP or less. Example of how to estimate viscosity by this correlation is presented in Chapter IV.

Pressure also affects viscosity due to the gas in solution. A pressure increase leads to increase in viscosity at constant temperature [11], although this effect is more pronounced in gases than in liquids and it is negligible for heavy oils.

Analysis of hundreds of samples of heavy crude oil all around the world indicates that distillation of heavy oil yields about 50 vol% residue with 22 wt% coke. On the other hand, distillation of light crude oils yields on average less than 20 vol% residue with low coke content of about 10 wt%. Heavy crudes are notorious for high sulfur and metal content; on the average, the concentration of nickel is about 86 ppm, vanadium is 269 ppm and sulfur is 44,700 ppm [7]. Properties of light and heavy crudes are summarized in Table 1.

Table 1 Comparison of heavy oil and light oil properties

Average property	Heavy Oil	Light Oil
API gravity	16°API	35°API
Viscosity	600 cP	10 cP or less
Sulfur Content	2.5 wt%	0.5 wt%
Asphalt Content	40 wt%	10 wt%

Petroleum does not have uniform chemical composition. It varies with location, age and the depth of oil field. Overall, petroleum is a complex mixture of hydrocarbons, including paraffinic, naphthenic, and aromatic groups. Acetylenic and olefinic groups usually are not present in crude oil. Ultimate or elemental composition of oils all around the globe on average yields: carbon, 83.0-87.0%; hydrogen, 10.0-14.0%; nitrogen, 0.1-2.0%, oxygen, 0.05-1.5%; sulfur, 0.05-6.0%.



Paraffins are saturated hydrocarbons with straight or branched chains. 2,2,4-Trimethylpentane or isooctane is an isomer, which is used as a standard in grading gasolines in terms of octane number. Octane number determines quality or resistance of the gasoline to the knocking “detonation” in the engine of the automobile. The higher the number, the higher the resistance, and therefore the better the gasoline, which leads to reduced engine wear during service and gives more power, efficiency and economy. Pure isooctane has an octane number 100. Isoparaffins have higher octane numbers than corresponding normal isomers.

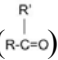
Later we will discuss the effect on gasoline quality by various hydrocarbon groups. Paraffins and naphthenes are thermally and chemically stable and burn with clean flame. Olefins are chemically unstable, reactive and toxic, but have high octane numbers. Aromatics are undesired, due to their high toxicity, and gradually their production has fallen to less than 20% in the US. Nevertheless, because of their high octane rating among hydrocarbons, some countries are increasing the aromatic content up to 50% in super unleaded fuels to replace lead containing octane enhancing additives like tetra ethyl lead. Alcohols and ethers are providing good antiknock value to the gasoline, are less toxic than aromatics and have been used as additives since 1979 in the

US. The most effective and ecologically sound additive nowadays is methyl tetra butyl ether, or MBTE. In order to obtain the desired effect of octane number boost from oxygenates, the volatility properties of hydrocarbon fractions have to be modified correctly. Otherwise, oxygen-containing additives will increase toxic and smog-forming properties of gasoline [12].

Naphthenes or cycloparaffins are saturated hydrocarbons containing one or more rings, each of which has one or more paraffinic side chains. Aromatics are hydrocarbons with benzene rings, which may or may not be linked up with naphthene rings and/or paraffinic side chains. Olefins or alkenes are unsaturated hydrocarbons with a double bond in the molecular structure. Acetylenes are another class of unsaturated hydrocarbons with a triple bond.

Nonhydrocarbon components are important parts of heavy oil composition because of their influence on the processing of crude oil: the presence of mercaptans leads to the metallic corrosion of equipment involved in the refining; the thermal decomposition of chlorides also contributes to the corrosion through formation of free hydrochloric acid; deposits of metals (vanadium and nickel) poison and cause deactivation of catalysts. Their presence in the final products cause discoloration, lack of stability during storage, reduced antiknock qualities, corrosion of engines and emission of harmful compounds to the environment [13].

Sulfur is present in crude oil in the form of elemental sulfur and various compounds, such as mercaptans (RSH), hydrogen sulfide (H₂S), sulfides (RSR'), cyclic sulfides () , thiophenes () and other more complex molecules [13].

Oxygen is present in various forms and total content is generally less than 2%. Higher percentage may be due to the prolonged exposure to the atmospheric air during production or storage, because crude oil is quite susceptible to oxygen. However, residue of vacuum distillation might contain up to 8% by weight. Generally, compounds containing oxygen in oil are carboxylic or naphthenic acids (RCOOH); oxygen also exists in the form of phenols (ROH), ketones () , esters (RCOOR') and ethers (ROR') [14].

Nitrogen may be present in two forms: nonbasic (pyrrole, indole, etc.) and basic (pyridine, indoline, etc.). Basic nitrogen compounds can be extracted by dilute mineral acids, whereas nonbasic compounds, containing a greater part of nitrogen, cannot. Even where nitrogen content is quite low (0.1-0.9%), the presence of nitrogen is undesirable, since it contributes to the poisoning of cracking catalysts.

Even very small amounts of metals, like iron, copper, nickel and vanadium, have a negative influence on the crude oil refining processes by decreasing the effectiveness of cracking catalysts, leading to excessive coke formation and decrease in gasoline yields. In addition, the presence of vanadium and sodium leads to ash deposits and corrosion on the turbine rotors of high-temperature power generators. Metals exist in the form of water-soluble inorganic salts, which can be removed by evaporation and subsequent water washing, and in the form of oil-soluble organometallic complexes (vanadium, copper, nickel, iron), metallic soaps (zinc, titanium, calcium, magnesium) or colloidal suspensions of elemental metals [13]. The majority of metal constituents remain in the residue after distillation; therefore, there is a demand for new metal removing technologies for thermal operations (gas oil processing).

Another, very important petroleum property is its fractional composition. To determine fractional composition, crude oil is slowly heated in a rectification column at atmospheric pressure, and separation of fractions is based on their boiling points as indicated in Table 2 [13]. The amount of light fractions differs from oil to oil.

Table 2 Common distillation fractions of petroleum [13]

Fraction	Boiling range	
	°C	°F
Light naphtha	-1–150	30–300
Heavy naphtha	150–205	300–400
Gasoline	-1–180	30–355
Kerosene	205–260	400–500
Stove oil	205–290	400–550
Light gas oil	260–315	400–600
Heavy gas oil	315–425	600–800
Lubricating oil	>400	>750
Vacuum gas oil	425–600	800–1100
Residuum	>600	>1100

Based on the separation of paraffin wax upon cooling crude oil, the industry divides petroleum into paraffinic and naphthenic oils. The US Bureau of Mines developed a correlation index (CI), which is based on the plot of specific gravity versus the reciprocal of the boiling point in degrees Kelvin. For pure hydrocarbons, members of the normal paraffin series is given a value of CI = 0 and of benzene is given as CI = 100:

$$CI = 473.7\gamma_o - 456.8 + \frac{48,640}{T(K)} \quad (3)$$

where $T(K)$ is the average boiling point for a petroleum fraction and γ_o is the specific gravity [15].

Values for the index between 0 and 15 indicate a predominance of paraffinic hydrocarbons in the fraction. A value from 15 to 50 indicates predominance either of naphthenes or of mixtures of paraffins, naphthenes, and aromatics. An index value above 50 indicates a predominance of aromatic species. Four classes are suggested, based on CI: paraffinic, naphthenic, aromatic, asphaltic and mixed base of four. Fig. 1 illustrates a ternary diagram with the classification defined according to their composition [13].

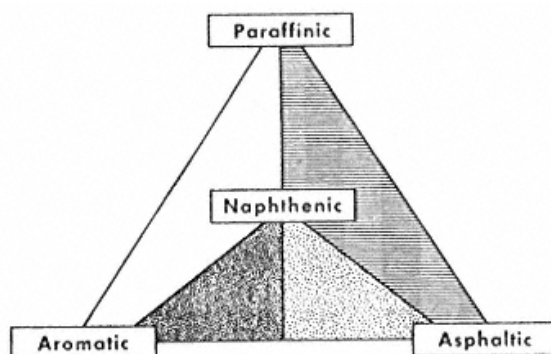


Fig. 1 Simplified composition diagram for crude oils [13]

2.2 Upgrading methods for heavy oil and chemistry of thermal cracking

Upgrading is a process of fractionation or chemical treatment of heavy oil to increase its economic value. The minimum objective of upgrading is to reduce viscosity without adding costly solvents, whereas the full upgrading approach is to process oil to obtain higher quality products, such as the lighter end products gas oil and gasoline [16].

There are several major methods of heavy oil upgrading: thermal cracking, fluid catalytic cracking and hydroprocessing. A schematic representation of a thermal cracking unit is shown in Fig. 2 [11].

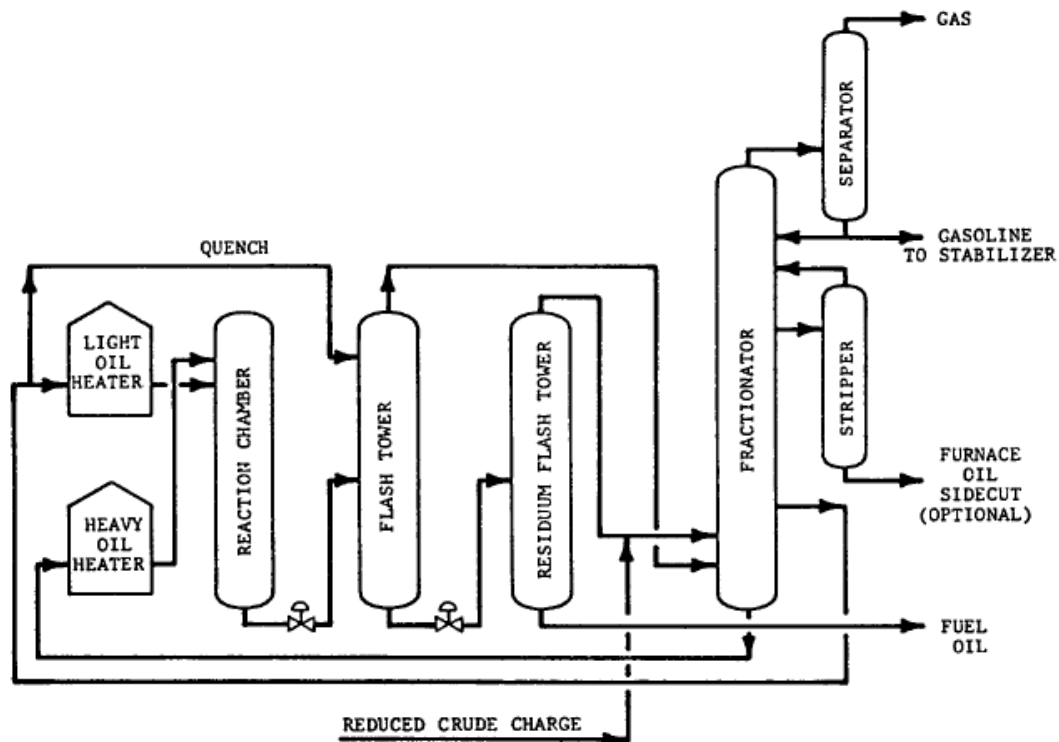


Fig. 2. Thermal cracking unit [11]

The objectives for upgrading include:

- Lowering metal content to reduce catalyst poisoning rate during catalytic cracking to fuels and middle distillates.
- Lowering sulfur content to meet product specifications or emission standards.
- Increasing hydrogen content to enhance selectivity for gasoline and middle distillates. Hydrogen content is the key fundamental quality parameter of residue
- Reduce boiling point and viscosity of heavy oil and bitumen [17].

Thermal cracking is the oldest and still the major technology of the refining industry and important improvements in this technology still continue to be made. Thermal cracking started as a simple batch process, when a batch of crude oil was heated until most of the kerosene was distilled from it and the color of the overhead material became dark. Hydrocarbon heating leads to decomposition, rearrangement and recombination of molecules. As thermal cracking proceeds, reactive unsaturated

molecules are formed that continue to react and can ultimately create higher molecular weight species that are relatively hydrogen deficient and readily form coke. Cracking takes place at temperatures above 400°C. Thermal decomposition does not require the addition of a catalyst. To minimize coke formation and to increase the yield of lighter products the essential variables are feedstock type, time, temperature and pressure.

The severity of thermal processing determines the type of conversion and the product characteristics [11]. Based on temperature ranges, two main processes of thermal cracking are distinguished as visbreaking and coking.

The objective of visbreaking is to reduce viscosity achieved by increasing residence time in a furnace reactor at elevated temperatures ranging from 450 to 520°C and adding steam for formed gas oil removal.

Coking consists of delayed coking and fluid coking. Delayed coking is conducted at milder temperatures, about 500°C, and used to produce a pure coke for electrode manufacturing. Fluid coking or flexicoking is still under development and major mechanical and process improvements are being made. For this method the fluidized bed technique is implemented to make the process continuous and to sustain high temperatures of 510-566°C in the reaction zone, resulting in lower coke but higher fuel gas yields [17].

Disadvantages of these technologies are the enormous thermal energy consumption and the environmental impact, such as sulfur dioxide emission, which causes bronchial irritation in humans and contributes to acidification of lakes. Delayed coking requires large amounts of water for hydraulic cleaning of the coke drum. All cracking products are rich in sulfur and nitrogen, so secondary upgrading is necessary to lower the concentration of sulfur below required levels for final product specification [16].

Both catalytic cracking and hydroprocessing can be thought of as a finishing process and not a conversion process. The purpose of these processes is the removal of heteroatoms or the reduction of aromatics in the final product [18].

If during thermal conversion hydrogen escapes as part of the hydrocarbon gas byproduct, hydroprocessing adds hydrogen and uses catalysts to enhance the process. Two main processes are fixed bed hydrogenation (hydrotreating) and the ebullating-bed process.

Fixed bed hydrogenation is a process of feedstock enrichment by hydrogen under the pressure and thermal treatment. Hydrotreating technology is one of the most popular refinery processes, since low-priced hydrogen became available from improvements in reforming¹ design. Thermal treatment (300-450°C), the presence of hydrogen at 0.7-15 MPa and a hydrogenation catalyst (Co-Mo, Ni-Mo, Al₂O₃) remove heteroatoms (nitrogen, sulfur, oxygen) and metals from crude oil, thus reducing coke formation. A drawback of hydrotreating is its fast catalyst poisoning by metals and coke, which leads to expensive plant shutdowns for catalyst replacement.

In the ebullating-bed process, catalyst particles are suspended in a fluidized bed by liquid moving them upward. By this technique it becomes feasible to transfer all of the regeneration heat to the reaction zone, to build larger units and to process heavier feedstock. Presently, there are a number of different configurations that allow catalytic cracking of heavy oils and residuals, such as H-Oil (Texaco), LC Fining (Amoco), CANMET and VEBA COMBI (PetroCanada). The problems encountered in this process come from complex, higher boiling constituents that require pretreatment. Knowledge of constituents is required for the choice of the right catalyst [11].

Fluid catalytic cracking, or FCC, is one of the most commonly used refinery processes to convert heavy gas oil to lighter distillates. As stated before, feedstock to FCC is limited to heavy gas oils, because of the sensitivity of catalysts to metals, heteroatoms and coke. If cracking heavier feedstock is desired, expensive metal tolerant catalysts and metal passivation additives should be purchased. When these measures were taken resid fluid catalytic cracking (RFCC) and resid oil cracking (ROC) emerged. Residue processing grew from basically nothing in 1980 to nearly 2 MMbpd² of installed

¹ Reforming is a process of converting naphthenes to aromatics with release of hydrogen

² Million barrels per day; 1 bbl= 158.97 liters=0.15897 m³

capacity in 1996. Total FCC capacity worldwide, by comparison, is about 13 MMbpd [19]. Fig. 3 [20] shows the relative distribution of processes as of 1998 used for primary upgrading in North America and Venezuela with coking contributing of about 50%.

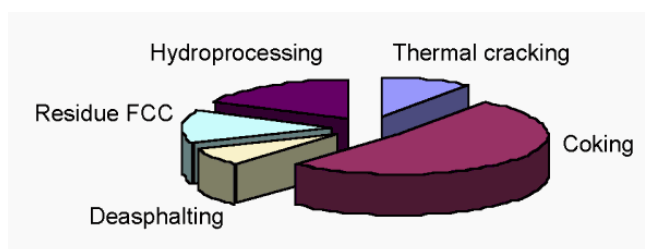


Fig. 3 Major thermal upgrading processes distribution [20]

Any of these thermal, hydro or catalytic processes can be combined to form a more effective overall process. Several important combinations practiced nowadays are Hydrotreating/FCC, used to produce high value gasoline and middle distillates and Hydrotreating/Delayed Coking, used to produce high quality coke [17].

In summary, thermal cracking for direct conversion of heavy crudes into lighter fractions is very energy intensive and environmentally hazardous; catalytic and hydrogenous processes are expensive and complex to operate.

During cracking, larger molecules break down to smaller via breakage of a C–C bond, which happens with free-radical chain reactions. Free radicals are molecular species with unpaired electrons and due to the highly reactive nature (life of methyl and ethyl radicals at temperatures of 600-900°C is of the order of 10^{-3} s), concentration is low but still measurable, which is confirmed by mass spectroscopy.

A chain reaction starts with an *initiation*, when the hydrocarbon chain is broken and free radicals are formed. For alkanes in general, the energy of the C–C bond is much lower than the energy of C–H bonds. Therefore, a C–C bond will be preferentially broken. For example, the dissociation energy of C₂H₅-H is 410 kJ/mole and the dissociation energy of CH₃-CH₃ is 360 kJ/mole. The energy of the C–C bond in *n*-

alkanes decreases as one moves towards the center of the molecule. For example, *n*-hexane would prefer to crack in two propyl radicals ($C_6 \rightarrow 2C_3$) rather than in ethyl and butyl radicals ($C_6 \rightarrow C_2 + C_4$) [18].

The initiation step is followed by a *propagation* step, when free radicals and stable molecules are interacting with each other, leading to isomerization and decomposition of free radicals. Isomerization type reactions must be taken into account only for molecules consisting of long chains. Since the forward reaction of decomposition is endothermic, it is favored at high temperatures characteristic of thermal processes and while the reverse reaction of polymerization is avoided. At atmospheric pressures, these decomposition reactions favor formation of light olefins and smaller radicals [16].

Chain *termination* is the last stage of every chain reaction. Free radicals recombine to form stable paraffin and olefin molecules.

Formed olefins react further to form higher molecular weight materials: olefins, coke, residue. Hydrogen deficient, noncatalytic conditions favor olefin formation and they participate in free-radical reactions similar to alkanes.

Thermal reactions of naphthenes are similar to paraffins, with additional reaction pathways of ring opening and dehydrogenation, like one with decalin (Fig. 4).

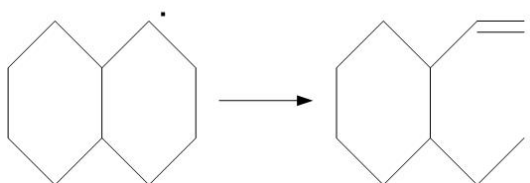


Fig. 4 Ring opening reaction of decalin molecule

Compared to paraffins, ring opening is energetically less favorable; that's why naphthenes are less reactive and somewhat more stable. Therefore, the residue fraction generally contains large amounts of naphthenic structures. A dehydrogenation reaction occurs at the absence of hydrogen to form either aromatics or olefins and diolefins.

The aromatic ring is considered stable at moderate cracking temperatures of 350–500°C. Cracking removes the side chains to give a distribution of alkylaromatics with shorter chains, alkanes and olefins. Alkylated aromatics, like the alkylated naphthenes, tend to dealkylation rather than to ring destruction. Ring destruction of the benzene derivatives occurs above 500°C; however, alkylaromatic radicals can also participate in condensation reactions, which give rise to condensed aromatics, which may undergo ring destruction at somewhat lower temperatures (450°C) [13], [16]. This is the greatest problem during thermal cracking, because polycondensation reactions of aromatics lead to coke formation. Coke formation decreases the yields of the desired gasoline and diesel fractions [12].

All major thermal cracking reactions can be viewed as series of simple thermal conversions as indicated in Fig. 5.

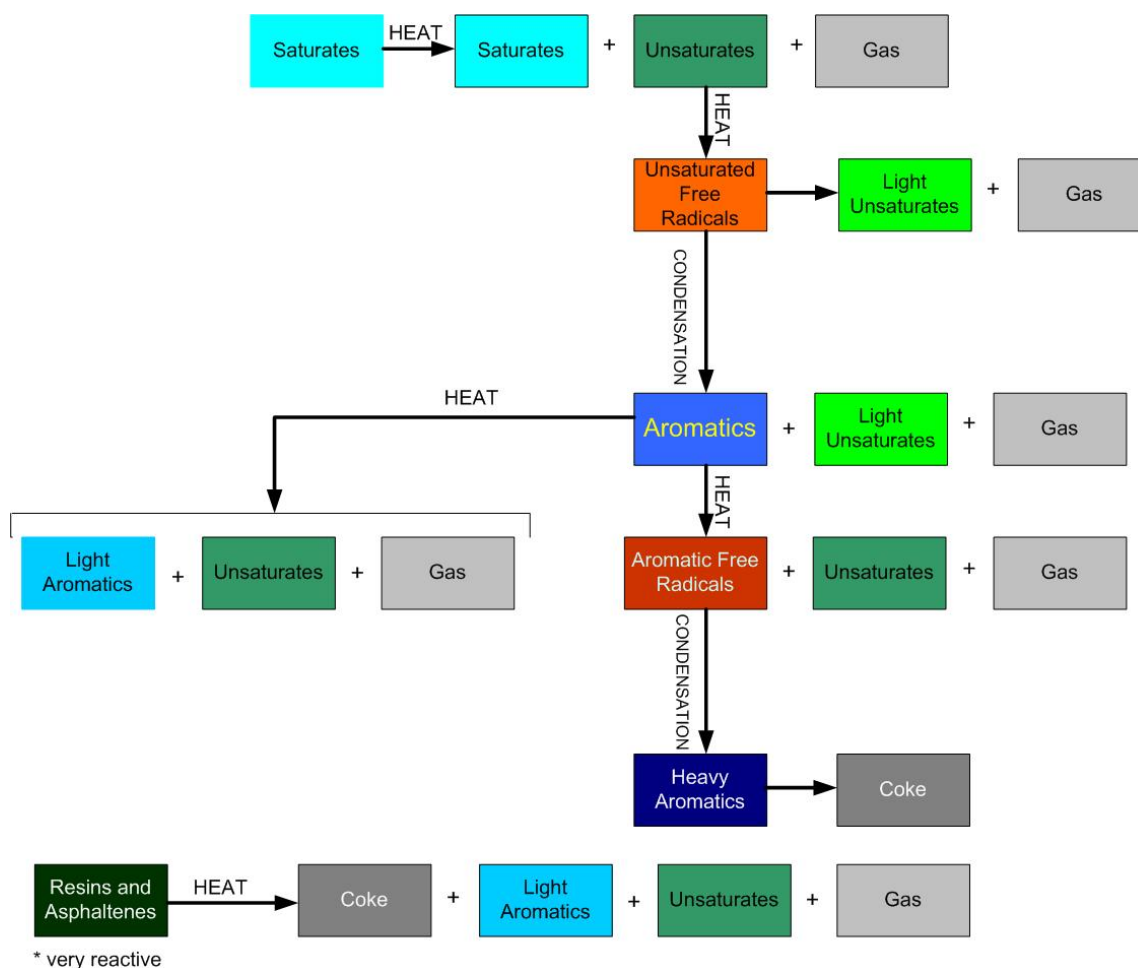


Fig. 5 Thermal decomposition of hydrocarbon components

2.3 Radiation background

2.3.1 Interaction of fast electrons with matter

The following discussion explains the basic interaction mechanism of charged particles traveling through a specific medium.

The energy of an electron is usually measured in *electron volts* (eV). An electron volt is the energy acquired by one electron at a potential difference of 1V.

Electrons passing through neutral material excite and ionize atoms, so that they can also emit energy [21]. When a charged particle interacts with a medium, it produces

an ionization event or ion pair production. That is why this type of radiation is called *ionizing radiation*. [22].

Electrons lose energy due to the radiation emission, elastic and inelastic scattering. Radiation emission predominates at high electron energies, which is favored by high atomic number stopping materials. When electrons with energies above 50 keV are decelerated by another charged particle, such as an atomic nucleus, they give off electromagnetic radiation in the X-ray region or *bremstrahlung*, which is translated from German as "braking radiation".

Elastic and inelastic scattering are dominant at low electron energies. Elastic scattering happens when an electron is an incident particle and it is diffracted in the Coulomb potential of atoms and molecules. Inelastic scattering is the only one of the processes that generates ionization and excitation in the stopping material and hence is the only process that brings about significant chemical or biological damage [23]. Inelastic scattering occurs when electrons interact with the electrostatic field of atomic electrons so that the atomic electrons are either raised to a higher energy level (i.e., the atom is excited) or are ejected from the atom (the atom is ionized).

The linear rate of energy loss in a medium is the basic physical quantity that determines the dose that the particle delivers to the medium. This quantity is called the *stopping power* of the medium for the particle [21]. The stopping power is expressed in MeV/cm. Dividing the stopping power by the material density yields a quantity known as *mass stopping power*. In particular, the total mass stopping power of a medium is defined as the sum of its mass collision and mass radiative stopping power. The general expression is given by,

$$\left(\frac{dE}{\rho dX}\right)_{Total} = \left(\frac{dE}{\rho dX}\right)_{collision} + \left(\frac{dE}{\rho dX}\right)_{radiative} \quad (4)$$

Radiative losses are a small fraction of the losses due to ionization and excitation for electrons and secondary electrons with energies of a few MeV, and become important only in absorbers with high atomic numbers like lead or titanium [24].

High energy electrons are called *beta particles* or beta rays. Electrons resulting from interactions of X-rays or gamma photons with matter are referred as *secondary electrons*. Some interactions of high energy electrons result in additional electrons called *delta rays* [24].

Electrons travel forward along tracks away from the initial beam direction when penetrating through a specific medium. These deviations from the incident beam direction result from elastic and inelastic *scattering* processes. The process continues with emission of secondary electrons along their tracks producing a cascade effect until the energy is dissipated in excitation and thermal processes [25].

The *range* of the charged particle is given by the distance it travels before coming to rest. Electrons follow a tortuous path through absorbing materials due to electron-electron, electron-nuclear interactions, which changes penetration direction. The range of penetration is approximated by the continuous-slowing-down approximation (CSDA), and the CSDA range is defined by equation [26]:

$$R_{CSDA} = \int_0^{E_0} \left(\frac{dE}{\rho dx} \right)^{-1} dE \quad (5)$$

where E_0 is the initial particle kinetic energy (MeV) and $dE/\rho dx$ is the mass stopping power (MeV·cm²/g). The definition of range is considered as the expectation value of the path length ℓ , which the electron follows until it comes to rest. Values are calculated and tabulated for various elements and compounds [26],[27].

The following empirical equations relate the range R_{HC} in gm/ cm² to the electron kinetic energy E_k in MeV, in materials composed of low atomic number elements, like hydrocarbons [21]: Note that in reality an electron slowing down is not a continuous process, since electrons do not lose large fraction of energy in a single collision.

$$\text{For } 0.01 \leq E_k \leq 2.5 \text{ MeV: } R_{HC} = 0.412 E_k^{1.27-0.0954 \ln E_k} \quad (6)$$

$$\text{For } E_k > 2.5 \text{ MeV: } R_{HC} = 0.530 E_k - 0.0106 \quad (7)$$

These relations fit the curve plotted in Fig. 6 [21]:

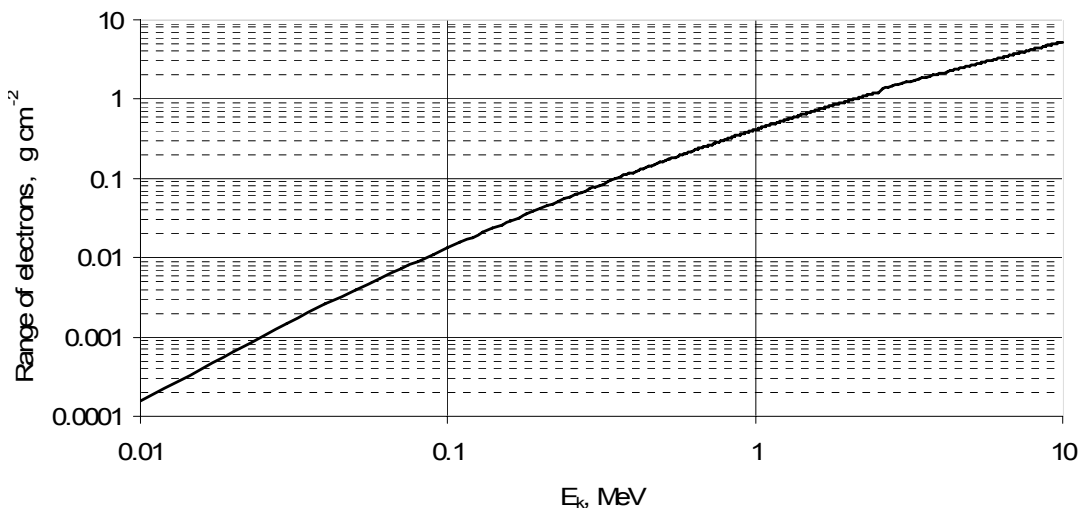


Fig. 6 Electron range-energy curve for materials composed of hydrocarbons [21]

2.3.2. Dosimetry methods for electrons

Management of the physical and chemical changes brought about by irradiation requires knowledge of the amount of energy transferred from the radiation source to the target material. The determination of these quantities constitutes *radiation dosimetry*.

Dosimetry is essential for quantifying the incidence of various changes as a function of the amount of radiation received, for comparing different experiments, for monitoring the radiation exposures of individual materials, and for surveillance of the environment.

Absorbed dose is a measure of the energy deposited in a medium by ionising radiation. It is equal to the energy deposited per unit mass of medium, and so has the unit J/kg, which according to the Standard International (SI) is given the special name gray

(Gy) [28]. The common SI dose unit is the kilogray (kGy). Another unit of dose is the rad, which represents 10^{-2} J/kg.

In water, a dose of 1 Mrad delivered adiabatically will increase the temperature 2.4°C , assuming a negligible change in chemical energy. In plastic materials with lower heat capacities, the temperature rise will accordingly be greater, typically about $5^{\circ}\text{C}/\text{Mrad}$.

The dose requirements for various applications extend over a very broad range, from less than 1 rad for radiography to more than 100 Mrad for the degradation of scrap Teflon [29]. In our experiments, we used absorbed dose from 10 to 30 kGy to investigate the effect of dose on the viscosity of heavy crude oil.

Exposure is an important fundamental quantity, which is defined as a quotient of the absolute value of the total charge produced in the air by the mass of volume element of air, when all liberated secondary electrons are completely stopped in the volume element and have produced all of their ionization in air. Note that exposure is a result of the radiation, not a measure of the radiation itself. Exposure is measured in coulombs per kilogram of air (1 C kg^{-1}) or *roentgen* (R).

The roentgen is defined as the radiation exposure equal to the quantity of ionizing radiation that will produce one e.s.e. (electrostatic unit of charge or $3.3364 \times 10^{-10} \text{ C}$) of electricity in 1 cm^3 of dry air at 0°C and standard atmosphere, and is conventionally taken to be worth $2.58 \times 10^{-4} \text{ C kg}^{-1}$ (using a conventional air density of about 1.293 kg/m^3). Using an air ionization energy of 33.97 J/C , we have:

$$0.01D_{air} = 2.58 \times 10^{-4} \frac{\text{C}}{\text{kg}} \times 33.97 \frac{\text{J}}{\text{C}} \times R \quad (8)$$

or

$$D_{air} = 0.876 \times R \quad (9)$$

where D_{air} is in rads and R in roentgen. Therefore $1 \text{ Gy} \approx 114.155 \text{ R}$.

Measurement of ionization, produced in a volume of a gas upon irradiation, has been used in dosimetry since the discovery of X-rays and radioactivity [23]. Most of the ionization chambers used for radiation monitoring of beta, gamma and X-ray radiation are air filled and unsealed types. Their sensitivity depends on the volume and pressure of the gas and on the associated readout components. Ionization chambers are available as both active and passive detectors [21]. Ionization chambers consist of two gas-filled electrodes separated by a space. The incoming radiations will go through this gas-filled space and cause ionization, and the resulting discharge of current is measured by applying a potential across the electrodes. These electrodes may be in the form of parallel plates or of coaxial cylinders. One of the electrodes may be the wall of the vessel itself.

The average amount of energy required to form an ion pair in a gas is usually given the symbol W and is measured in eV. For a beam of electrons, the length of the plates should be made greater than the range of the electrons in the gas, so electrons will expend all their energy between the plates, ionizing and exciting the gas molecules. The total number of ion pairs formed is determined from the current in the external circuit, which is operated under conditions where recombination and gas multiplication do not occur. The total amount of energy required to form this number of ion pairs is determined from the energy of the incident electrons and the number of them entering the gas. The ratio of this amount of energy to the number of ion pairs formed gives the average value of the energy required to produce one ion pair.

Values of W are more or less independent of the gas in which the ionization is produced. In air, the gas most frequently used in ionization chambers, the value of W is about 33.97 eV per ion pair [26] and this value is believed to be independent of electron energy. Note that *ionization potential*, which is the least amount of energy required to remove an electron from a free, unexcited atom, is less than W [30].

As the collecting voltage is increased, the ions move under the influence of the electric field between the plates, Fig. 7 [30]. The negative ions drift towards the positive plate (P_1) and the positive ions drift towards the negative plate (P_2). Opposite charged

ions have to move against each other along the lines of force until they arrive at the plates. On arrival at P_1 the electron is driven round the circuit by the battery until it arrives at P_2 , where it neutralizes a positive ion. The current indicated by the meter is due to the negatively charged ions produced in the air between the plates. The positive ions do not travel in the external circuit, because of their comparatively larger sizes.

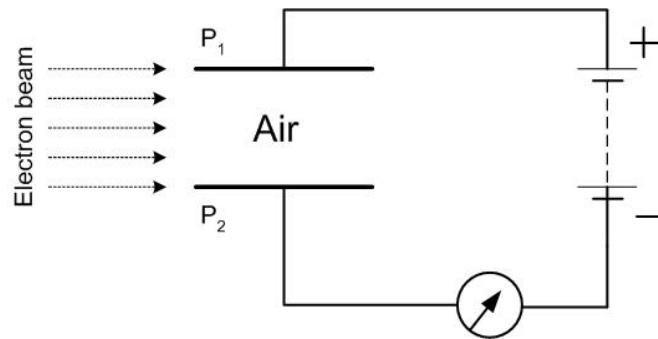


Fig. 7 Ionization chamber [30]

As the collecting field is increased, less recombination occurs and the current indicated by the meter increases. The increase of meter reading with collecting voltage continues until, eventually, no recombination occurs and all of the ions are extracted by the collecting field, which is indicated by the plateau in Fig. 8 [30] and called the saturation current.

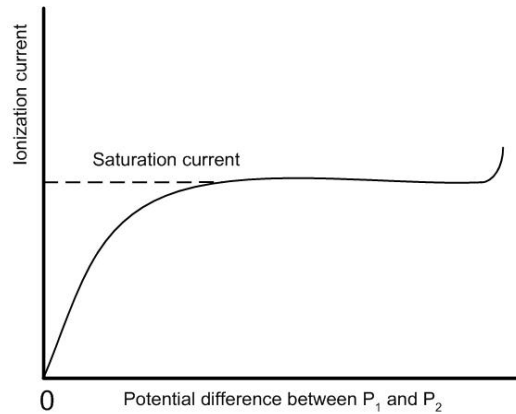


Fig. 8 Saturation curve [30]

As we see from Fig. 8, when the electric field applied to an ionized gas containing free electrons is increased to a high value, we observe a sharp increase in the ionization current above the plateau value. This can be explained by the fact that the electron in the intervals between collisions with neutral gas molecules was accelerated by the field and gained kinetic energy. Moreover, average distance between collisions was small, so the electron did not gain sufficient energy to produce ionization of the molecules when it collided with them, and instead it transferred its energy to them as excitation energy. However, when the electric intensity is increased or the pressure of the gas is reduced, the amount of kinetic energy the electron gains between collisions may exceed the energy needed to ionize a gas molecule. In this case, the electron, colliding with a neutral molecule, ionizes it, producing a positive ion and another free electron. This free electron is also accelerated by the field, and the two electrons may each produce ionization when they collide, yielding four electrons, and so on. This effect is known as gas multiplication. This effect should be avoided in ionization chambers since it leads to a spurious value of the ionization current.

Ionization current is proportional to the rate at which ions are produced in the gas, which is proportional to the rate of arrival of the ionizing particles at the gas volume. Integration of the current, by allowing it to charge a capacitor, gives the total charge produced by the radiation, which is proportional to the total number of particles

entering the chamber. As a result, ionization measurements can be used to measure both the intensity of the radiation and the total amount of radiation in a given time.

LET or *linear energy transfer* is the amount of energy deposited by a charged particle of specified energy as it travels a distance $d\ell$. Radiation is often described as having high or low LET [31].

All sources of ionizing radiation with the same LET produce the same chemical effect with the same dose, provided the energy is delivered at the same dose rate. LET effects are small with the two principal sources used in industrial radiation processing, but dose rate effects can have a major influence on the results.

Dose rate is a fundamental aspect of the reaction kinetics. At low dose rates (10^{-2} kGy/s), free radical reaction kinetics vary directly with the square root of the dose rate. Thus, an increase in dose rate of 100 times will increase the rate of conversion 10 times. At very high dose rates (above 10^5 kGy), where spur overlap phenomena begin to occur, the reaction rate tends to become independent of dose rate [23].

The term “dose rate” is complicated to some extent by the characteristics of the radiation source. Some accelerators produce a beam of electrons whose electrical characteristics are constant with time. Others, such as the linear accelerator, produce a continuous train of short, high current pulses separated by periods of zero current. Thus, different devices can produce different effects even when the time average dose rate is the same.

2.4 Radiation-thermal processing

2.4.1 Industrial radiation processing

Application of radiation technology in industry is various: sewage water and stack gas treatment, polymer processing, radiation sterilization of food and medical products and many others. The principal sources of ionizing radiation for industrial processes are *high voltage electron accelerators* and radioactive materials or *gamma-ray*

emitters. Both operate in such way that neither of them is capable of inducing radioactivity in the irradiated product.

Industrial electron accelerators are capable of producing up to 200 kW of electron beam power at 4 MeV and 100 kW at 5 MeV [32]; the lowest limit is 0.2 MeV, and the highest is 12 MeV. Any accelerator consists of accelerator tubes and high voltage supplies. The maximum useful penetration depth of a dual electron beam is 8 cm in a material of unit density (1 g/cm^3), which is quite small compared to the 30 cm penetration depth of gamma sources in the material of the same density [33].

Industrial gamma ray facilities utilize a Co-60 source or a Cs-137 source from nuclear wastes. The curie (Ci) is a former unit of radioactivity, which is defined as $1\text{Ci}=3.7\times 10^{10}$ decay per second. The SI unit of radioactivity is becquerel (Bq), which equates to one decay per second or $1\text{Bq}=2.7\times 10^{-11}$ Ci [28]. Gamma facilities are capable of producing a radiation source from a few hundred kilocuries (kCi) up to several megacuries (MCi). A typical 1.0 MCi facility provides about 15 kW of gamma ray power [29].

Compared to gamma ray facilities, electron accelerators are cheaper to operate because of their high thruput rates. In addition, the efficiency of energy absorption in electron accelerator processes can be perhaps twice that of gamma processes. However, electrons are limited to the treatment of thin material streams. Gamma ray implementing processes are costly, but have greater penetration and are used mainly for the treatment of bulky objects [29].

The major problem arising from implementation of radiation technology is the *radiation safety*. Radiation safety consists of many elements: procedural, equipment and facility design, shielding. *Shielding* is the most important element of radiation safety and mainly designed to stop harmful primary irradiation from gamma sources and secondary irradiation from electron absorption in a target material, like bremsstrahlung. For an electron beam, the required thickness of shielding decreases as electron energy decreases. Shielding can be made from a combination of enforced (poured) concrete with gravel, sand and lead. The facility should include a sufficient ventilation system to

remove products of ionizing radiation in air, like nitrogen oxides and ozone. Overall, the higher the power source, the higher the expenses related to radiation safety.

Electron beam accelerators are becoming more popular than gamma source facilities. The reasons are their ecological safety due to the absence of radioactive material disposal problem; the absence of related to waste disposal security concerns; their versatility due to the ability of accelerator to operate in X-ray production mode by simply installing high Z material at the exit beam window; and the ability to adjust dose rate to technological requirements.

Overall, the advantages and disadvantages of radiation induced industrial processes can be summarized as follows [23].

Advantages are:

- Absence of catalyst results in purer product and reduced cost of operation.
- Temperatures of operation are relatively low.
- Run-away reactions can be easily avoided by variation of radiation intensity.
- Complexity of equipment is reduced.
- Electron beams can be deflected by electric or magnetic fields so as to scan large areas or particular areas.

Disadvantages are:

- Capital and operating costs are high.
- Ionizing radiation is less specific in its action than chemical initiation and might result in undesired side reaction production.
- The public has a misconception of radiation hazards.
- Dose-rate depends on chain reactions, when thruput can not be increased by simply increasing dose rate.

2.4.2. Radiation chemistry of hydrocarbons

Radiation chemistry studies chemical transformations and chemical reactions occurring in chemical systems under the action of energy absorbed from ionizing radiation.

Radiation promoted activation energies of chemical reactions are lower than chemical reactions proceeding in the absence of a catalyst. This accounts for the increase in reaction rates caused by the irradiation. An essential advantage of radiation promoted chemical reactions is a considerable reduction and sometimes elimination of the induction period.

At present, attention is focused on processes in which a small amount of absorbed energy results in a large amount of valuable products that are difficult to attain by other methods. In radiation chemistry, the most important quantity is the absorbed dose because chemical changes occur as a result of the substance absorbing the energy of the ionizing radiation. Any chemical change (synthesis, decomposition, etc.) occurring in a system under the influence of radiation at ambient conditions is called *radiolysis*. The main quantitative characteristic of any chemical reaction occurring under the influence of radiation is called the *radiation-chemical yield*. It is a useful concept for rating the molecular yields of various radiation induced reactions and often just called the *G value*. It is defined as the number of chemical reactions produced per 100 eV of absorbed energy. G values for many reactions lie in the range of 0.1 to 10, indicating average energy requirements of from 10 to 1000 eV per event. The relation between the absorbed dose *D*, the *G* value and the molecular weight *MW* is:

$$\frac{100 \text{ eV}}{1 \text{ molecule}} \left| \frac{1.602 \times 10^{-19} \text{ J}}{1 \text{ eV}} \right| \left| \frac{1 \text{ mole}}{10^{-3} \text{ kg}} \right| \left| \frac{6.02 \times 10^{23} \text{ molecule}}{1 \text{ mole}} \right| = 9.644 \times 10^7 \text{ J/kg}$$

$$D(\text{kGy}) = \frac{9.644 \times 10^4}{G \cdot MW} \quad (10)$$

For example, if the *G* value is 3 and the molecular weight is 10,000 then the dose requirement will be about 3.2 kGy [29].

Early interest in the effects of ionizing radiation on organic materials stemmed from their use as insulators and lubricants by the electrical industry and somewhat later their use in the same capacities in the developing field of nuclear technology. Thus, many of the early investigations concentrated on the radiation chemistry of

hydrocarbons, which have been studied extensively [23]. The various types of radiation (alpha, gamma, X-rays, electrons, etc.) cause ionization and cleavage of C-C and C-H bonds in hydrocarbon molecules, resulting in new substances with lower molecular masses than those of the initial substances.

Although it is known that irradiation conditions and radiolysis products tend to have a great influence on yields in organic systems, radiation chemical yields are not established for crude oils as in the case for pure organic compounds. This is because of the presence of impurities and complex composition [23].

Most organic compounds give complex mixtures of products that include hydrogen and other molecules that are smaller, about the same size as — and up to twice as large as — the original molecule due to the polymerization. Yields are lower in the solid than in the liquid phase, in part because of the more efficient energy transfer from excited species, but also in part because of the greater probability that radical pairs formed by the dissociation of excited molecules will become trapped and eventually recombine. Bond scission tends to be almost random in straight chain hydrocarbons such as hexane, giving a large number of products. Unsaturated compounds tend to give relatively high yields of high molecular weight products formed by chain reactions. In contrast, aromatic hydrocarbons tend to give low yields of radiolysis product because the energy states of the molecule allow efficient degradation of excitation energy without any chemical change in the molecule, i.e. the energy of excited molecules is channeled to relatively low-energy excited states that have a low probability of dissociation [23].

2.4.3 Radiation-thermal cracking

Despite the fact that thermal cracking is the earliest process available for crude processing, developed countries, like the USA, convert more than 70% of crude by thermal processes [34] This is why there is still demand for new technologies, and why research and development are needed to lower the energy consumption in these thermal processes.

A new, promising approach for effective and efficient processing of highly viscous and high sulfuric crude oil is the use of highly economical and environmentally

friendly irradiation technology. Irradiation processing makes it possible to induce a great variety of electron beam induced radiation reactions in hydrocarbons, without the use of catalysts or any other chemical agents. The opportunity to use ionizing irradiation for oil processing was proved theoretically and demonstrated experimentally in the 1960s [1, 35]. However, Schuler in 1981 doubted the feasibility of a practical application of radiation to the processing of petroleum [36] because of the availability of light crude oils, which made implementation of radiation in petroleum refining not economic. Fortunately, it was not abandoned entirely and nowadays interest has flashed again. As mentioned earlier, densities of extracted crude oils increased in last ten years by 30-40%, which of course largely affected the refinery industry. Processing heavier crudes comes at the expense of increase in the thermal energy consumption, faster catalyst poisoning, increased environmental standards for fuels, more complex refining facilities, etc. Adoption of very efficient and ecologically sound irradiation technology may allow the industry to:

- Add flexibility to the refining facilities to process different feedstock, without major, very expensive changes in the main configuration.
- Keep the configuration of processing units simple, making control and operation easy and safe.
- Deeply desulfurize light hydrocarbon fractions (not analyzed in this thesis).
- Produce fuels with higher octane number (due to increased isomerization).
- Decrease energy consumption up to 30-40% compared to conventional thermal cracking [37].

Hydrocarbon enhancement electron beam irradiation technology (HEET) is more energy efficient, as the chemical reactions take place at lower temperatures (350°C-450°C) and pressures than those needed for the thermal cracking process [38]. According to authors [2, 39], radiation, coupled with thermal cracking during gas oil processing at T=400°C, by 4 MeV energy electrons with a dose rate of 1 kGy/s gives an increase in gasoline yields almost three times higher compared to conventional thermal cracking.

HEET involves a series of chain reactions similar to those in classic thermal cracking based on a heating technology. However, in electron beam induced thermal cracking, irradiation replaces the most energy consuming stage of the chain reaction – initiation [1, 40]. Another difference between thermal and radiation-thermal processing is that radiation induced energy has the capability of breaking any of bonds, while in the conventional case primarily weak chemical bonds are broken [4]. Thermal energy is coupled most strongly to the translation, rotational and vibrational modes; only a small fraction goes into the electronic modes of the absorber. Thus, ionization, bond rupture, and all other processes leading to chemical reaction occur only in the high-energy tail of the Maxwellian distribution: ionizing radiation is absorbed almost entirely by the electronic structure of an absorber. Therefore, ionizing radiation is a very effective and efficient generator of the reactive species that initiate chemical reactions [33].

Experiments conducted on crude oil with high contents of sulfur have shown that radiation induced chemical conversion differs much from reactions in the thermal cracking model hydrocarbons. For example, sulfur content in the final product was reduced significantly and about 90% of the total sulfur was concentrated in the heavy residuum fractions. Based on this, specific approaches to process high-sulfuric oils by applying radiation were developed [41, 42]. Other recent works on this problem [3, 43-49] are also pointing to advantages of radiation utilization in heavy oil and gas oil processing.

The polymerization and isomerization effects in the distillate from radiation-thermal cracking (RTC) [38], the so called “synergy” effect [2, 49] or polycondensation [43, 50] are of a high interest. The synergetic processes in complex hydrocarbon mixtures that have been exposed to the action of ionizing radiation increase antiknocking quality of motor fuels, i.e. they increases octane and cetane numbers.

Conventional thermal cracking does not produce a significant degree of branching in products, other than that already present in feedstock [13]. Therefore, in order to produce higher quality gasoline, high pressures are applied, which promotes branching of *n*-alkanes (isoparaffins have higher octane numbers than corresponding

normal isomers) and prevents gas production. Therefore, utilization of electron beam radiation would allow production of high quality motor fuels without high pressures.

Few patents existing in this area describe pilot-plant scale design, which are not suitable for laboratory scale research.

Gomberg [51] investigated effects of ionizing radiation on the yields of liquid hydrocarbon products from tar sands and coals. Crashed solid fuel samples were mixed with hydrogen-donor solvent and irradiated by a gamma source at or above ambient temperatures and pressures. Different combinations of solvent, absorbed dose and fuel sample were investigated. There was an increase in the yield of light fractions, and elemental analysis showed that there was a significant drop in sulfur and nitrogen concentrations compared to non-irradiated control samples.

Pokacalov [46] describes a method and an apparatus for treating heavy fractions of crude oil. According to the results of test runs, there was an increase in yields of lighter fractions from 4 vol.% to 24 vol.%, when a thermal treatment of 11°API gravity oil is combined with the action of gamma-electron-proton irradiation compared to the sole thermal treatment. The action of gamma-electron-proton thermal treatment gives higher yields at lower absorbed doses than gamma-electron thermal treatment, thus facilitating energy conservation. Energy of electrons is used for activation or destruction of long molecules of residual oil, creating free radicals. Protons are compensating free valence bonds of broken molecules, preventing recombination of radicals, which might lead to the formation of even bigger hydrocarbon chains. Therefore, simultaneous action of a flow of two differently charged accelerated particles assists liberation of light fractions. The energy of protons might be lower than the energy of electrons. Pokacalov observed that with increasing absorbed dose the yields were increasing, too.

Yet the author of another patent [45] claims that output of light fractions can be increased, if ultrasonic generator or pressure pulsator were installed to the feed running system described in the previous patent by Pokacalov. Such device creates nonuniformity of density and flow rate in the irradiated volume of feed, increasing the

useful percentage of destruction energy induced by combined flux of accelerated particles and ionizing radiation.

Zhuravlev *et al.* [3] proposes to use heat from nuclear reactor, and ionizing radiation coming with it, for radiation-thermal cracking of vacuum gas oil. They observed that the rate of conversion of heavy gas oil into lighter fractions (gasoline and diesel) increased 1.5-2 times for radiation-thermal method, compared to conventional thermal methods. Additionally, the concentration of sulfur in products of RTC was 2 times lower than in products of TC.

Differences between ordinary thermal cracking and radiation-initiated thermal cracking can be given on the example of heptane thermal conversion. Radiation-initiated thermal cracking of natural petroleum fractions follows a similar pattern.

As discussed previously, thermal cracking is the result of C–C bond cleavage of paraffins, and the initiation step gives two alkyl radicals:



Followed by radical propagation reactions of dehydrogenation:



and β -scission



Olefin yields depend on operating temperatures (the higher the temperature, the lower is the molecular weight of the olefins), partial pressure of hydrocarbons (lower pressure favors the olefin yield) and residence time in the reactor (longer residence times lower the yield due to the increased possibility of secondary reactions).

Radiation assisted cracking of natural petroleum fractions follows a pattern similar to the radiation-thermal cracking of heptane. Implementation of radiation in the

cracking of heptane molecules resulted in temperature reduction and higher yields of olefins and methane compared to the non-irradiated processing scheme. At the process temperature of 450°C and low dose rate of 6.4×10^{-4} kGy/s, the G value for alkene production is equal to 5500, which gives information about the chain reaction and chain length and tells us that the olefin yield is high for low dose rates. Radiolysis of heptane at ambient conditions (atmospheric pressure and temperature of 25°C) yielded a G value of 3, which is very small compared to the previous G value, and this indicates that free radical chain reactions occur only at high temperatures. Moreover, chain reactions were not observed at temperatures below 300°C and further increase in temperature resulted in lower molecular weight olefin production. This is explained by the fact that the initiation step has high activation energy and without radiation the molecule initiates at temperatures around 500°C, whereas RTC proceeds at lower temperatures (450°C). Therefore, radiation provides a source of radicals; the overall products of cracking are determined by propagation steps of the radical chain reaction rather than by the radiolysis mechanism [23].

CHAPTER III

EXPERIMENTAL METHODOLOGY AND MATERIALS

This chapter describes the facility for irradiation, the properties of the research material, sample preparation procedure and radiation-thermal cracking experiment setup.

3.1 Facility for irradiation

We used the Food Engineering Safety laboratory at the Biological and Agricultural Engineering Department of Texas A&M University to irradiate crude oil under electron beam. This facility consists of an electron Van de Graaff accelerator and concrete shielding around it. The machine is placed within 2 ft thick concrete walls, made of concrete blocks with staggered joints. Section #1 of Fig. 9 houses an accelerator; section #2 is an entrance into the irradiation chamber, which is shielded by a sliding door with a 5-mm-thick lead sheet inside. The ceiling of the facility is covered by sand bags. Next to the concrete shielding is a control room (Fig. 10), which houses the accelerator control panel (Fig. 11).

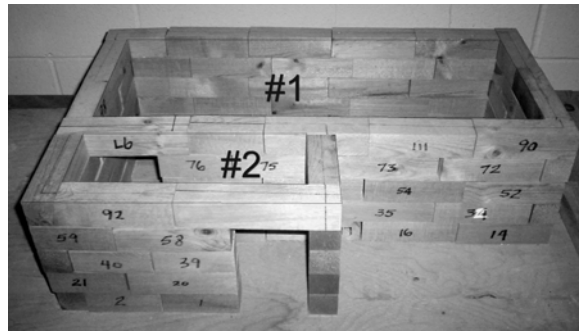


Fig. 9 Design model of facility at the Biological and Agricultural Engineering Department



Fig. 10 General view of VDG facility at the Biological and Agricultural Engineering Department



Fig. 11 Control room equipment

3.2 Van de Graaff accelerator

A Van de Graaff or VDG is an electrostatic accelerator to produce a beam of fast (high-energy) electrons in continuous mode. VDG is a versatile research tool, because it provides a steady-state beam with good energy regulation [52]. This machine is generally used only for laboratory research and has found practical application in nuclear physics, food irradiation and other fields [53].

The principle of the work is based on the mechanical transfer of charge from ground to high voltage terminal; thus, high voltage potential is produced [54]. Fig. 12 [53] shows the main parts of a VDG, which are the charge producing system and the accelerating system.

The rubber belt of high dielectric strength is placed in the high-pressure atmosphere of an insulating gas. The DC-power generator is used as a source of electrons. Electrons from corona discharge are sprayed onto a rapidly moving belt and transported against the potential gradient to a high voltage (HV) terminal, where the charge is collected upon contact with a metal brush. Further, the charge is accelerated back to the ground [52].

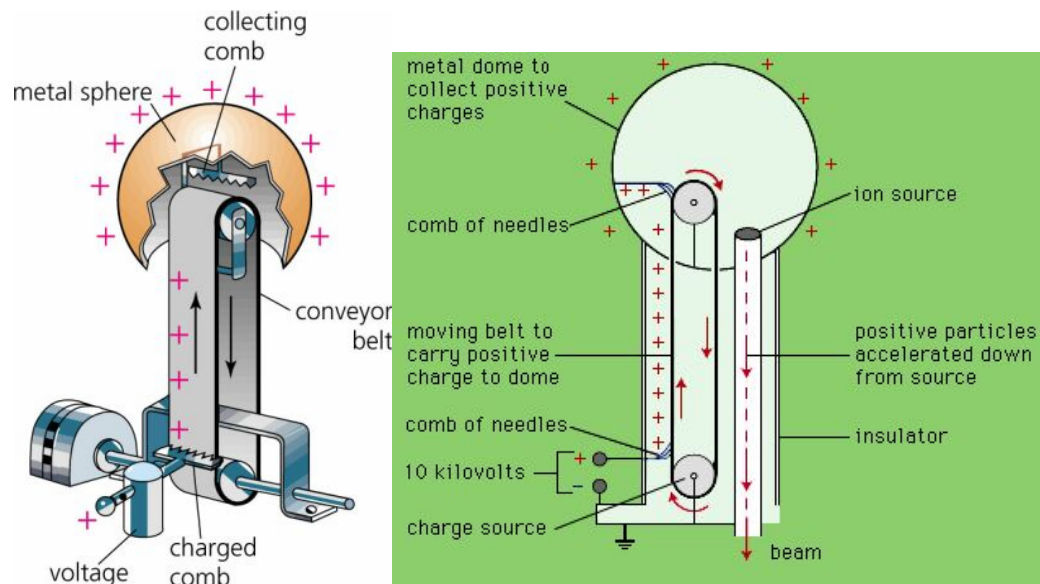


Fig. 12 Schematics of Van de Graaff accelerator [53]

To describe the physics behind VDG we let a force, F_x , act upon a charged particle. To make acceleration possible we have to change momentum (p_x) of a charged particle, which will increase electrical field (E_x):

$$\frac{dp_x}{dt} = F_x = q \cdot E_x \quad (14)$$

where q is in coulombs (C), E_x is in N/C or V/m.

Within a uniform electric field, E , a charged particle moves between two parallel plates at a potential difference v_x (V), as shown in Fig. 13:

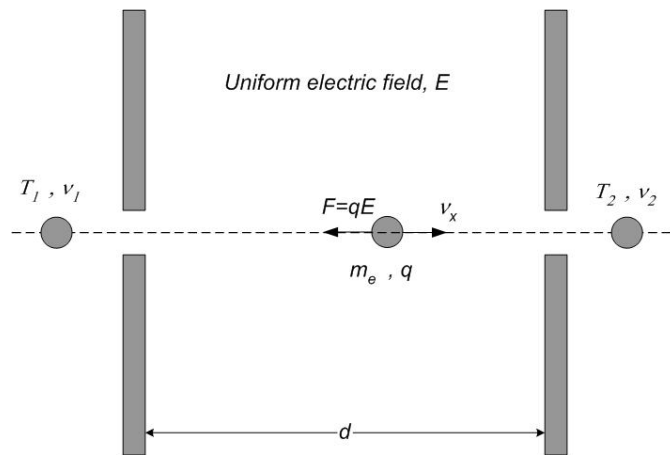


Fig. 13 Acceleration of charged particle between two parallel plates

As electrons move in the direction of electric field, E , potential difference increases up to v_x :

$$v_x = v_1 - v_2 \quad (15)$$

This potential difference is proportional to the distance, d (m) [55]:

$$v_1 - v_2 = Ed \quad (16)$$

Charge density, collected on the belt depends on the dielectric strength of the environment. For a flat belt, the maximum charge density, σ_{max} (C/cm²) is:

$$\sigma_{max} = 2\epsilon\epsilon_0 E_{max} \quad (17)$$

where ϵ_0 , is an electric constant (electric flux/m) and ϵ is permissivity of the environment surrounding belt. E_{max} is the breakdown strength of the electric field (V/m). For a charged particle moving within this field, the maximum possible voltage, V_{max} , will be:

$$V_{max} = E_{max} d \quad (18)$$

The VDG we used for heavy oil irradiation was designed and manufactured by High Voltage Engineering Corporation in Burlington, MA in 1954. This system is able to accelerate electrons at selected energies between 0.75 and 2 MeV. A general view of the machine is shown on Fig. 14.

The accelerator consists of 3 main parts: generator, vacuum system and control system. The generator for the VDG is a cylinder shaped tank 0.8 m in diameter, 1.8 m long and set 1 m above the floor. Fig. 15 and Fig. 16 show the accelerators main external parts.

In the VDG, the two parallel plates are the high voltage terminal within the tank, which is connected to the ground.

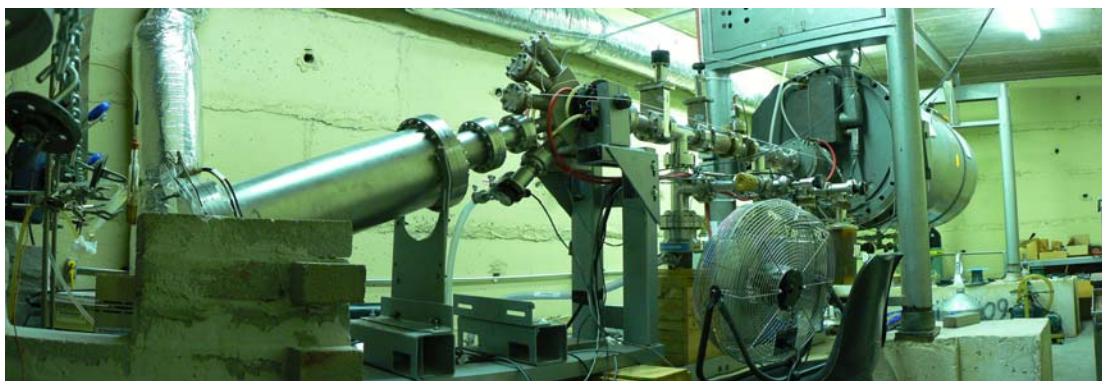


Fig. 14 General view of Van de Graaff machine

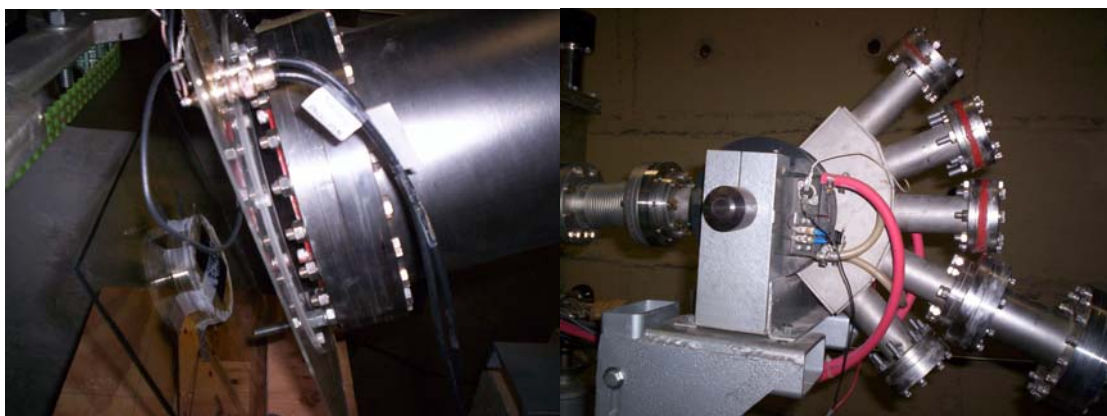


Fig. 15 E-beam exit window with parallel plate transmission ion chamber and sample of crude oil placed in front of it (left). E-beam bending magnets (right)



Fig. 16 System of vacuum pumps (left). Pressurized tank, where, in the atmosphere of inert gas, the accelerating column is placed (right)

3.4 Preparation of Hamaca oil sample

To study effects of radiation on crude oil we used heavy Hamaca crude oil from Venezuela's Orinoco Basin. Table 3 [56] provides the composition and main fluid properties of the oil. The liquid is heavy enough not to have any yield by atmospheric distillation.

Table 3 Hamaca hydrocarbon fluid composition and properties [56]

Component	Gas composition, mole %	Liquid composition, mole %	Fluid composition, mole %
N ₂	0.1	0	0.03
CO ₂	5.995	0.06	1.92
C1	91.918	0.34	29.04
C2	0.864	0.03	0.29
C3	0.389	0.05	0.15
i-C4	0.143	0.04	0.07
n-C4	0.202	0.08	0.12
i-C5	0.08	0.08	0.08
n-C5	0.068	0.09	0.08
C6	0.113	0.4	0.31
C7	0.108	1.01	0.72
C8	0.015	0.15	0.11
C9	0.004	0.09	0.06
C10+	0.001	97.58	67.02
Total	100	100	100
Molecular weight		523	
Oil specific gravity		1.005 (9.3 °API)	
Viscosity (50 °C)		25,000 cP	

To find the optimum thickness of the sample for uniform irradiation MCNP, general Monte Carlo N-Particle Transport Code program was used to numerically simulate neutron, photon and electron transport [57].

Fig. 17 [58] is a result of simulating a single and dual beam irradiation of a 5-mm-thick Hamaca oil sample.

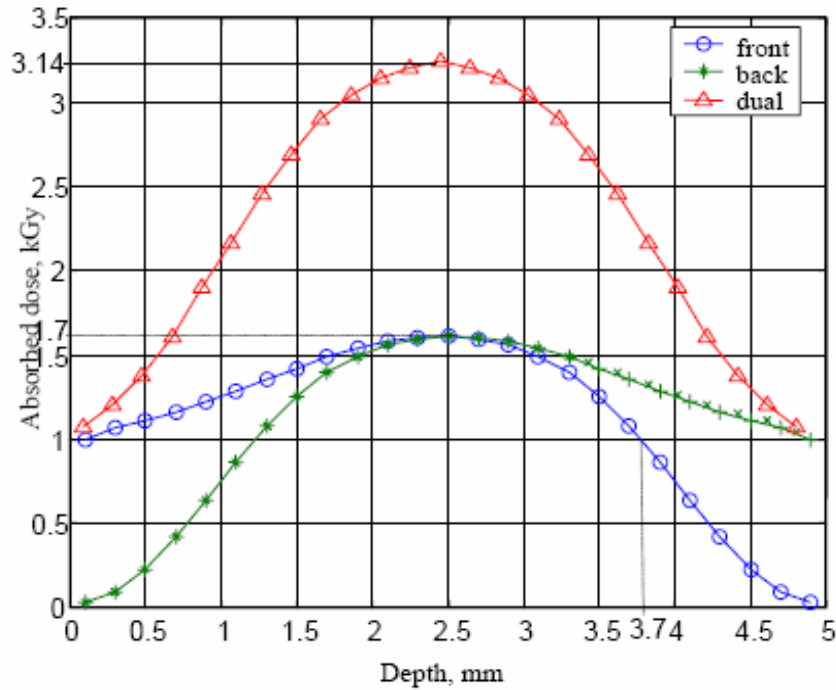


Fig. 17 Depth-dose curve at 5 mm Hamaca crude oil

Single side irradiation of a 5-mm-thick sample results in the maximum dose of 1.7 kGy at a depth of 2.5mm, if the entrance dose is 1 kGy. At the thickness of about 3.7 mm, the absorbed dose is equal to the entrance dose. This thickness we defined as an optimal range (R_{opt}). For a process load of thickness between 2.5 and 3.7 mm, the dose uniformity ratio (ratio between maximum and minimum absorbed doses) yields a constant value of 1.7. Usually this value does not exceed 2.0, while a ratio of 1.5 is a more typical figure. To improve the dose uniformity ratio, dual-side irradiation should be implemented [59].

A steep increase in the uniformity ratio is observed as soon as the thickness exceeds the optimal range (R_{opt}). It approaches infinity when the maximum range of electrons, which is about 5 mm for 1.35 MeV electrons, is exceeded. For dual-sided irradiation, the position of D_{max} is in the center of two outside planes, and the dose uniformity ratio is equal to 3.14. Therefore, to obtain a uniform target absorbed dose, an

optimum average thickness for the sample should be between 2.5 and 3.7 mm. Based on these calculations, average dimensions for all prepared samples were set to 7x6x0.25 cm, which gives an average mass of 10.5 gm.

After determination of optimal sample size and mass, we needed to develop a procedure to prepare samples. The reported viscosity of Hamaca oil is 25,000 cP at 50°C [56], so it needs preheating in order to pour onto the sample holder. For this purpose, we used a water bath. Sample preparation involved the following steps:

- Heat up water bath up to 80°C.
- Place the vessel with oil in it and wait until oil starts to flow.
- Pour some amount of oil on piece of polyethylene packaging film.
- Seal with Scotch tape and spread oil evenly.

Fig. 18 shows schematics of sample preparation and Fig. 19 shows the actual sample, ready for irradiation.

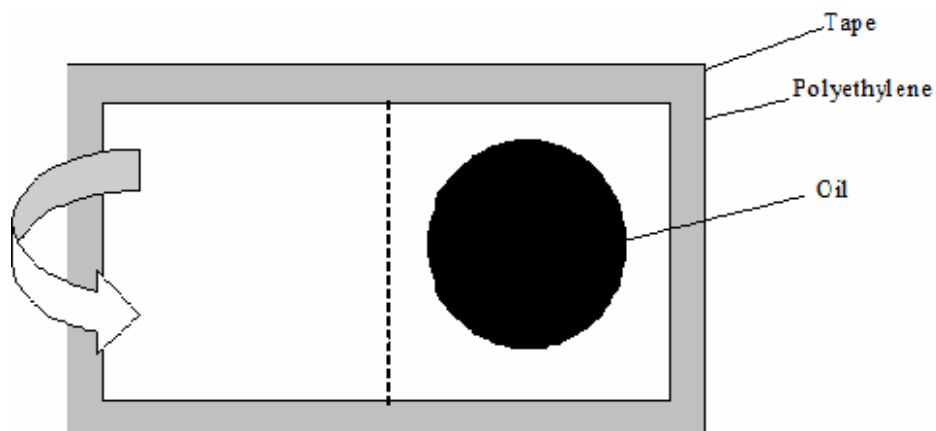


Fig. 18 Sample preparation

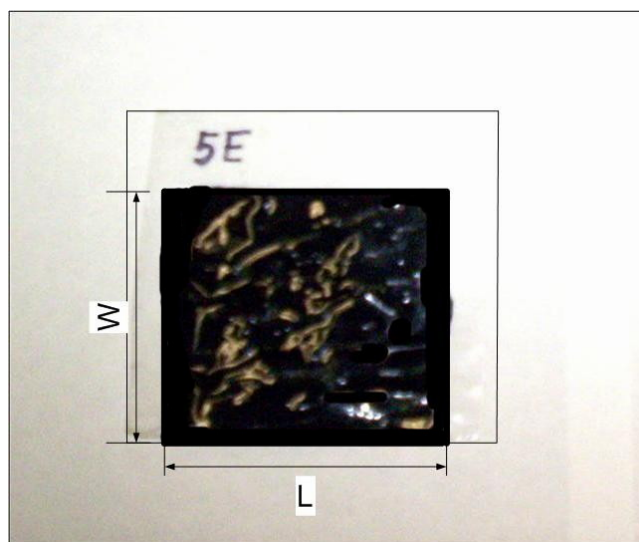


Fig. 19 Sample of Hamaca crude oil ready for irradiation

The volume of the oil in the sample is based on the average thickness of the sample t and calculated from the following equation:

$$V = Area \times t = W \times L \times t = 7 \text{ cm} \times 6 \text{ cm} \times 0.25 \text{ cm} = 10.5 \text{ cm}^3 \quad (19)$$

After preparation of samples with pure crude oil, we prepared samples with mixtures of crude oil with petroleum distillates and distilled water. The procedure followed for preparation of the mixture of Hamaca oil and petroleum distillates (PD) included the following steps:

- Place an empty beaker on the balance and set balance to zero.
- Heat a water bath up to 80°C with a vessel containing oil in it.
- Ensure that oil flows, and once it reaches the pour point, transfer it into the calibrated beaker to measure its weight.
- Note the mass of oil and add a proportional amount of PD with a syringe to obtain the following weight percentage values: 10, 5 and 2.5 %.
- Stir the mixture for about 10 minutes to homogenize it. This procedure takes place at 80°C (petroleum distillates are not volatile at this temperature).

- Prepare another sample by the same procedure as the prepared sample with Hamaca crude, i.e. pour it on the sample holder and seal with Scotch tape.

Samples with mixtures of oil and distilled water (5 and 10 wt.%) were prepared in the same way as we prepared samples of petroleum distillate and Hamaca oil.

3.5 Irradiation of crude oil sample by electron beam

In Chapter II, we defined exposure and absorbed dose and now we can implement those terms in the dose measurement procedure. Using direct-reading dosimeters, and knowing that exposure values in roentgens are numerically similar to dose values expressed in rads, we can measure absorbed dose at the target [31]. Note that the absorbed dose, defined in terms of exposure in air, is $D_{\text{air}}(\text{rad})=0.876xR$ [equation (9) in Chapter II], where R is the number of roentgens. The Farmer-type absolute ionization chamber of 3.03 cm^3 air volume and operating range of 500-1000 R was placed at the distance parallel to the exit window at point P, as showed in Fig. 20.

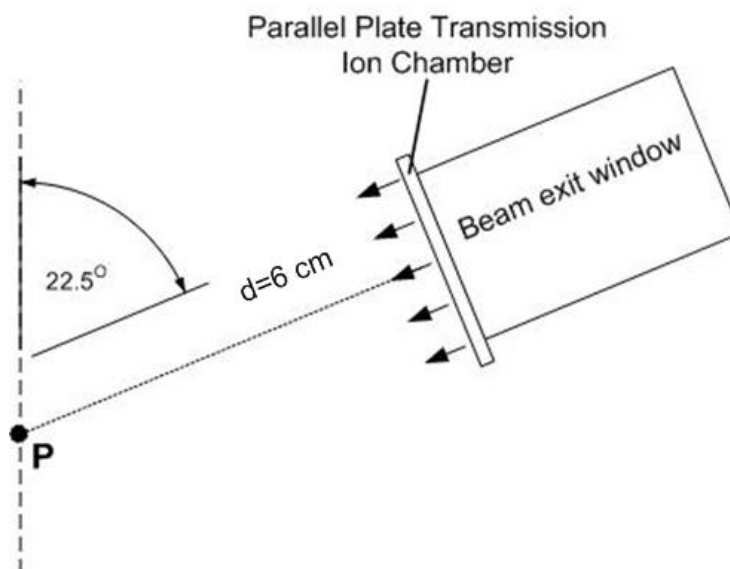


Fig. 20 Lateral view of irradiation point P positioned in front of exit window

The ionization chamber was used to measure exposure in air in kR, which was converted to absorbed dose in kGy ($1 \text{ kGy} = 10^5 \text{ rad}$), assuming that the target is a muscle-tissue equivalent material. The mixture of organic components in the crude oil is similar in “effective atomic number,” i.e. elemental composition, to the soft biological tissue (i.e., muscle), making the oil an approximately “tissue-equivalent” material with respect to electron energy absorption. Thus, if one is interested in the estimation of the absorbed dose in the element volume of crude oil, muscle tissue can be substituted as a reference medium.

The parallel plate transmission ion chamber was always placed at the exit beam window and used to collect charge C , resulting from passing electrons through it. Charge was measured and readings were taken from the control room, Fig. 21. Voltage is supplied to the parallel plate transmission ion chamber by 9V batteries connected in series.



Fig. 21 Front panel of charge counter from transmission ion chamber

Therefore, the number of counts from the transmission ion chamber can be translated in terms of absorbed dose in the sample of Hamaca crude oil. We needed only

the number of counts from the transmission ion chamber to determine the duration of irradiation. For example, total absorbed dose of 10 kGy corresponds to 626148 counts from the transmission ion chamber and the target dose of 5 kGy corresponds to half of this value or 313074 counts.

Next, we irradiated a sample with Hamaca crude oil and observed that after irradiation, a slight rustling sound was coming from a sample. This might be due to the gas production from crude oil initiated by radiation. There was no increase in temperature of the sample, mainly because it was irradiated at a low dose rate. However, for high-power e-beams, thermal effects of radiation are well-known [60].

We did not measure the beam current and beam power, but if we know the absorbed dose at the target, we can estimate them.

The total mass stopping power [$S/\rho = (dE/dx)/\rho$] is the amount of energy dE lost by a charged particle traversing a distance dx in a material of a density ρ . The values of total mass stopping power are calculated and tabulated for different density materials [23, 26].

Fluence (ψ) is a measure of the number of ionizing particles entering a sphere of unit cross-sectional area at the point of interest, units being electrons/cm². Distribution of fluence with respect to energy of the particle is defined as:

$$\psi(E) = \frac{d\psi}{dE} \quad (20)$$

where $d\psi$ is the fluence of particles with energy between E and $E+dE$. For a differential fluence $\psi(E)$ of identical charged particles, the absorbed dose D is given by:

$$D = \int \psi(E) \frac{S}{\rho} dE \quad (21)$$

For charged particles having constant energy, the dose is approximately fluence times mass stopping power, although this might have an error factor of two because of

the backscatter of electrons. Since crude oil can be approximated as a “tissue-equivalent” material, the value for mass stopping power is indicated in the literature [26]: the mass stopping power for 1 MeV electrons in a muscle tissue is $1.84 \text{ MeV}\cdot\text{cm}^2/\text{g}$. Now we only need the absorbed dose at the target to calculate fluence. For an absorbed dose of 10^4 Gy , fluence is:

$$\psi = \frac{1 \times 10^4 \text{ Gy}}{1.84 \frac{\text{MeV cm}^2}{\text{g}} \cdot 1.6 \times 10^{-13} \frac{\text{J}}{\text{MeV}} \cdot 1 \times 10^3 \frac{\text{g}}{\text{kg}}} = 3.4 \times 10^{13} \frac{\text{electrons}}{\text{cm}^2} \quad (22)$$

The radius of uniform electron field at the target is approximately 4 cm. The total beam current (I) is fluence times beam area. Thus,

$$I = \psi \times \pi \times r^2 = 3.4 \cdot 10^{13} \text{ electrons/cm}^2 \times 3.14 \times 42 \text{ cm}^2 = 1.71 \times 10^{15} \text{ electrons} \quad (23)$$

To obtain a target dose of 10 kGy, time of irradiation was 284 seconds; thus, electron rate is $6.02 \cdot 10^{12}$ electrons/second. The elementary charge of an electron is $1.6 \cdot 10^{-19} \text{ C}$. The beam current is calculated as:

$$I = 6.02 \times 10^{12} \frac{\text{electrons}}{\text{second}} \times 1.6 \times 10^{-19} \frac{\text{coulombs}}{\text{electron}} = 0.96 \times 10^{-6} \text{ amps or } 1 \mu\text{A} \quad (24)$$

For 1.33 MeV electrons, beam power (P) is equal to:

$$P = \left(6.02 \times 10^{12} \frac{\text{electrons}}{\text{second}} \right) \times \left(1.33 \times 10^6 \frac{\text{eV}}{\text{electron}} \right) \times \left(1.6 \times 10^{-19} \frac{\text{J}}{\text{eV}} \right) = 1.28 \text{ W} \quad (25)$$

Average dose rate (\dot{G}) is an absorbed dose at the target divided by the time of irradiation and equal to $\dot{G} = 10 \text{ kGy}/284 \text{ s} = 0.035 \text{ kGy/s}$, which is quite a low dose rate [61]. Here it should be noted that the dose rate was not a constant value for all experiments, because change in the geometry, material for irradiation and some other

factors would lead to different dose rates with the same accelerator. For example, for the experiment with radiation-thermal cracking in the aluminum can, with a change in the oil density, distance from the exit beam window and material of the container, the dose rate was estimated to be 0.0018 kGy/s.

Since for viscosity measurement we needed a very small amount of oil, it was necessary to know whether dose distribution within the crude oil sample is uniform or not. GAFCHROMIC® HD-810 radiochromic film was used to determine distribution of the absorbed dose within the sample of Hamaca crude oil. Films were attached to the front and back side of the sample and irradiated up to a target dose of 1 kGy. After irradiation, films were scanned in transmission mode using the full dynamic range scale. Fig. 22 through Fig. 25 [62] show dose distribution.

An average absorbed dose of the sample №1 was 0.96 kGy and 0.90 kGy of the sample №2 (see Table 4). In addition, 75% of the absorbed dose in both samples lay in the interval 0.8 kGy–1.2 kGy, which indicates a good uniformity.

Table 4 Average dose and percentage in the interval of 0.8 – 1.2 kGy

	Sample number №1		Sample number №2	
	Front	Back	Front	Back
Average dose, kGy	0.98	0.94	0.92	0.88
Percentage in the interval 0.8 – 1.2 kGy, %	81.4	74.8	79.1	71.9

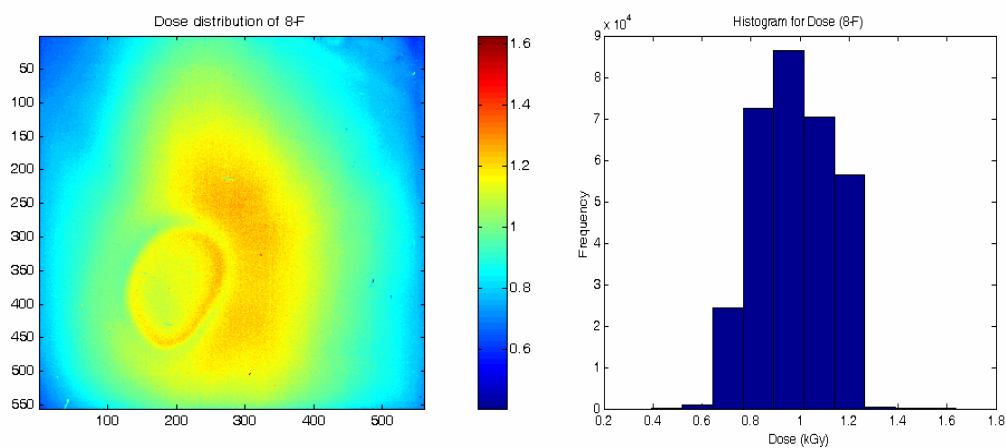


Fig. 22 Dose distribution and histogram in sample №1-front side

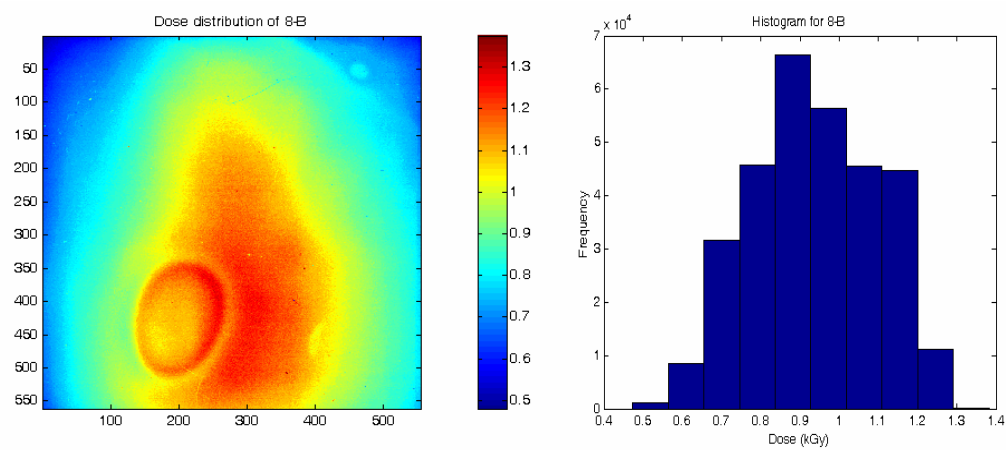


Fig. 23 Dose distribution and histogram in sample №1-back side

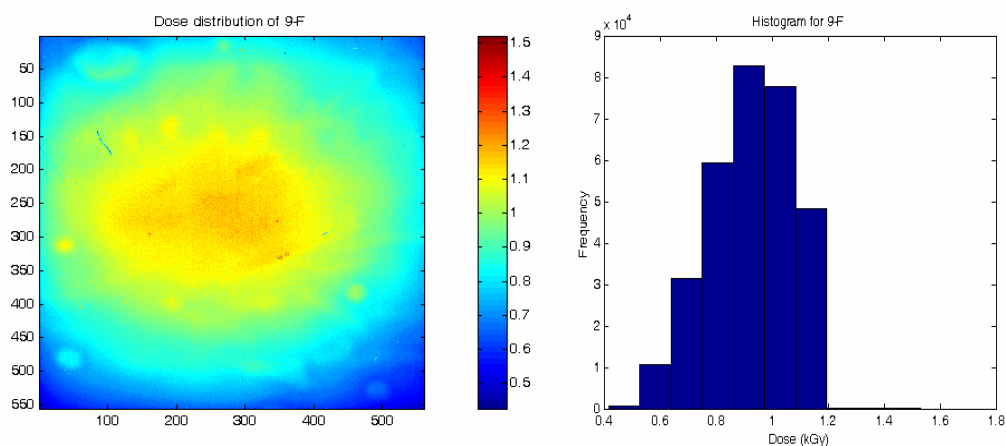


Fig. 24 Dose distribution and histogram in sample №2-front side

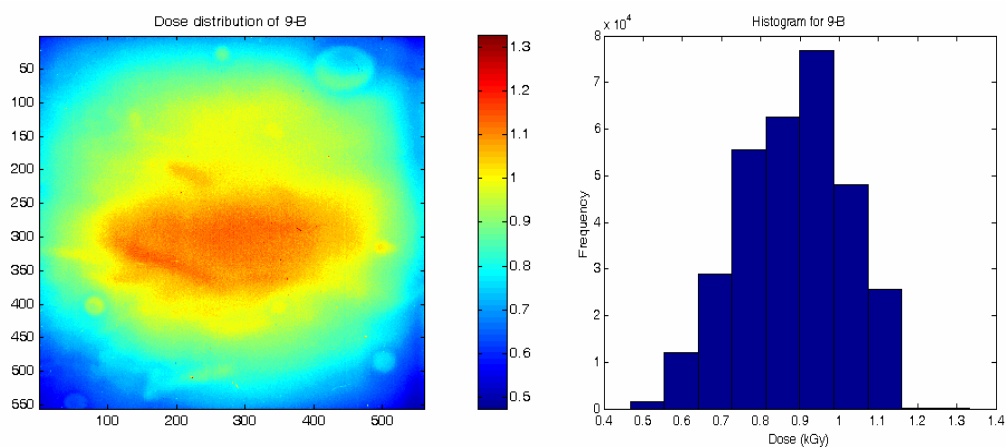


Fig. 25 Dose distribution and histogram in sample №2-back side

Doses around the center were higher than the values of the boundary because the oil samples did not contact the radiochromic films uniformly. Films contacted the crude oil more around the center than at the boundary, Fig. 26.

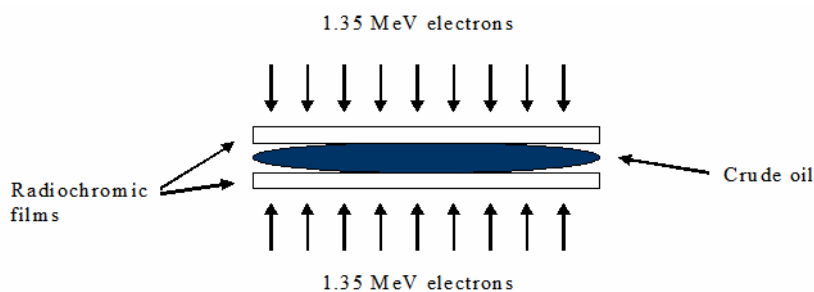


Fig. 26 Schematics of radiochromic films and crude oil

The dose uniformity could be significantly improved if the sample size were reduced to 2 cm x 2 cm. However it is important to keep the amount of crude oil in the sample sufficiently large for viscosity measurements. Once the sample was opened, the oil content was mixed and the required amount was placed in the viscometer.

3.7 Radiation-thermal cracking experiment layout

Radiation-thermal cracking of crude oil required another approach to the experimental design. Therefore, the next step was to design a container that would not attenuate electrons in which it would be feasible to conduct thermal cracking at high temperatures. Experimental glassware is widely available, but the problem is in its thick walls made of Pyrex glass, that would significantly reduce the absorbed dose due to electron attenuation. We could build custom-made flasks from very thin glass. However, those would be handmade vessels, and as a result, they might not be identical in terms of volume and mass, which would cause discrepancies in yields. Besides a very thin glass vessel is hazardous because it might not withstand the pressure fluctuations and break easily. Another option was to modify an empty aluminum can. Walls of the can are very thin and should not attenuate electrons substantially. We needed to verify this through dose calculation.

3.7.1 Estimation of absorbed dose for Pyrex glass and aluminum can

Initial kinetic energy of electrons generated by a Van de Graff accelerator is $E_k=1.35$ MeV. However, the kinetic energy of the electron beam just after passing the exit beam window with transmission ion chamber is lower than this value, since it has to pass through the following barriers, Fig. 27:

- i. a 0.0127 cm thick Al foil, which is situated inside the chamber to seal the exit window and keep low pressure vacuum in the chamber
- ii. a 2.54 cm air gap between the Al foil and the transmission ion chamber
- iii. a transmission ion chamber consisting of 3 layers of Al foils 0.0076 cm thick.

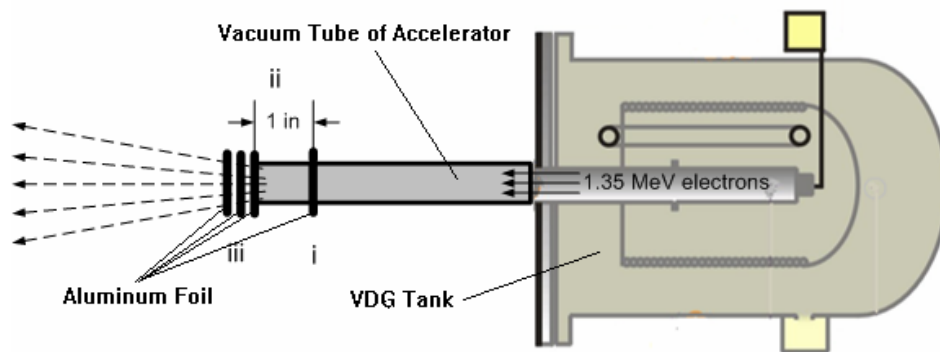


Fig. 27 VDG tank and attached tube with aluminum foil inside

The loss in the kinetic energy of 1.35 MeV electrons is calculated from equation [26]:

$$dE = \frac{dE}{\rho dX} \times \rho \times dX \quad (26)$$

where dE is loss of kinetic energy in MeV; $dE/\rho dX$ is total stopping power in $\text{MeV}\cdot\text{cm}^2/\text{g}$ from [63]; ρ = density of the material in g/cm^3 ; dX = thickness of the material in cm. Results of these calculations are presented in Table 5.

Table 5 Electron energy losses in accelerator tube

Material	dE/(ρ dX), (MeV cm ² /g)	ρ , g/cm ³	dX, cm	dE, MeV
i. Al foil	1.488	2.6989	0.0127	0.051
ii. Air gap	1.674	0.0012	2.54	0.005
iii. Al foil	1.488	2.6989	0.0076	0.030
Total loss ~				0.09 MeV 6.67%

As a result, the kinetic energy of electrons, after exiting the beam window, is $E_{kl}=1.35\text{MeV}-0.09\text{MeV}=1.26\text{ MeV}$.

Placing a heater with a flask too close to the exit beam window may deform the Lucite plate of the transmission ion chamber. Therefore, it should be placed at some distance. As we can see from previous calculations, kinetic energy losses in air are negligible. However, the absorbed dose at the target is largely affected by the distance from exit beam window. The reason is electron scattering. Beam intensity is very high near the exit beam window, and with the increase in distance, electron scattering occurs, as indicated in Fig. 27. Thus, based on the empirical data, it is assumed that the efficiency is only 66% at the distance of 6 cm, 50% at 12 cm, 33% at 18 cm, 28% at 24 cm and 25% at 30 cm [64]. Efficiency is determined by the scattering of electrons and as scatter increases efficiency decreases. Taking all these into account, the target absorbed dose is estimated from [65]:

$$D = \frac{E_k \cdot I \cdot t}{m_{oil}} \quad (27)$$

where I is a current density in μA and t is time of irradiation in seconds, m_{oil} is a mass of oil in grams and E_k is an electron kinetic energy in MeV.

The calculated beam current is 1 μA , the time of irradiation of crude oil in the flask from Pyrex glass is 1200 sec (20 min) and the mass of crude oil is 92 g. As an example, we showed dose calculation for a distance of 12 cm from the exit beam

window when the container is made of Pyrex glass. The rest of calculations are condensed in Table 6.

Given: $E_{k2}=0.8875$ MeV; Efficiency=50%; $I=1$ μ A; $t=1200$ sec; $m_{oil}=92$ gm

$$D = \text{eff}\% \cdot \frac{E_k \cdot I \cdot t}{m_{oil}}$$

$$D = 0.5 \cdot \left[\frac{0.8875 \text{ MeV}}{1 e^-} \frac{1 \text{ J}}{6.24 \cdot 10^{12} \text{ MeV}} \times \frac{1 \times 10^{-6} \text{ A}}{1.6 \times 10^{-19} \text{ C/e}^-} \times \frac{\text{C/A}}{1 \text{ sec}} \times \frac{1200 \text{ sec}}{92 \text{ gm}} \times \frac{1000 \text{ gm}}{1 \text{ kg}} \right]$$

$$D=5787.97 \text{ J/kg}=5.79 \text{ kGy}$$

Dose calculated in this way is only a preliminary estimate of the absorbed dose for a design purpose and complex calculations are required to estimate dose more accurately. Table 6 shows dose estimations for radiation-thermal cracking in a Pyrex glass flask and in an aluminum can. Assuming that the dose rate and the amount of crude oil is constant we could obtain an average 35% increase in the absorbed dose in the container made of a thin aluminum compared to the container made of Pyrex glass. Based on these calculations we selected 12 cm as an optimum distance from the electron beam exit window, because it is far enough from the Lucite plate of the transmission ion chamber and sufficiently close to obtain a substantial absorbed dose.

Table 6 Theoretical calculations of absorbed dose and optimum distance from exit beam window

Material	Stopping Power $dE/(\rho dX)$, (MeV cm^2/g)		ρ , g/cm^3	dX, cm	$dE = \left(\frac{dE}{\rho dX}\right) \cdot \rho \cdot dX$, MeV
Pyrex	1.562		2.23	0.1	0.348
Aluminum	1.488		2.6989	0.01	0.041
Distance, cm	%eff/100	dE(air), MeV	dE (Pyrex), MeV	$E_{k2}=E_{k1}-dE(\text{air})-dE(\text{Pyrex})$, MeV	$D = \%eff \cdot \left(\frac{E_{k2} \cdot I \cdot t}{m_{oil}}\right)$, kGy
6	0.66	0.012	0.348	0.8996	7.74
12	0.50	0.024	-	0.8875	5.79
18	0.33	0.036	-	0.8754	3.77
24	0.28	0.048	-	0.8633	3.15
30	0.25	0.060	-	0.8512	2.78
Distance, cm	%eff/100	dE(air), MeV	dE (Al), MeV	$E_{k2}=E_{k1}-dE(\text{air})-dE(\text{Al})$, MeV	$D = \%eff \cdot \left(\frac{E_{k2} \cdot I \cdot t}{m_{oil}}\right)$, kGy
6	0.66	0.012	0.041	1.2071	10.39
12	0.50	0.024	-	1.1950	7.79
18	0.33	0.036	-	1.1829	5.09
24	0.28	0.048	-	1.1708	4.28
30	25	0.060	-	1.1587	3.78

The range of electrons in low atomic number materials, like crude oil, is calculated from the following equation [21]:

$$\text{for } 0.01 \leq E_k \leq 2.5 \text{ MeV: } R_{HC} = 0.412 \times E_k^{1.27-0.0954 \ln E_k} \quad (28)$$

where E_k is a kinetic energy of electrons in MeV.

The calculated range of electrons in crude oil through a Pyrex glass wall at the distance of 12 cm from the exit beam window is equal to $0.3536 \text{ g}/\text{cm}^2$; and for the case of a thin aluminum wall it is equal to $0.5150 \text{ g}/\text{cm}^2$. The depth of penetration is equal to $d = R_e/\rho$, where ρ is density of the material. Assuming that no convection from boiling fractions is present and taking density of oil as $0.92 \text{ g}/\text{cm}^3$, the depth of electron penetration into crude oil via a Pyrex wall is 0.38 cm, whereas via an aluminum wall electrons would penetrate as deep as 0.56 cm.

These dose calculations are only a rough estimate of the real absorbed dose. To get accurate results, more rigorous and complex calculations are required, which would

take into account convection, heterogeneous media properties, mass transfer of light fractions and subsequent decrease in the mass of irradiated oil.

3.7.2 Design of setup with aluminum can

Since it is very important to conduct consequent runs in exactly the same conditions for good replication and consistency of results, in this section we give information about instrumentation and setup configuration.

A resistance coil heater³ with 500 W rating was used as a heating source. A gooseneck distilling condenser CG-1212-20 from Chemglass was used to cool and condense vapor light fractions coming from the flask. The CG-1212-20 is a one-piece distilling condenser with a 75° adapter, highly efficient coil and vacuum adapter. The joint size is described by a number of the form xx/yy. The first number denotes the outside diameter of the top of the tapered male joint (or inside diameter of the top of the female joint) and the second number denotes the length of the joint. For example, a 24/40 joint is 24 mm wide at the top and is 40 mm long [66]. The condenser has a top thermometer joint of 10/30 size, receiver joint of 24/40 size and a sealed-in drip tip. The coil of the condenser is 6 mm in diameter and 200 mm in length, and the jacket of the condenser is 25 mm in diameter with overall width of 390 mm.

The receiver is placed on the balance to receive the distillate from the dripping end of the condenser. It is important to avoid contact between the condenser and the receiver, since any vibration from the condenser will cause error in readings. Vibration in this case comes from the pump⁴ used to circulate ice-cold water through the jacket of the condenser. A 3-gallon-capacity cooler is used to keep the temperature of the ice bath (2-3°C) constant during the experiment. To determine the temperature profile, a J-type thermocouple with a transition joint is used. To measure the mass of condensing distillate, an electronic balance XD-12K of Denver Instrument Co is used. Details about thermocouple configuration and balance settings are given in Appendix B.

³ Petroleum heater 61560 by Precision Scientific with moving rheostat

⁴ Manostat VERA is a variable speed peristaltic pump to pump fluids through 1/4" ID tubing

Before any tests are carried out, it must be recognized that the presence of more than 0.5% water in the test samples of crude oil causes several problems. For example, during the thermal cracking test, water requires the application of additional thermal energy due to the high heat of vaporization. As a result, water is easily superheated and violent boiling occurs, leading to erroneous readings caused by mechanically transported oil. Steam formed during distillation can act as a carrier gas, and high boiling point components may end up in the distillate contaminating it [11]. Water condenses on the thermocouples tip which drops into the oil, resulting into a burst, violent bubbling and subsequent reduction in temperature. This process is recurrent, causing undulating behavior in the temperature profile and inconsistency in the yield. Therefore, it is important to dewater oil before experiments.

TC and RTC experiments were done with a blend of different dewatered oils with an average density of around 0.9 gm/cm^3 or 20°API . To obtain this density we mixed at room temperature in a closed container two different oils: Remington light (0.85 g/cm^3) and Jobo extra heavy (0.96 g/cm^3). Crude oils were mixed at room temperature, and the ideal mixture is assumed, i.e. the following relation for mixture density can be applied:

$$\rho_m (\text{g/cm}^3) = \frac{(\text{Mass of Light Crude}) + (\text{Mass of Heavy Crude})}{(\text{Volume of Light Crude}) + (\text{Volume of Heavy Crude})} \quad (29)$$

To check API gravity we used Standing's correlation to correct this density from ambient temperature to API standard temperature of 60°F :

$$\rho = (0.0133 + 1524 \rho_{@60^\circ\text{F}}^{-2.45}) [T(^{\circ}\text{F}) - 60] - (8.1 \times 10^{-6} - 0.0622 \times 10^{-0.0764 \rho_{@60^\circ\text{F}}}) [T(^{\circ}\text{F}) - 60]^2 \quad (30)$$

where density is calculated in units of lbm/ft^3 and converted to g/cm^3 .

When two crudes are being mixed, one should keep in mind that asphaltenes are soluble in aromatics and insoluble in paraffins. Therefore, when heavy and light oils are blended, a heavy oil should be compatible with a light one, i.e. light oil should be

aromatic. To check the nature of the blended oil, we calculated Bureau of Mines Correlation Index (CI) from equation (3) in Chapter I:

$$CI = 473.7\gamma_o - 456.8 + \frac{48,640}{T(K)} \quad (3)$$

where $T(K)$ is the average boiling point for a petroleum fraction and γ_o is the specific gravity [15].

The index is equal to 41, which signifies predominance of paraffins, naphthenes, and aromatics. An index value above 50 indicates predominance of aromatic species. Therefore, the choice of light oil was correct. In addition, when we again measured density several weeks after mixing, we observed that density did not change considerably (<3%).

A general view of the experimental setup for radiation-thermal cracking in aluminum cans is shown in Fig. 28, and Fig. 29 presents schematics of the experimental configuration for RTC.

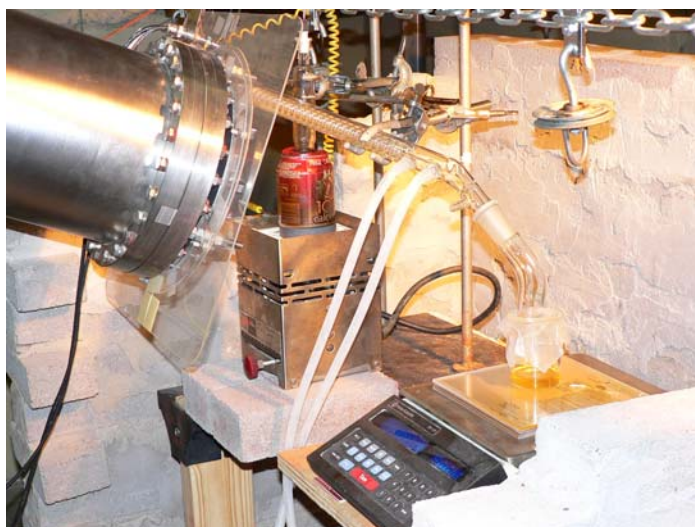


Fig. 28 General view of radiation-thermal cracking in can

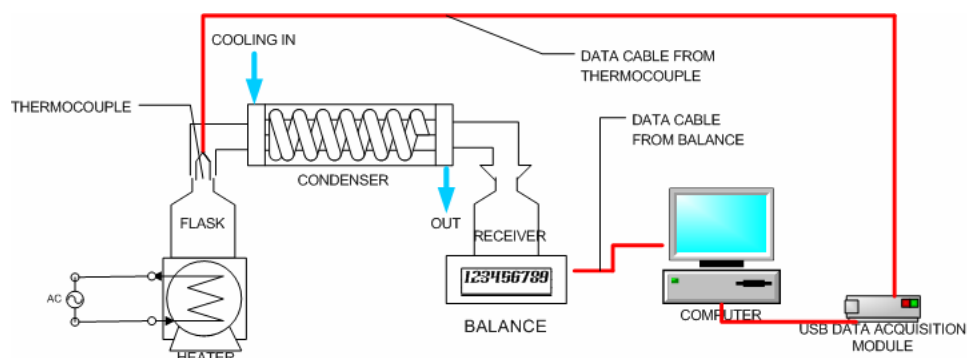


Fig. 29 Configuration for thermal cracking experiment

Since the bottom of an aluminum can is not flat, we used a copper base, which fits the bottom precisely. This is done in order to increase heat transfer from the heater to the crude oil in the can. Copper was chosen as a material for the base, because it is one of the best heat conductors available (about 400 W/m/K) and conducts heat almost instantaneously (only silver has a higher thermal conductivity than copper), whereas such material as stainless steel is a relatively mediocre heat conductor. In addition, the melting point of pure copper is above 1600 °C, so we don't have to worry about deformation of the base.

To check whether the temperature of the heater was stable or not, a hole was drilled in the lower portion of the base and a K-type thermocouple was placed to take temperature measurements. The temperature profile of the heater is indicated in Fig. 30.

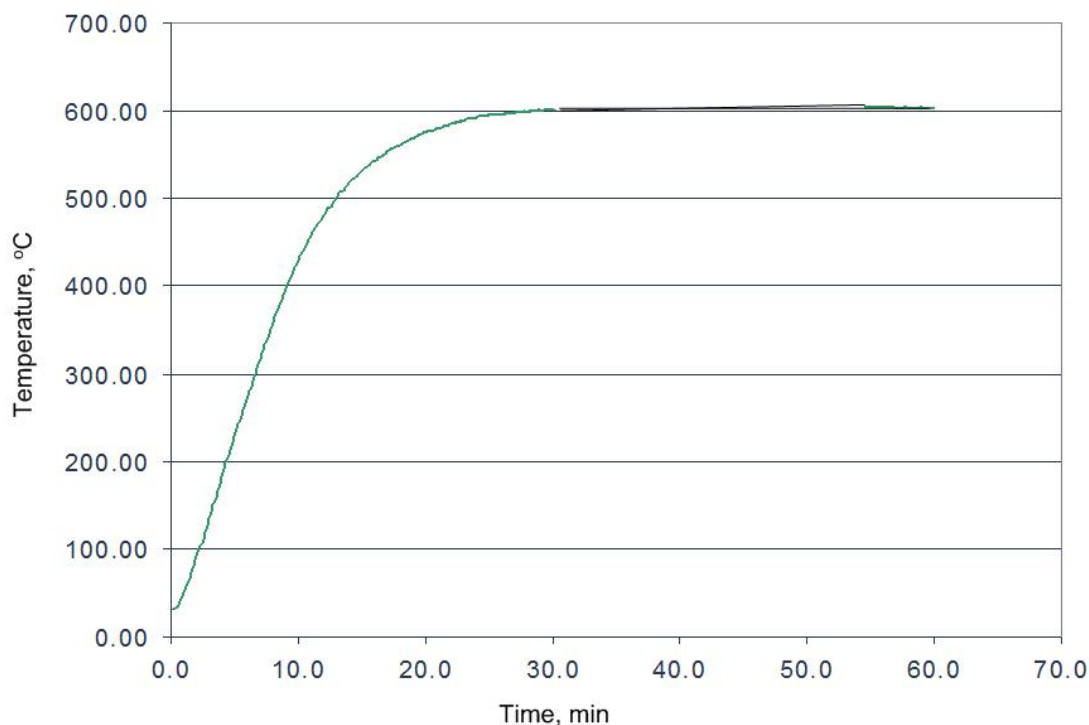


Fig. 30 Temperature profile of the heater

To conduct thermal cracking in an aluminum can, it has to be customized to allow proper collection of the distillate. In the top portion of the can a hole was cut to place a silicone cork. Solid silicone rubber stoppers of size 8 (41-mm top diameter) were purchased from an online retailer. The manufacturer [67] indicated that the working temperature range is from -62 to 232 °C. The stoppers were proven heat resistant since during the test run, which was conducted for 2 hours, the temperature of outcoming light fractions was above 300 °C and no decomposition of silicone rubber was observed. Ordinary rubber stoppers were starting to decompose at significantly lower temperatures. After placing the stoppers in place, the sides were sealed with a high temperature silicone gasket to prevent vapor losses.

To provide better fit of the can to the condenser we placed a glass insert in the cork hole. This was done to ensure that consequent runs were conducted in exactly the

same way for good replication and consistency of results. Glass inserts can be cut from any glassware with female type joint size of 24/40.

The schematic of the can design is presented in Fig. 31:

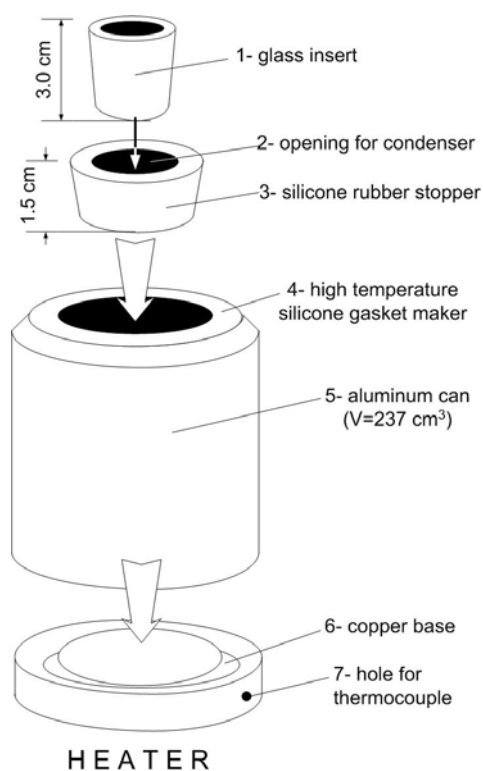


Fig. 31 Aluminum can design

The procedure for the thermal cracking experiment in an aluminum can included the following steps:

- Charge 54 grams of crude oil in the flask, which is approximately 60 ml. The reason for filling the can only $\frac{1}{4}$ of the total can volume is to allow some space for liquid oil to expand and while boiling to prevent oil flowing in the overhead, contaminating the distillate.
- Place can on the heater and attach the condenser.

- Ensure that the computer is taking readings from thermocouple and balance.
- Start the experiment by plugging the heater into the electric socket and note subsequent time as zero.
- Close the sliding door of the irradiation chamber.
- Conduct the experiment for 60 minutes. The duration of the experiment is based on the results of test runs, when 60 minutes were enough to collect a sufficient amount of distillate, obtain substantial absorbed dose and prevent decomposition of the silicone cork.
- After 60 minutes stop taking readings from the balance and thermocouple; this signifies the end of experiment. Note the last recorded mass reading as “Mass of distillate.”
- Unplug the heater and remove all connections.
- Record weight and volume of the distillate. Those are marked as “Final mass of distillate” and “Volume of distillate” respectively.
- Record weight of residual oil and calculate losses from the material balance.
- Prepare experimental setup for another run by cleaning the condenser, checking the temperature of the bath, and cooling the heater to room temperature.

Experimental results and discussion are presented in Chapter IV.

CHAPTER IV

RESULTS AND DISCUSSION

4.1. Viscosities of oil and mixtures before and after irradiation

We irradiated samples with Hamaca heavy oil and measured their viscosity. The apparatus used to measure the viscosity is Brookfield LVDV-III viscometer. The temperature is maintained constant by a fluid circulating from a water bath with automated thermostat. This type of viscometer is generally used when only small sample volumes are available. The rotating viscometer measures fluid parameters of shear stress and viscosity at given shear rates. The viscometer has a cone spindle, which is driven through a calibrated spring. The viscous drag of the fluid against the cone spindle is measured by the spring deflection. Then a rotary transducer measures the spring deflection.

The range of the viscosity (in centipoises) is determined by the rotational speed of the cone spindle, the size and shape of the spindle, the container the cone spindle is rotating in, and the full-scale torque of the calibrated spring. The viscometer utilized in this project was a cone-and-plate spindle CPE-52 (cone angle 3.0°). The CPE-52 spindle is used to measure high viscosities in the range of 4.6–92,130 cP, and appropriate sample volume for it is 0.5 ml.

An appropriate selection will result in measurements made between 10 and 100 on the instrument % torque scale. In other words, to measure high viscosity, choose a slow speed of spindle rotation. If the chosen speed results in a reading above 100%, then the speed should be reduced. The cone spindle must rotate at least five times before a viscosity reading is taken. For example, if the speed is 1 RPM, at least 5 minutes should pass before recording a viscosity. Also, the viscosity reading should be verified that it is within the allowable 1% deviation. In this work, all viscosity measurements are reported with corresponding fluctuation in readings. The methodology and results of viscometer calibration are described in Appendix A.

To analyze changes in oil viscosity, first we needed to determine viscosity of non-irradiated oil. These values were used for comparative analysis of irradiated and non-irradiated sample viscosities. Viscosity measurements were not intended to characterize the rheological behavior, which is complex and beyond the scope of this work. We merely wanted to evaluate irradiation effects on the viscosity of crude oil and its mixtures with solvents.

If more than two viscosity measurements are available, viscosities at any other temperature can be estimated from Walther's correlation [equation (2) in Chapter II] or Arrhenius equation:

$$\log[\log(\mu + c)] = A + B \log T \quad (2)$$

$$\mu = A \exp(B/T) \quad (31)$$

For example, consider the following viscosity measurements of the blend from various heavy oil residues (oil XYZ) Table 7:

Table 7 Viscosity values of XYZ heavy crude oil

Temperature, °C	Shear rate, s ⁻¹	Viscosity, cP (mPa·s)
50	0.20	25,000±15
60	0.60	16,350±11
70	1.00	12,600±10
80	2.00	9,860±7
90	4.00	7,740±3

As we see from Fig. 32 and Fig. 33, calculated values are in very good agreement with measured ones.

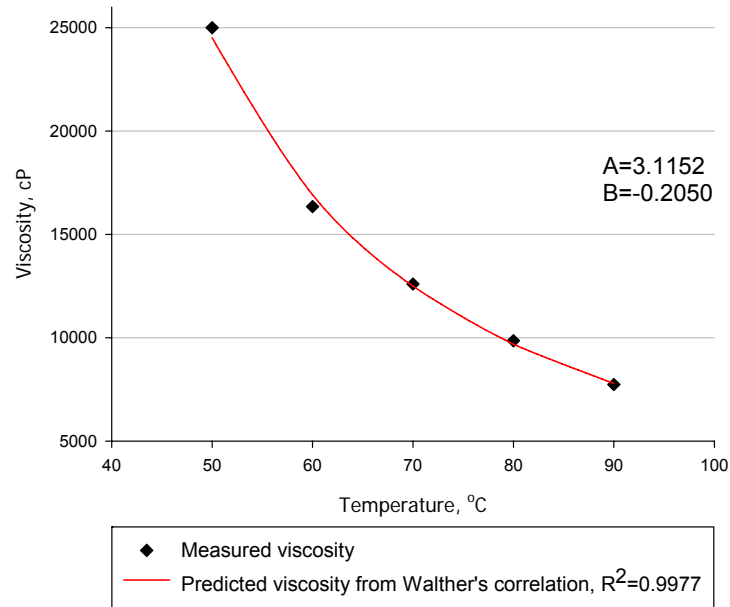


Fig. 32 Predicted and measured viscosities for XYZ oil, Walther's correlation

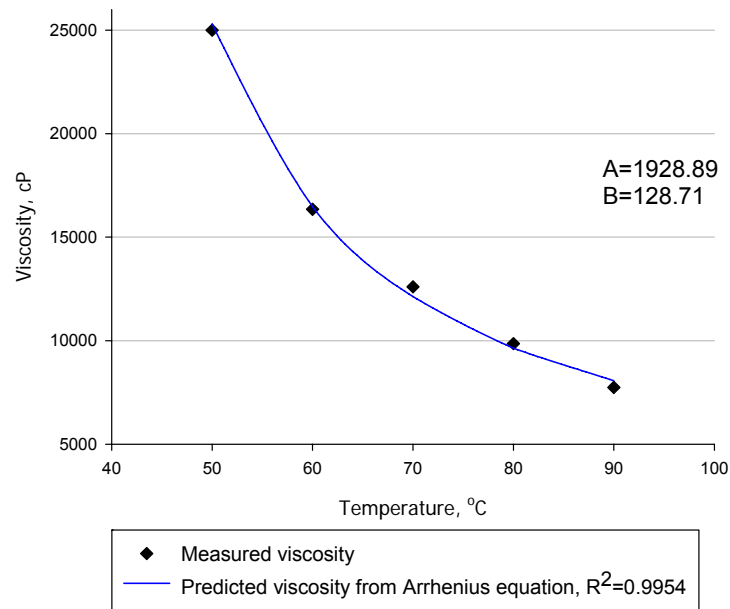


Fig. 33 Predicted and measured viscosities for XYZ oil, Arrhenius equation

Average error for Walther's correlation is $1.7 \pm 0.5\%$ with a median 1.75%. Average error for Arrhenius equation is $2.4 \pm 0.7\%$ with a median 2.24%. In Fig. 34 is shown error distribution for both equations.

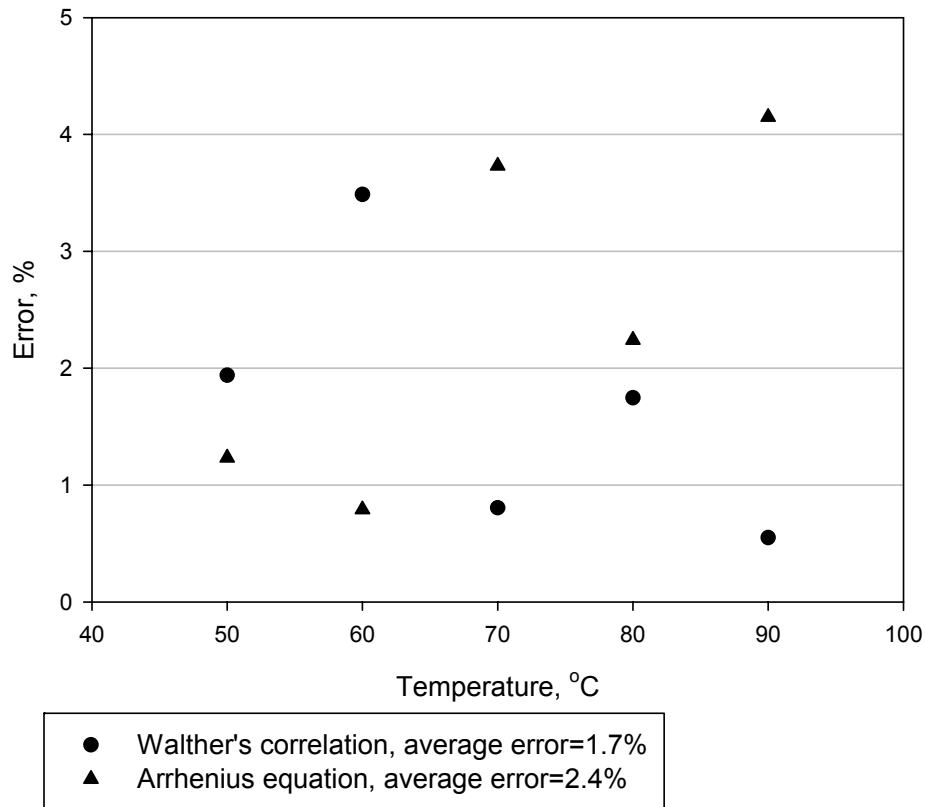


Fig. 34 Error distribution

As we can see, Walther's correlation fits data better than Arrhenius equation. Therefore, Walther's correlation will be used to interpolate and extrapolate viscosity of heavy oil, like Hamaca heavy crude.

Hamaca heavy oil is found to be a Newtonian fluid, Fig. 35.

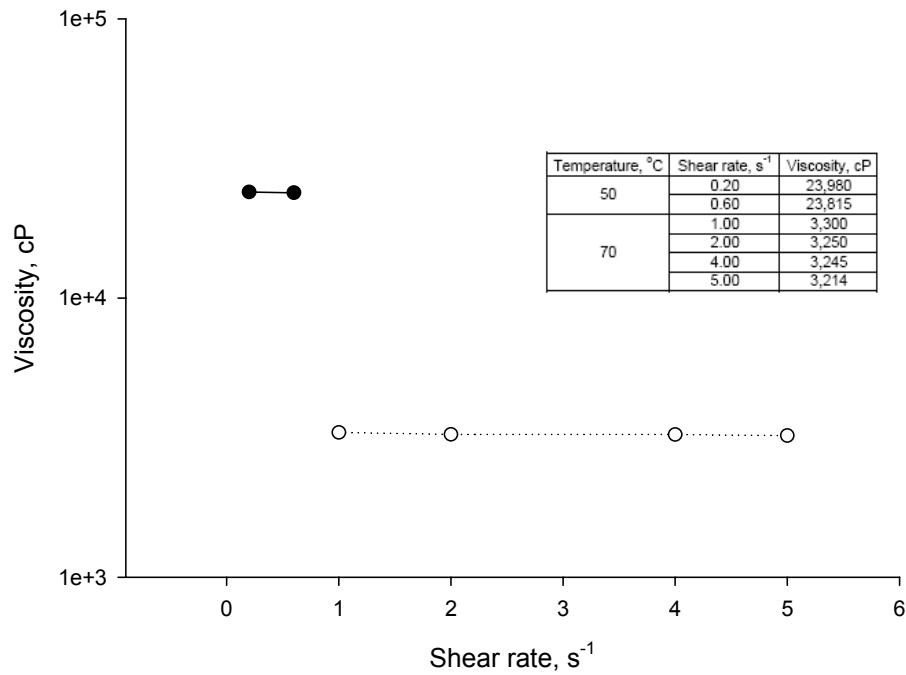


Fig. 35 Shear rate and viscosity dependence of Hamaca heavy oil

As it was discussed earlier, increase in the viscosity is closely correlated with increase in the molecular weight. Molecular weight of crude oil (MW) can be approximated from the viscosity values taken at 100 and 210°F (38 and 100°C) by the Riazi-Daubert correlation [68]:

$$MW = 233.56\gamma_0^{-0.665} v_{100}^{(-1.2435+1.1228\gamma_0)} v_{210}^{(3.4758-3.038\gamma_0)} \quad (32)$$

where γ_0 is a specific gravity at a given temperature and v is a kinematic viscosity in cSt. This equation gives only a rough estimate of average molecular weight, so if someone is interested in relative percentage change in the molecular weight, only two viscosity measurements are needed.

To convert units of dynamic viscosity (cP or g/cm/s) into units of kinematic viscosity (cSt or cm²/s), we need density of the oil at corresponding temperature. The density of liquid crude oil is calculated from Standing's correlation [69], equation (30):

$$\rho = (0.0133 + 1524\rho_{@60^{\circ}F}^{-2.45})[T(^{\circ}F) - 60] - (8.1 \times 10^{-6} - 0.0622 \times 10^{-0.0764\rho_{@60^{\circ}F}})[T(^{\circ}F) - 60]^2 \quad (30)$$

Due to the physical constraints on the viscometer, viscosity of the Hamaca oil could not be measured at 100 and 210°F (38 and 100°C). Therefore, first we estimated viscosity by Walther's correlation from viscosity measurements at available temperatures, in the same way as we estimated viscosity of XYZ oil, and then, viscosity values were extrapolated to 38 and 100°C. Results of viscosity measurements and molecular weight estimates are summarized in Table 8.

Irradiation of oil samples up to 10, 20 and 30 kGy led to the increase in viscosity with absorbed dose. There was a slight increase in the viscosity of the sample irradiated up to 10 kGy (1.3% in average) and the effect of radiation on the viscosity was more pronounced on the samples irradiated to higher doses (20 kGy — 6.3% increase and 30 kGy — 7.7% increase). Relative reduction in the molecular weight of the sample irradiated up to 30 kGy, compared to 20 kGy, can be attributed to the variability in the measured viscosity at higher temperatures. It is doubtful that this happened due to the destruction of the molecular structure by high energy electrons at elevated doses.

Skripchenko et al. [43] indicated that the change in the molecular structure and the increase of the molecular weight of heavy petroleum fractions irradiated by γ -radiation is attributed to the increased role of polycondensation at higher doses. Other researchers [44] discussed γ -radiation treatment of oil bitumen at room temperature and found that experiments with radiolyzed samples showed increase in the asphaltene content, produced by the crosslinking reaction of the resins into the asphaltenes.

Therefore, electron beam irradiation of heavy oil leads to the same result: with increasing dose, viscosity of irradiated oil increases linearly from 0 kGy and 10 kGy, and exponentially after that.

Table 8 Results of the viscosity measurements and molecular weight estimates

Absorbed Dose	Temperature, °C	Shear Rate, s ⁻¹	Measured Viscosity, cP	Predicted Viscosity, cP	Coefficient of Determination, R ²	Relative Error, %	Density, g/cm ³	v, cSt	Estimate of Molecular Weight	Increase in MW, %
Control	38	-	-	231,356	0.9963	-	0.993	233,071	1509	-
	50	0.60	23,815	25,399		6.7	0.986	-		
	70	4.00	3,245	2,879		11.3	0.976	-		
	90	10.00	730	772		5.8	0.965	-		
	100	-	-	476		-	0.960	496		
10 kGy	38	-	-	227,056	0.9964	-	0.993	228,739	1534	1.64
	50	0.60	23,850	25,429		6.6	0.986	-		
	70	4.00	3,288	2,929		10.9	0.976	-		
	90	10.00	748	791		5.8	0.965	-		
	100	-	-	488		-	0.960	508		
20 kGy	38	-	-	231,790	0.9965	-	0.993	233,508	1575	4.35
	50	0.60	24,830	26,352		6.1	0.986	-		
	70	4.00	3,445	3,067		11.0	0.976	-		
	90	10.00	789	832		5.4	0.965	-		
	100	-	-	514		-	0.960	535		
30 kGy	38	-	-	247,021	0.9964	-	0.993	248,852	1558	3.28
	50	0.60	25,600	27,315		6.7	0.986	-		
	70	4.00	3,490	3,105		11.0	0.976	-		
	90	10.00	786	832		5.9	0.965	-		
	100	-	-	512		-	0.960	533		

Next, we measured viscosities of irradiated and control samples after prolonged storage to evaluate whether other transformations have taken place over time. Samples were irradiated up to 10 kGy and after irradiation, irradiated oil was transferred from the polyethylene sample container into the glass vial and was kept tightly closed for 17 days. Viscosities were measured 17 days later and results of control and irradiated sample viscosity measurements are given in Table 9. There is no certain rationale why viscosity was measured 17 days later. We just wanted to evaluate viscosity after some relatively long time. More experimentation is needed to determine how viscosity would change from day to day and whether viscosity increase stops or not. We can see that viscosity of the irradiated oil measured 3 hours after irradiation was not changed significantly compared to the control sample (non-irradiated). On the other hand, viscosity of the irradiated sample measured 17 days later showed significant increase compared to the viscosity of non-irradiated sample, kept at the same conditions for 17 days.

Table 9 Effect of aging in the irradiated oil

Sample	Temperature, °C	Shear Rate, s ⁻¹	Fresh μ , cP	Aged μ , cP	Relative Increase in μ , %
Control	50	0.60	23,815±15	24,340±14	2.20
Irradiated	50	0.60	23,850±15	26,650±11	11.74
Control	70	4.00	3,245±12	3,321±11	2.34
Irradiated	70	4.00	3,288±10	3,816±9	16.06

Effect of aging on the increase in viscosity can be explained by the oxidation of irradiated products. Skripchenko et al. [43] irradiated mixtures of coals with heavy petroleum residues by γ -radiation and after prolonged storage (2 months) asphaltenes content rose and oil content fell. In addition, there was an increase in the intensity of the absorption bands of oxygen-containing groups (C=O, -OH) in its IR spectrum, which signifies increased activity with respect to atmospheric oxygen. Thus, storage of the irradiated petroleum for 17 days lead to processes of condensation and increased susceptibility to atmospheric oxygen.

Highly viscous oil, like Hamaca, contains not only residua from the cracking processes, but also small portions of asphaltenes, and since 1914 various solvents have been added to petroleum to separate asphaltenes [13]. It would be interesting to observe changes in the viscosity of the mixture of Hamaca heavy oil and petroleum distillates used as solvents before and after treatment by electron beam irradiation. For this purpose, 3 different samples were prepared: 2.5, 5 and 10 %wt. of petroleum distillate (PD). As we can see from Table 10, even a small addition of PD decreases viscosity significantly.

Viscosity of oil mixtures has been studied extensively for transportation purposes and enhanced oil recovery methods. Mixing rules can be used to estimate viscosities of mixtures by taking a weighted average of the properties of each component to obtain the property of the mixture.

One general assumption of the mixing rule is that the two mixed components do not interact with each other. The most common mixing rule is a power-law mixing rule, which is:

$$\mu = (x_o \mu_o^n + x_s \mu_s^n)^{1/n} \quad (33)$$

where n is an adjustable exponent that depends upon the components and the proportions in the mixture; x_o and x_s represent a mole fraction of oil and solvent respectively.

The mole fractions of solvent and oil can be found from the following expression

$$x_o = (1 - m_s) \cdot MW_s \cdot \frac{x_s}{m_s \cdot MW_o} \quad \text{and} \quad x_s = 1 - x_o \quad (34)$$

where m_s is a mass fraction of the solvent in the mixture, and MW_o is a molecular weight of Hamaca crude oil, which is equal to 523. Molecular weight of petroleum distillate is estimated to be 186 and viscosity – 0.89 cP at 50 °C. Results of viscosity correlation are presented in Table 10 and Fig. 36.

Table 10 Results of power-law correlation

%wt Solvent	m_o	m_s	x_o	x_s	$\mu_{\text{measured, cP}}$	$\mu_{\text{predicted, cP}}$	Error, %	$\mu_o=23815$ cP $\mu_s=0.89$ cP $MW_o=523$ $MW_s=186$ $n= -0.00337$
100	0	1	0	1	0.89	0.89	0	
10	0.9	0.1	0.762	0.238	2,362	2,037	13.8	
5	0.95	0.05	0.871	0.129	7,720	6,273	18.7	
2.5	0.975	0.025	0.933	0.067	10,340	11,866	14.8	
0	1	0	1	0	23,815	23,815	0	

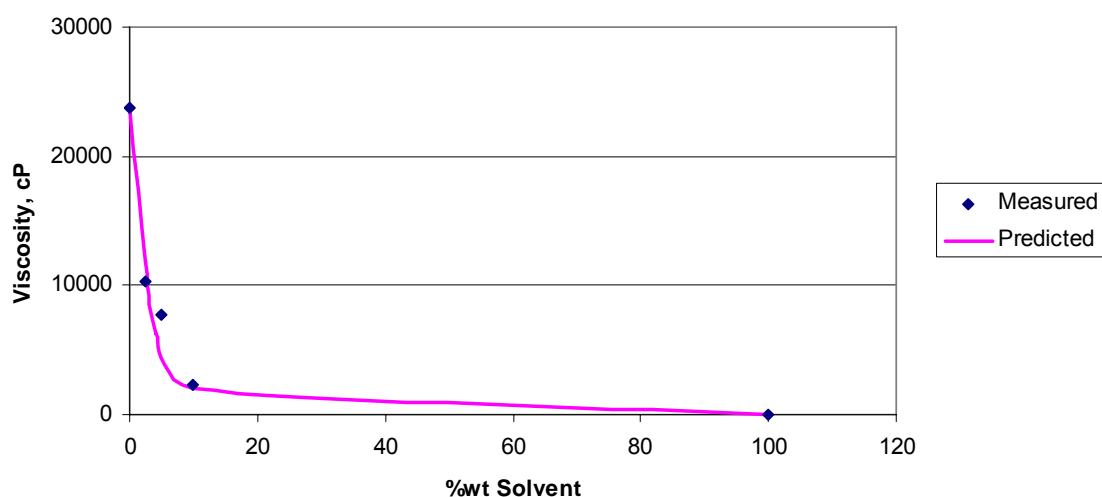


Fig. 36 Results of power-law correlation

We tested another correlation developed by Shu [70] for predicting viscosities of binary mixtures of heavy oil, bitumen and petroleum fractions, with particular emphasis on a heavy-oil/solvent mixture. A power-law mixing rule is generalized by use of the Einstein-type relationship for the viscosities of infinitely dilute solutions. This correlation requires only density and viscosity of the two fluids to predict blending viscosity at any mixture composition. The correlation was tested with heavy oil/solvent mixtures and gives an excellent prediction of the blending viscosities. This correlation is useful for predicting diluent quantities required to reduce oil viscosity for pipeline transportation of heavy oil.

$$\log \mu = \left(\frac{\alpha V_o}{\alpha V_o + V_s} \right) \log \mu_o + \left(1 - \frac{\alpha V_o}{\alpha V_o + V_s} \right) \log \mu_s$$

$$\gamma = 17.04 (\gamma_o - \gamma_s)^{0.5237} \gamma_o^{3.2745} \gamma_s^{1.6316}$$

$$\alpha = \frac{\gamma}{\ln(\mu_o / \mu_s)}$$
(35)

where γ is the specific gravity of hydrocarbon fluid, V is a volume fraction. As we see from Fig. 37 and Table 11, Shu's correlation gave relatively better results.

Table 11 Results of Shu's correlation

%wt Solvent	V_o	V_s	$\mu_{\text{measured, cP}}$	$\mu_{\text{predicted, cP}}$	Error, %	$\mu_o(50^\circ\text{C})=23815 \text{ cP}$ $\mu_s(50^\circ\text{C})=0.89 \text{ cP}$ $\gamma_o=0.986$ $\gamma_s=0.81$ $\alpha=0.455626$ $\gamma=4.644925$
100	0	1	0.89	0.89	0	
10	0.881	0.119	2,362	2,309	2.3	
5	0.940	0.060	7,720	6,788	12.1	
2.5	0.975	0.025	10,340	12,394	19.9	
0	1	0	23,815	23,815	0	

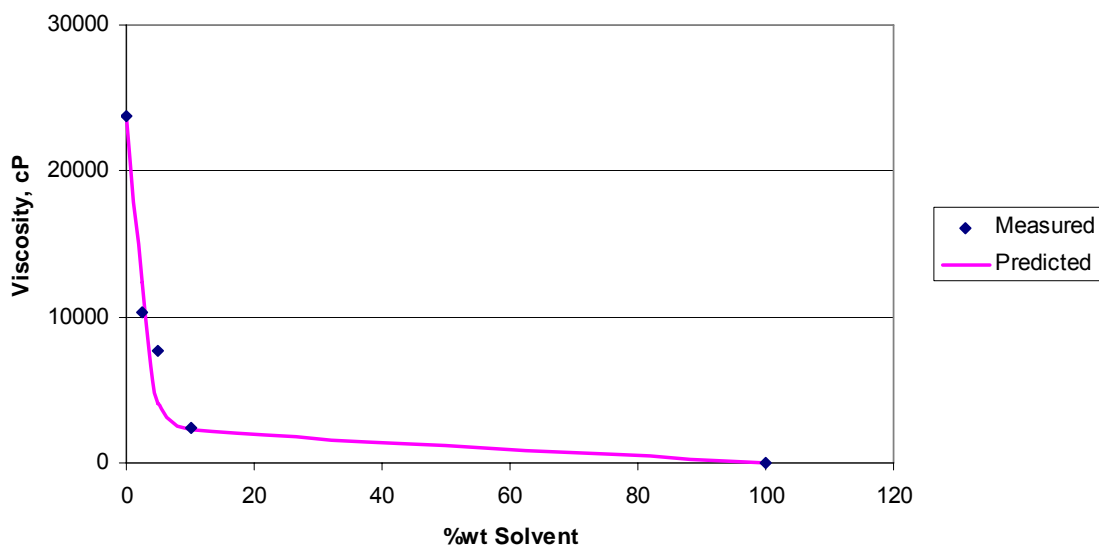


Fig. 37 Results of Shu's correlation

All three samples of petroleum distillate (solvent) and heavy oil were irradiated up to 10 kGy and viscosities were measured at 50°C. Results presented in Table 12 indicate that there is a small increment in viscosities of irradiated mixtures, compared to control ones. Since addition of light petroleum distillates, like naphtha, to reduce viscosity of bitumen is a common practice in bitumen transportation, mixtures should not be exposed to radiation.

Table 12 Viscosity test report for oil and PD samples at 50 °C

Percentage of PD	Shear rate, s ⁻¹	Viscosity of control sample, cP	Viscosity of irradiated sample, cP	Increase %
10wt.% PD	5.00	2,362±12	2,440±11	3.3
5wt.% PD	2.00	7,720±18	8,000±12	3.6
2.5wt.% PD	1.20	10,340±15	11,840±19	14.5

Emulsion consists of a continuous external phase and an encapsulated discontinuous internal phase [71]. If the sample is a mixture of two or more components, a biohomogenizer is used to create the mixture. Stir the mixture while adding the second component for 3 to 4 minutes. Good mixing leads to the formation of normal emulsion, which means that water droplets are distributed evenly in oil.

The time dependent non-Newtonian or thixotropic fluids have a decreasing viscosity under constant shear rate over a period of time. The oil-water emulsion exhibits this kind of behavior because of the emulsion stability. Setiadarma [72] found that a water-in-oil emulsion becomes stable at a constant shear rate over time. Therefore, before viscosity was recorded, we spent sufficient time waiting until viscosity readings were stable, i.e. within the allowable 1% deviation.

Since at higher water weight percentages, oil-water emulsion gets less stable and because the main objective of the experiment was to determine effect of radiation on the viscosity of oil, where small amount of water present. Thus, we prepared two different oil and water mixtures, 5 and 10 wt.%, were investigated for this part of the experiment. A biohomogenizer was used to create the mixtures at 10,000 RPM for 3.5 to 4 minutes. The mixture was created by adding water gradually. The first mixture formed a very stable and viscous emulsion with viscosity around 29,000 cp at 50°C and around 3,600 cp at 70°C. When we added more water to form the second mixture, the viscosity dropped to about 28,000 cp at 50°C and about 3,400 cp at 70°C. As we see from Fig. 38 and Fig. 39, viscosities of mixtures are higher than viscosity of pure oil and decrease with percentage weight of water in the mixture.

Because oil and water are immiscible liquids, their emulsions are not stable and to obtain reliable results they needed to be irradiated within a few hours after preparation. Table 13 presents results of viscosity changes in a 10 wt.% DW mixture irradiated up to 10 kGy and Table 14 presents results of viscosity changes in a 5 wt.% DW mixture irradiated up to 10 kGy.

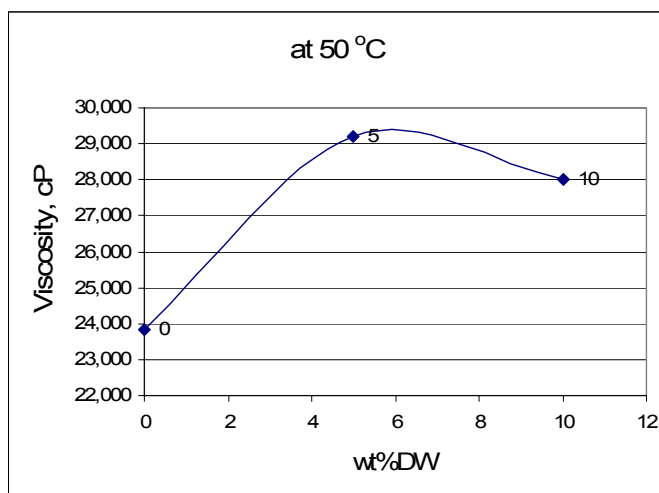


Fig. 38 Changes in viscosity with wt.% DW at 50°C

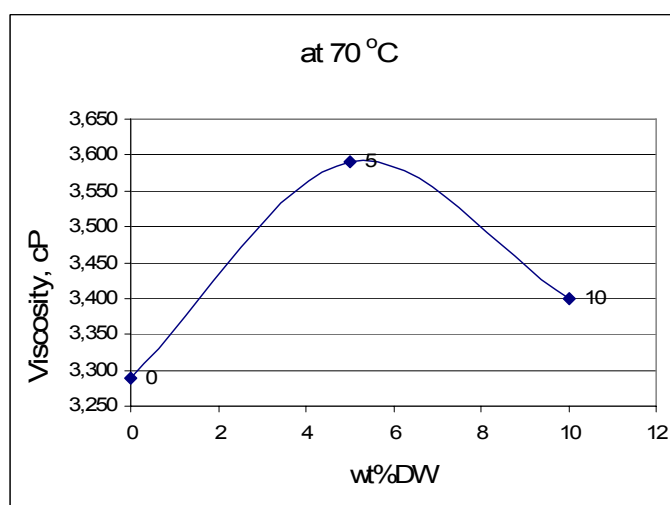


Fig. 39 Changes in viscosity with wt.% DW at 70°C

Table 13 Viscosity of 10wt.% DW sample before and after irradiation up to 10 kGy

Temperature (°C)	Control Sample Viscosity, cP	Irradiated Sample Viscosity, cP	Increase in Viscosity, %
50	28,000±14	32,200±19	15.0
70	3,400±10	3,907±11	14.9
90	842±3	1,160±8	37.8

Table 14 Viscosity of 5wt.% DW sample before and after irradiation up to 10 kGy

Temperature (°C)	Control Sample Viscosity, cP	Irradiated Sample Viscosity, cP	Increase in Viscosity, %
50	29,200±10	33,300±12	14.0
70	3,590±11	3,980±7	10.9
90	790±5	890±5	12.7

As we can see from Table 13 and Table 14, viscosity increased by 13% for a sample with 5 wt.% DW in average. There was considerably high increase in the viscosity of the sample with 10 wt.% DW measured at 90°C, which signifies instability of oil-water emulsions at high temperatures. Neglecting this value, viscosity increased by 10% for a sample with 10 wt.% DW in average. Therefore, viscosity increase of irradiated sample is independent of water content.

The main idea of water addition was due to the report of considerable rise in the yields of liquid radiation-thermal cracking products, when 5-6 wt.% of water was added to the feedstock [39]. Since thermal treatment was not considered for this part of the irradiation experiment, we wanted to see effects of water addition on the viscosities of the mixture after irradiation. It was expected that as a result of radiation-induced oxidation-reduction reactions at ambient conditions, such compounds as peroxides and hydroxides would be hydrogen donors and viscosity would drop with the reduction in average molecular weight of hydrocarbon chains. As we see, this did not happen, mainly because the thermal component was absent in the activation energy and if any hydrogen was produced from radiolysis of water molecules in crude oil, it was not consumed by hydrocarbon molecules.

4.2. Yields from RTC experiment

According to the literature, radiation, coupled with thermal cracking during oil processing at T=400°C, by 4 MeV energy electrons with dose rate of 1 kGy/s gives increases in gasoline yields almost three times higher than after conventional thermal

contact cracking [2, 39]. More recent works in this field also provide the advantages of using radiation to increase the yields of lighter fractions [3, 43-49].

The purpose of this part of the research was to compare yields obtained from conventional thermal cracking and yields from thermal cracking under the electron beam. Experiments were conducted on the Van de Graaff (VDG) accelerator facility of the Biological and Agricultural Department of Texas A&M University. Estimated dose rate of VDG was low, around 0.0018 kGy/s, compared to the above-mentioned dose rate of 1 kGy/s. To compare yields from TC and RTC, the experiment should be conducted at identical conditions: same experimental setup (identical flasks, heat source, crude oil), same ambient conditions (ambient temperature and pressure) and at the same site.

4.2.1 Dose measurement

Since theoretical dose calculations show higher absorbed doses than those measured experimentally, we conducted a series of experiments to simulate RTC in can and measure actual absorbed dose. An empty aluminum can was positioned at the same height and distance from the exit beam window of the VDG as if we were conducting RTC. We placed a Farmer ion chamber in it to measure exposure in air in kR (kilo roentgen) and knowing that 1 kR is proportional to 8.76×10^{-3} kGy [26], we measured absorbed dose in kGy. The distance from the beam exit window to the aluminum can was 12 cm. A dosimeter was placed to the longitudinal cylindrical side facing the electron beam, so that the beam would hit directly on the outer cylindrical surface of the aluminum can, Fig. 40. Three sets of measurements were done to assess uncertainty of the results, and each set of measurements was done until the Farmer ion chamber showed a reading of 5 kR. Table 15 gives the measurements and average absorbed dose.

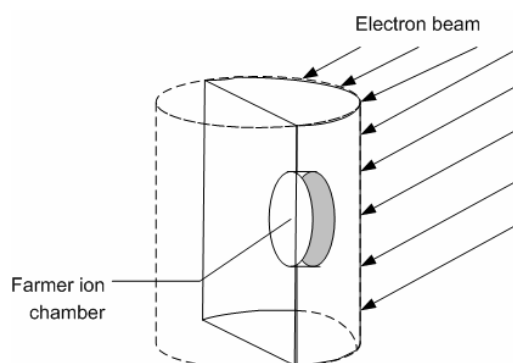


Fig. 40 Simulation of radiation thermal cracking in the can

Table 15 Results of experimental calculation of the absorbed dose

Trial	Transmission count	Farmer ion chamber, kR	Dose, Gy	Counts/Gy
A	9237	5.01	43.70	211.44
B	9516	5.04	43.95	216.53
C	9469	5.06	44.12	214.60
Average				214.19

We already mentioned in Chapter III calculation of the optimum thickness of the sample for uniform irradiation by MCNP (Monte Carlo N-Particle Transport Code) program [58]. There we assumed the entrance dose (dose at the surface of the sample) to be 1 kGy. The result of the simulation was a 2-D dose distribution within the sample, and knowing the entrance dose we could scale it up to any dose we needed [62]. The average dose for simulation of radiation-thermal cracking experiments in the aluminum can was calculated in a similar way. In this case, 3-D simulation was done, and from the 1 kGy entrance dose, 0.769 kGy of average absorbed dose throughout volume of the crude oil in the can was calculated [58]. The 1 kGy of entrance dose corresponds to 214228 counts from the transmission ion chamber. An extrapolation of the number of counts obtained from transmission ion chamber with the number of counts for the RTC experiment gives the entrance absorbed dose (dose at the longitudinal side of crude oil facing electron beam) and the average dose. Results of dose calculations are shown in Table 16:

Table 16 RTC simulation results

RTC	Transmission ion chamber counts	Entrance dose, kGy	Average dose, kGy
1	214,228	1	0.769
2	500,000	2.334	1.795
3	563,506	2.631	2

As it was expected, theoretical calculations showed higher absorbed doses than simulated ones: 7.79 kGy versus 2 kGy. This can be explained by the specifics of VDG operation. At the time the machine started, the kinetic energy of electrons was significantly below 1.35 MeV and only after 5-10 minutes did it start to work at its peak capacity. In addition, VDG rarely operates at full capacity of electron generation because of the excess bremsstrahlung (X-ray) production. Once the X-ray indicator signals, the machine is shut down and the procedure starts over again. Fluence of electrons starts from zero again and rises with increasing cathode temperature, until it reaches its peak and operates safely. Thus, peak capacity is limited by X-ray production.

4.2.2 *Material balance of radiation-thermal cracking in aluminum can*

The next set of experiments was done in 237-ml-volume modified aluminum cans. The top of the can was removed and a silicone rubber stopper with an opening for the condenser was placed instead. The design of the can and procedure are described in Chapter III.

As it is defined in Chapter III, “final mass of distillate” is the mass of distillate measured some time after stopping the experiment and term “mass of distillate” stands for the mass recorded by computer at the end of the experiment, i.e. 60 min after start.

Material balance on the initial amount of crude oil, final mass of distillate and mass of residue shows that there is an average 5 gram of losses, which corresponds to 10% of initial mass of crude oil. Losses are associated with distillate trapped in the condenser and some evaporation from hot residue. This is the reason why after each run the condenser has to be cleaned and dried, so each experiment starts at the same conditions as the previous one to ensure repeatability of results. Both TC and RTC are

conducted at the closed sliding door of the irradiation chamber to avoid variability in convection during the experiment.

There was in average 35 wt.% increase in yields of radiation-thermal cracking, compared to conventional thermal cracking, as indicated in Table 17.

Table 17 Results of experiment

Experiment	Mass of distillate, gm	Final mass of distillate, gm	Mass of residue, gm	Volume of distillate, ml	Number of counts	Estimated absorbed dose, kGy
TC-1	8.4	8.7	40.74	10.7	-	-
TC-2	7.5	8.05	41.66	10.3	-	-
TC-3	6.9	7.28	43.32	9.3	-	-
RTC-1	10.5	12.82	36.87	16	1,793,684	6.44
RTC-2	9.5	10.43	42.33	13.2	1,653,000	5.93
RTC-3	10.7	12.93	36.32	16.2	1,782,352	6.4
Avg. mass of distillate for TC= 7.6 gm		Density of crude oil=0.9 gm/cm ³ Voume. of input crude oil=60 ml Mass of input crude oil=54 gm Time of experiment=60 min Time of irradiation=60 min				
Standard deviation= 0.755 gm						
Avg. mass of distillate for RTC= 10.23 gm						
Standard deviation= 0.643 gm						
Increase in yield= 35%						

Temperature profiles of TC and RTC are similar. Outcoming fumes during RTC stabilized at around 345°C, whereas during TC, stabilized at around 335°C. The general observation is that at higher temperatures of outcoming fumes we are getting higher yields of distillate. Increase in temperature can not be attributed to heater instability. Heater output is stable and the temperature of the base stabilized at around 600°C for both TC and RTC. From irradiation experiments of heavy Hamaca crude at ambient conditions, we know that the temperature of the irradiated material is not increasing due to the radiation. Therefore, increase in the temperature of the process by 10°C can be explained by recalling effects of low dose radiation, which is not heating, but steadily providing a source of free radicals in the irradiated media, increasing kinetics of the radical propagation step of the thermal process. Also, it is well-known that increase of the temperature by 10°C leads to an increase in the reaction velocity of 2-4 times [12], so

the opposite also should be true. Thus, the thermal cracking reaction proceeds faster under the beam, and more distillate is accumulated in a shorter amount of time.

It is likely that yield of light fractions would increase with absorbed dose, Fig. 41. Since VDG produces low dose rate electron beam, higher absorbed dose can be obtained only if time of irradiation increased. In our case we set duration of the experiment to 1 hour. Further increase in time tends to result in silicone cork decomposition, leading to leak and loss of light fractions. Therefore, further experimentation is needed to determine yield dependence on absorbed dose with accelerator capable to produce higher dose rates. Overall, the yields and compositions of RTC products must be complex functions of the radiation parameters, such as radiation source, dose rate and dose. This complexity is increased further if one varies temperature and pressure of the process. Topchiev et al. [1], in his experiments with gasoline, believed that the dose rate is connected with the yield by non-linear relation and therefore, the dose rate, not the absorbed dose, is a fundamental parameter of RTC. By varying the dose rate it would be possible to change the radiation-chemical yield from practically zero to very high values.

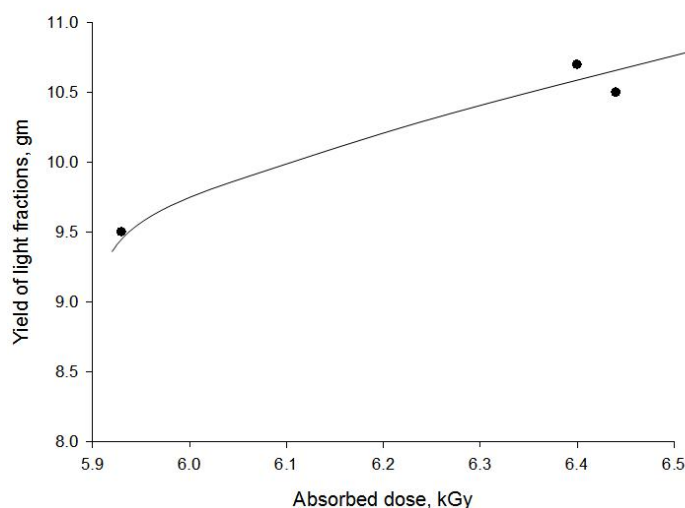


Fig. 41 Dose-yield relation

Distillates of RTC should have more unsaturated hydrocarbons (olefins) of higher molecular weight than TC. From GC analysis we observed that there is no significant difference in the physical properties, composition, concentration of isoparaffins and naphthenes of RTC and TC products. The residue of RTC and TC products display a similar pattern. Therefore, increase in the yield of RTC products can be attributed only to the increased chemical kinetics, when the rate of the free radical chain reaction increases due to the higher concentration of free radicals, i.e. in a shorter time interval, RTC is producing more product. Gas chromatography results are available in Appendix D.

Fig. 42 through Fig. 47 shows the results of thermal and radiation-thermal cracking experimental runs (TC-1 through TC-3, and RTC-1 through RTC-3). From Fig. 46 it is clear that the distillate production decreased in the 20th minute of the RTC-2. That is due to the X-ray production and subsequent VDG shut down. When the machine started again, there was time lag during which the dose rate was extremely low. This shutdown affected the final mass and the absorbed dose, which happened to be the lowest among the three. At low dose rates (10^{-2} kGy/s), free radical chain reaction kinetics vary directly with the square root of the dose rate, i.e. an increase in the dose rate of 100 times increases the rate of conversion 10 times. Thus, it is evident that radiation directly affects the whole process of radiation-thermal cracking.

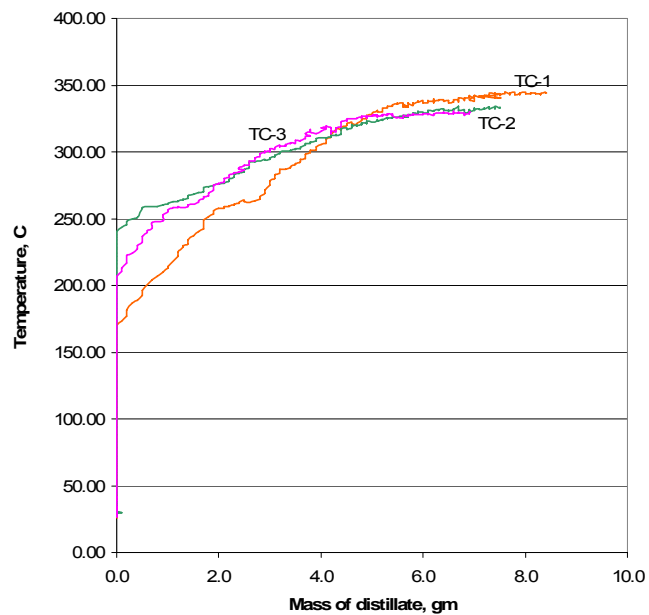


Fig. 42 Overlapped graphs of mass of distillate vs temperature profile for thermal cracking

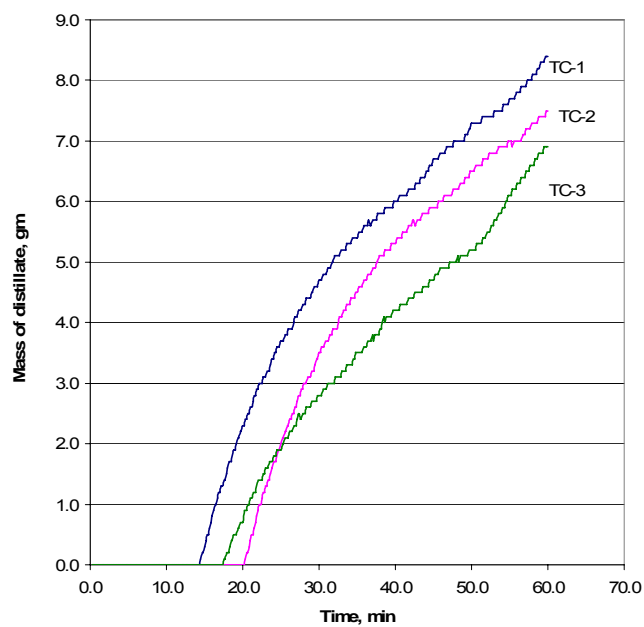


Fig. 43 Overlapped graphs of time vs mass of distillate for thermal cracking

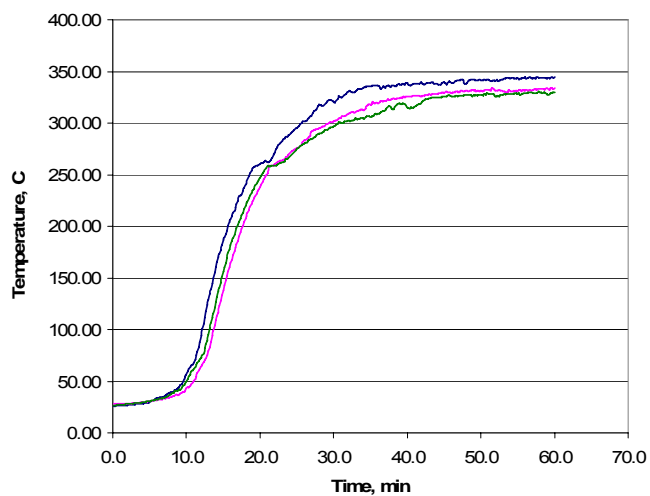


Fig. 44 Overlapped graphs of time vs temperature of outgoing fumes for thermal cracking

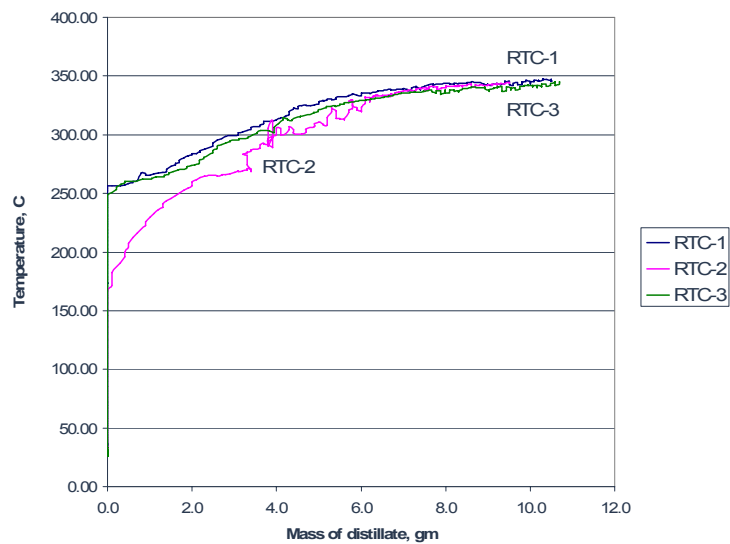


Fig. 45 Overlapped graphs of mass of distillate vs temperature of outgoing fumes for radiation-thermal cracking

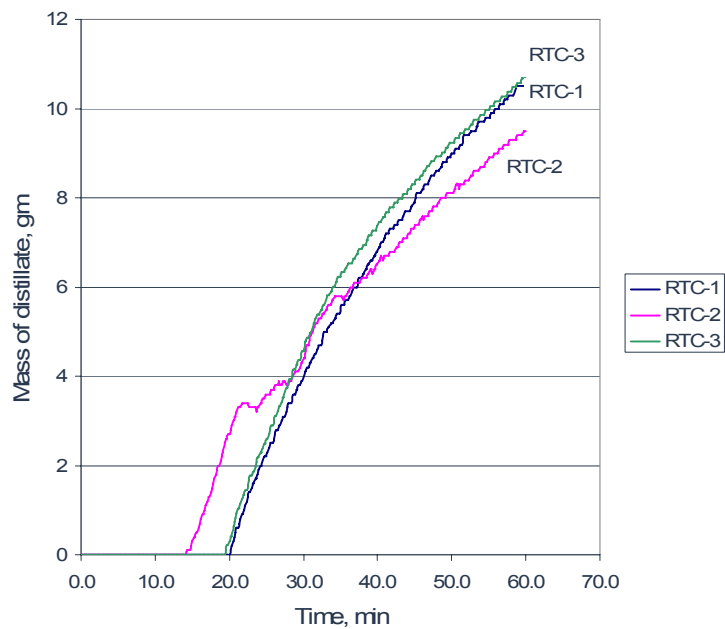


Fig. 46 Overlapped graphs of time vs mass of distillate for radiation-thermal cracking

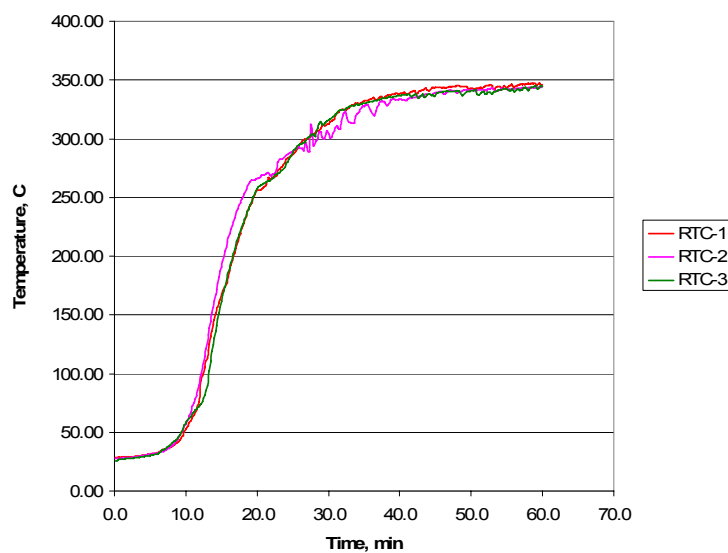


Fig. 47 Overlapped graphs of time vs temperature of outcoming fumes for radiation-thermal cracking

CHAPTER V

ECONOMIC ANALYSIS OF RADIATION THERMAL PROCESS

Companies always decide to proceed with a new technology based on the economics, unless legislation becomes overriding, e.g. zero emissions/waste would favor alternative process. The case with radiation-thermal cracking is exceptional in its own way. Implementation of radiation coupled with thermal cracking allows reducing fuel consumption, which will reduce emissions to the atmosphere, and produce ecologically sound motor fuels due to the reduction in sulfur and heavy metals concentration according to literature claims. In addition, increased octane and cetane numbers of motor fuel allow selling the product for a higher price.

This economic analysis is based on the patented pilot plant of the radiation thermal cracking process designed by Zaykin's group [5]. The pilot plant has a capacity to process 20,000 bbl/day of an 18°API gravity feedstock. The source of high energy electrons is an ELU-4 electron accelerator, which is able to produce 4 MeV electrons with a beam power up to 200 kW. The operating volume of the irradiation chamber (reactor) is 400 cm³ with a residence time of 1.087×10^{-2} s and an optimal absorbed dose of 1 kGy. For the economic analysis, we used cost data of a Rhodotron-type resonant cavity accelerator with a maximum power rating of 200 kW [73]. High energy electrons are produced by repeatedly passing electrons through a coaxial resonant cavity to increase their energy. Electrons gain 1 MeV in each pass, and they make 4 passes to accumulate 4 MeV. The overall power efficiency is usually less than 50% because power is lost by heating the cavity. We selected a conservative 40% efficiency, i.e. for the accelerator to produce 200 kW beam power, it consumes 500 kW. Total capital cost for installing the Rhodotron adjusted to inflation by the consumer price index of 115.83% [74] is given in Table 18 [32, 75].

Table 18 Baseline capital cost for a high-power accelerator facility

	\$MM (1998)	Adjusted to Inflation, \$MM (2006)
High Power Accelerator	3.500	4.054
Accessories	1.218	1.411
Shielding and Support Systems	2.783	3.224
Total Cost	7.500	8.689

The shielding designed for 5 MeV electron energy and a 200-kW power beam accelerator requires a 233-cm-thick concrete wall in the sideward direction and 326 cm in the forward direction. To decrease cost of the facility, the accelerator should be placed underground, where earth is the primary shielding material. In addition, doing so eliminates restrictions on the floor plan. Moreover, it allows the introduction of the accelerator to an existing thermal cracking unit with minimal modifications.

The design of the pilot plant is described in the patent [5]. After considering the details, we chose a layout similar to the modified visbreaking process, Fig. 48.

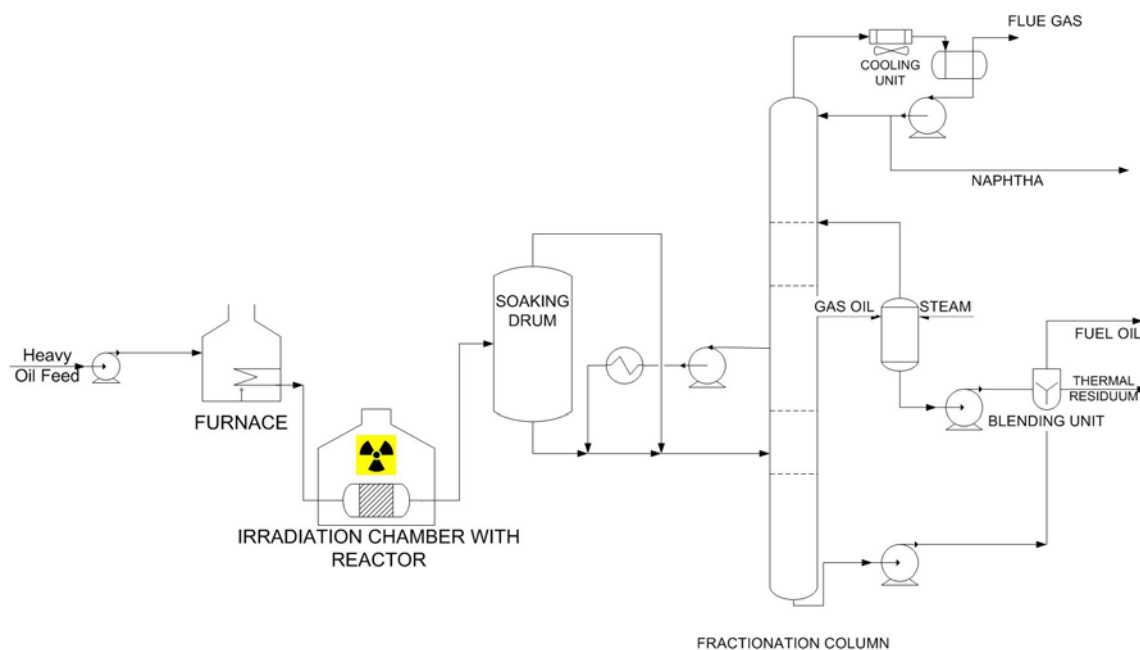


Fig. 48 Combined VB and RTC unit

Visbreaking is a mild thermal cracking process that takes place at a temperature of 450 to 520°C and yields naphtha, gas oil and small amounts of gas and thermal tar. Gas oil is blended with a soluble part of thermal tar to produce fuel oil. Residuum is either sent to the coking unit or disposed.

Two versions are practiced: the furnace process and the soaker process. In the soaker version, a soaker is placed between a furnace and a fractionator, which allows additional time for a reaction to proceed at lower temperatures than in a furnace process, resulting in reduced fuel consumption. Most of thermal cracking reaction takes place in the soaker drum. If the preheated feedstock is irradiated prior to the soaker, this will significantly increase concentration of free radicals, thus increasing reaction kinetics and decreasing residence time in the soaker.

The soaker visbreaker requires shutdown of the unit once a year for a period of 10 days to decoke the heater and the soaker drum. Therefore, the plant will be operational only 355 days per year. The total annual value of products is based on this number.

Maples [76] estimated that a 25,000 bbl/day processing capacity visbreaking plant costs \$24 million (price as of January 1991). To estimate the cost of another facility which has a similar process plant configuration, we can use the capacity ratio method with exponent. The total capital investment of the new facility *B*, with a processing capacity of 20,000 bbl/day, is equal to the total capital investment of the existing facility *A*, with a processing capacity of 25,000 bbl/day, multiplied by the ratio of the capacity of the new facility and the capacity of the existing one, raised to a power *n*:

$$\begin{aligned} \text{Capital Investment B} &= \text{Capital Investment A} \left[\frac{\text{Capacity B}}{\text{Capacity A}} \right]^n \\ &= \$24MM \cdot \left[\frac{20,000 \text{ bbl/day}}{25,000 \text{ bbl/day}} \right]^{0.7} = \$20.53MM \end{aligned} \quad (36)$$

This power is equal to 0.7 for the thermal cracking process [77]. Total capital investment (TCI), adjusted to inflation by a producer price index⁵ of 117.7% [78] results in \$24.164 million. Average operating requirements are presented in Table 19 [76]:

Table 19 Visbreaker annual operating requirements and cost

Utility	Utility requirement per barrel of crude oil	Annual utility requirement	Cost of utility units	Total annual cost of utilities, million \$/y
Fuel	0.08 MMBtu/bbl	584000	\$1.87/MMbtu	1.092
Electric Power	0.5 kWh/bbl	3650000	\$0.058/kWh	0.211
Steam	0.05x1000 lbs/bbl	365000	\$2.59/1000 lbs	0.945
Cooling Water	Essentially zero, maximum air cooling	-	-	-
TOTAL = 2.248 million \$/y				

Costs of utilities change upon the installation and utilization of an electron accelerator, Table 20. Since the RTC process consumes less energy than traditional thermal processing methods [38], a reduction of annual fuel consumption by 10% can be achieved.

⁵ The producer price index measures changes in the wholesale prices of finished goods.

Table 20 RTC annual operating requirements and cost

Utility	Utility requirement per barrel of processed crude oil	Annual utility requirement	Cost of utility units	Total annual cost of utilities, million \$/y
Fuel	0.08 MMBtu/bbl	525600	\$1.87/MMbtu	0.983
Electric Power	1.1 kWh/bbl	7910000	\$0.058/kWh	0.457
Steam	0.05x1000 lbs/bbl	365000	\$2.59/1000 lbs	0.945
Cooling Water	Essentially zero, maximum air cooling	-	-	-
TOTAL = 2.385 million \$/y				

The plant processing 20,000 bbl/day of heavy crude oil is capable of producing 1,200 bbl/day of 40 API gravity N&A (naphthenic and aromatic) naphtha and 18,800 bbl/day of fuel oil. Material balance is completed by a 360 bbl/day of residuum thermal tar, which is deposited in the soaker drum and furnace, and the rest, insoluble in gas oil, is sent to the coking unit.

Table 21 presents January-May 2006 averaged prices for 18°API gravity heavy crude oil and heavy fuel oil from EIA's (Energy Information Administration) website [79]. The price of a 40°API gravity N&A naphtha in the US Gulf Coast region is an averaged price of the period from January through April 2006 from the world's largest information provider for the chemical and oil industry, ICIS [80].

Table 21 Current prices of crude oil and petroleum products

Name of Material	Price, \$/bbl
Heavy Crude Oil (20 API or less)	51.56
40 N&A Naphtha from VB process	70.88
40 N&A Naphtha from RTC process	70.98
High Sulfur Fuel Oil from VB process	57.53
Low Sulfur Fuel Oil from RTC process	60.27

Addition of an electron accelerator increases the number of visbreaking process operators per shift from 3 (minimum number of operators required for continuous process) to 4 operators per shift, which results in the increase of the annual operating labor cost [32]. The annual cost of raw material, labor and product revenues for VB is summarized in Table 22.

Table 22 Annual cost of raw material, labor and value for products for VB

Products			
Name of Material	Price, \$/bbl	Annual Amount, million bbl/y	Annual value of product, million \$/y
40 N&A naphtha	70.88	0.426	30.19
High sulfur fuel oil	57.53	6.674	383.96
Total annual value of products (TAVP) =			414.15
Raw Materials			
Name of Material	Price, \$/bbl	Annual Amount, million bbl/y	Annual raw materials cost, million \$/y
Heavy crude oil	51.56	7.1	366.08
Total annual cost of raw materials =			366.08
Operating Labor			
Number of operators per shift	Shifts per day	Operator rate, \$/hr	Annual operating labor cost, million \$/y
3	3	33.67	0.885
Total annual cost of operating labor =			0.885

Zaykin et al. [81] claims that utilization of electron beam irradiation to the thermal process increases the yields of light fractions by 30 wt.% and we observed the same increase (35 wt.%). Such increase in the yields of light fractions are also observed in our experiments. In our case, the low dose rate and the low beam power accelerator are used to process heavy oil, which reduces capital cost of the accelerator facility, since lower thickness shielding would be required.

An increase in the naphtha yield by 30% weight approximately corresponds to 30% increase by volume; thus the production of naphtha increases from 1200 bbl/day to 1560 bbl/day.

Another claim relates to a significant reduction in the sulfur concentration. In test runs 80% mercaptans conversion was reached, resulting in more than 90% of the total sulfur concentrating in the heavy residuum fractions. Therefore, as a result of radiation-induced conversion, sulfur presents in light fractions mainly in the forms of high-molecular oxidized compounds (sulfones, sulfoxides, sulfonic acids) that can be easily extracted by well-known, inexpensive methods using appropriate solvents (water solutions of sulfuric acid, acetone, ethylene glycol, methyl alcohol). Sulfur concentration in fuel oil is decreased from 3.4 wt.% to 1.6 wt.%, thus increasing its retail price from \$57.53/bbl to \$60.27/bbl [79]. A deep destructive processing of crude oil with initial sulfur concentrations up to 4 mass% by radiation-thermal methods provides liquid RTC products with sulfur concentrations 2–4 times lower than sulfur content in the corresponding product of conventional thermal cracking. The heavier the residuum is the higher the sulfur concentration in the residuum. Therefore, total concentration of sulfur in fuel oil is reduced and most of the sulfur is concentrated in the residuum.

Since N&A naphtha is used as an additive to gasoline from an atmospheric distillation unit to increase its octane number, the resale price of the naphtha is also increased by 10¢ [80], as the octane number of RTC-produced naphtha is increased. The absolute rates of hydrocarbon isomerization during the conventional visbreaking are very low, and isomer concentrations in a hydrocarbon mix usually do not exceed $1\pm 2\%$ after processing. Isomerization rates and isomer yields after radiation-induced cracking are much higher, which is demonstrated by increase in the isobutane yield of 1.4 wt%, i.e. 200 times higher than that in the case of thermal cracking. Cost changes are reflected in Table 23.

Table 23 Annual cost of raw material, labor and value for products of RTC

Products			
Name of Material	Price, \$/bbl	Annual Amount, million bbl/y	Annual value of product, million \$/y
40 N&A naphtha	70.98	0.554	39.31
High sulfur fuel oil	60.27	6.546	394.54
Total annual value of products (TAVP) =			433.85
Raw Materials			
Name of Material	Price, \$/bbl	Annual Amount, million bbl/y	Annual raw materials cost, million \$/y
Heavy crude oil	51.56	7.1	366.08
Total annual cost of raw materials =			366.08
Operating Labor			
Number of operators per shift	Shifts per day	Operator rate, \$/hr	Annual operating labor cost, million \$/y
4	3	33.67	1.18
Total annual cost of operating labor =			1.18

All other expenses related to visbreaking and RTC processes are summarized in Table 24 and Table 25. Major component of an economic analysis is the total of all costs of operating the plant, selling the products, recovering the capital investment, and contributing to corporate functions such as management and research and development. These costs usually are combined under the general heading of *total product cost* (TPC). TPC, in turn, is divided in two categories: total cost of manufacturing (sum of variable cost, fixed charges, and plant overhead) and general expenses (administrative costs, expenses related to the distribution and marketing of the product, research and development costs). Rest of definitions used in the first column of tables are available at [77], (pages 262-271).

Table 24 Annual total product cost at 100% capacity for VB

Fixed Capital Investment, FCI	20.539	million \$		
Item	Factor	Basis	Basis cost, million \$/y	Cost, million \$/y
Variable Cost				
Raw materials				366.08
Utilities				2.248
Operating labor				0.885
Operating supervision	0.1	of operating labor	0.885	0.088
Maintenance and repairs	0.06	of FCI	20.54	1.232
Total cost of labor, supervision and maintenance =				2.206
Operating supplies	0.1	of maintenance & repair	1.232	0.123
Laboratory charges	0.1	of operating labor	0.885	0.088
Royalties (not on lump-sum basis)	0.01	of TPC	401.456	4.015
Catalysts and solvents	0	--		0.00
Fixed Charges				
Taxes (property)	0.02	of FCI	20.54	0.411
Insurance	0.005	of FCI	20.54	0.103
Amortization	0.03	of FCI	20.54	0.616
Plant Overhead				
Plant overhead, general	0.5	of labor, supervision and maintenance	2.206	1.103
Total cost of manufacturing =				376.927
General Expenses				
Administration	0.2	of labor, supervision and maintenance	2.206	0.441
Distribution & selling	0.02	of TPC	401.456	8.029
Research & Development	0.04	of TPC	401.456	16.058
TOTAL PRODUCT COST (TPC) =				401.456
INCOME TAXES (35%) =				2.107
Annual Net Profit (ANP) =				3.913
Total Capital Investment (TCI) =				24.164
RETURN ON INVESTMENT (ROI), % =				16

Table 25 Annual total product cost at 100% capacity for RTC

Fixed Capital Investment, FCI	29.228	million \$		
Item	Factor	Basis	Basis cost, million \$/y	Cost, million \$/y
Variable Cost				
Raw materials				366.08
Utilities				2.385
Operating labor				1.18
Operating supervision	0.1	of operating labor	1.18	0.12
Maintenance and repairs	0.057	of FCI	29.23	1.67
Total cost of labor, supervision and maintenance =				2.96
Operating supplies	0.1	of maintenance & repair	1.67	0.17
Laboratory charges	0.1	of operating labor	1.18	0.12
Royalties (not on lump-sum basis)	0.01	of TPC	403.65	4.04
Catalysts and solvents	0	--		0.00
Fixed Charges				
Taxes (property)	0.02	of FCI	29.23	0.58
Insurance	0.005	of FCI	29.23	0.15
Amortization	0.03	of FCI	29.23	0.88
Plant Overhead				
Plant overhead, general	0.5	of labor, supervision and maintenance	2.96	1.48
Total cost of manufacturing =				378.84
General Expenses				
Administration	0.2	of labor, supervision and maintenance	2.96	0.59
Distribution & selling	0.02	of TPC	403.65	8.07
Research & Development	0.04	of TPC	403.65	16.15
TOTAL PRODUCT COST (TPC) =				403.65
INCOME TAXES (35%) =				10.592
Annual Net Profit (ANP) =				19.672
Total Capital Investment (TCI) =				32.853
RETURN ON INVESTMENT (ROI), % =				60

The calculation of profitability is performed by a *rate of return on investment* (ROI) method that does not consider time value of money. This profitability measure is defined as the ratio of *annual net profit* to *total capital investment*:

$$\text{ROI} = \frac{\text{Annual Net Profit}}{\text{Total Capital Investment}} = \frac{\text{ANP}}{\text{TCI}} \quad (37)$$

Annual Net Profit (ANP) is a difference between Total Annual Value of Products (TAVP), calculated in Table 22 and Table 23, and Total Annual Expenses (TAE). Total Annual Expenses is a sum of Total Product Cost (TPC), calculated in Table 24 and Table 25, and Income Taxes (IT), which is based on a tax rate of 35%. It is common in evaluations to use a fixed income tax rate, such as the 35% noted above [77].

$$\text{ANP} = \text{TAVP} - \text{TAE} = \text{TAVP} - \text{TPC} - \text{IT} = \text{TAVP} - \text{TPC} - (\text{TAVP} - \text{TPC}) \times 0.35 \quad (38)$$

Total Capital Investment (TCI) is a sum of Fixed Capital Investment (FCI) and Working Capital (WC). WC typically represents 15% of TCI.

$$\text{TCI} = \text{FCI} + 0.15 \times \text{TCI} \quad \text{or} \quad \frac{20}{17} \cdot \text{FCI} \quad (39)$$

In the process of making an investment decision, the profits expected from a project are judged in accordance to a certain profitability standard. The profit must be judged relative to investment. A commonly used profitability standard is the minimum acceptable rate of return. It is a rate of earning that must be achieved by an investment in order for it to be profitable. The symbol m_{ar} is used and expressed as a percentage per year.

A calculated ROI is compared directly to an m_{ar} value selected from Table 26 [77]. If the ROI equals or exceeds the minimum acceptable rate of return m_{ar} , the project offers an acceptable rate of return. If it does not, the conclusion is that the project is not desirable for the investment of either borrowed or corporate funds.

Table 26 Suggested values for risk and m_{ar}

Investment Description	Level of Risk	Minimum acceptable return m_{ar} (after income taxes), %
Safe corporate investment opportunities of cost of capital	Safe	4-8
New capacity with established corporate market position	Low	8-16
New product entering into established market, or new process technology	Medium	16-24
New product or process in a new application	High	24-32
Everything new, high R&D and marketing effort	Very High	32-48+

Profitability analysis showed that implementation of radiation-thermal processing resulted in increase of return on investment (ROI) from 16% to 60%. The minimum acceptable rate of return (m_{ar}) for a high level of risk investment like a new process in a new application is 24-32%. Even for a product/raw material price fluctuation of $\pm 10\%$, ROI for RTC is approximately $\pm 11.2\%$, which is above the specified profitability standard.

Thruput of the process depends on the thruput of the reactor in the irradiation chamber, which, in turn, depends on the dose rate, configuration of the irradiation point and configuration of the accelerator itself. Therefore, the irradiation reactor is a bottleneck of the process, and rigorous optimization technique should be applied in order to operate the facility at a maximum processing capacity.

Reducing processing capacity down to 15,000 bbl/day resulted in ROI of 13% and 49% for VB alone and RTC respectively. Increasing processing capacity up to 25,000 bbl/day resulted in ROI of 19% and 68% for VB alone and RTC respectively. These calculations confirm that process should be operated at the maximum processing capacity in order to increase profitability.

CHAPTER VI

CONCLUSIONS AND FUTURE WORK RECOMMENDATIONS

6.1 Conclusions

Literature review part of the thesis is the most thorough list of the literature sources, pertaining topic of heavy oil upgrading by electron beam irradiation.

Described design of the pouch is an effective solution for a container for heavy oil irradiation. It provides uniform irradiation, cheap and easy to prepare.

Viscosity of irradiated heavy crude oil is found to increase, both with the absorbed dose and with the time after irradiation. We found that the irradiation of pure oil leads to the increase of the molecular weight calculated from Riazi-Daubert correlation. Thus, irradiation up to 10 kGy resulted in the 1.64% increase in the molecular weight, 20 kGy – 4.35%, 30 kGy – 3.28%. It was found that if irradiated oil was stored for 17 days, its viscosity increased by 14% in average.

Addition of water or solvents also leads to an increase in viscosity, above that of non-irradiated oil with added water or solvent. Thus, the irradiation of samples with added solvent in the following weight percentages 10, 5, 2.5wt.% resulted in the increase of the viscosity by 3.3, 3.6 and 14.5% respectively. The 5 and 10wt.% water-oil emulsion was irradiated up to 10 kGy and viscosity was measured at 50, 70, 90°C. The viscosity increased by 15% at 50 °C, by 14.9% at 70°C and by 37.8% at 90 °C for a 10wt.% water-oil sample. The latter high value is attributed to the instability of oil-water emulsions at higher temperatures. The viscosity increased by 14% at 50 °C, by 10.9% at 70°C and by 12.7% at 90 °C for a 5wt.% water-oil sample.

We conclude that irradiation at room temperature leads to the synthesis of longer molecules, rather than a fractionation. Readily available correlations can be implemented to predict viscosities of pure oil and hydrocarbon mixtures.

The described laboratory-scale layout and procedure for radiation-thermal cracking at low dose rates is expected to give consistent results. Aluminum can has very

thin walls and because of it, electron attenuation is minimal, compared to walls of the flask made of Pyrex glass. The temperature profile of petroleum vapors is sensitive to convection due to the thin walls of the aluminum can. Therefore, any source of instability in the ambient air should be avoided to ensure repeatability and accuracy of experimental results. Crude oil used for experimentation must be dewatered in order to avoid steam formation and violent boiling. Steam formed during cracking can act as a carrier gas, and high boiling point components may end up in the distillate contaminating it. Yields of light fractions can be increased by decreasing temperature of the cooling water-circulating jacket of the condenser. However, it should be recognized that in order to compare yields of light fractions from TC and RTC, the temperature of cooling water should be the same for both processes.

Implementation of radiation increased yields of light fractions by 35wt.% in average compared to the process where no radiation was present. Gas chromatography analysis revealed that there was no change in the molecular structure and density of RTC products, compared to products from conventional thermal cracking. This signifies that increase in the yield did not happen due to the increase in density and/or increase in the molecular weight of RTC products, but mainly because radiation assisted process extracts more light fractions out of residue, than the conventional process in the same amount of time. Therefore, ionizing radiation is shown to be a very effective and efficient generator of the reactive species that initiate chemical reactions, and thus catalyze thermal cracking reactions in the absence of catalysts.

Preliminary economic evaluation of the hypothetical radiation-thermal visbreaking unit shows that profitability of heavy oil processing increases compared to visbreaking alone. The calculation of profitability is performed by a rate of return on investment (ROI) method. It shows that implementation of radiation-thermal processing results in the increase of ROI from 16 to 60%. Therefore, investment in the installation of the electron accelerator is a reasonable decision. In addition, in this part of the thesis are given installation cost estimates and technical characteristics of the electron beam accelerator.

6.2 Recommendations for future work

Introduction of electron beam processing of materials in 1950 gave birth to various applications, the most recent of which is radiation-thermal cracking of hydrocarbons. This area of research is still ongoing and these preliminary results are very promising.

Therefore, a detailed analysis is necessary to determine the physical properties and chemical composition of radiation-thermal cracking products. This information is crucial to correctly model kinetics of the radiation-thermal process. Further experimentation is needed to determine the limits of radiation-thermal cracking with increasing dose rates and pressures. No research known to the author has shown the effect of catalysts presence. Thus, it is imperative to investigate the action of radiation and catalysts on the feedstock and on the catalyst itself. Further study should also include computer simulations of this process and a comparative analysis of various RTC processing techniques, as well as optimization of equipment and configurations. More realistic and detailed economic analysis is among the future avenues for research.

Development of a technique that would allow accurate measurement of the absorbed dose in the heterogeneous media of boiling crude oil with a subsequent mass transfer of light fractions is a challenging task. However, to do any economical evaluation and optimization of the process, it is important to develop such technique, as it may ensure that the absorbed dose and corresponding dose rates are accurately estimated.

REFERENCES

- [1] A.V. Topchiev, L.S. Polak, The radiation-thermal cracking of petroleum hydrocarbons, *Neftekhimiya* 2 (2) (1962) 196-210.
- [2] Y.A. Zaykin, R.F. Zaykina, J. Silverman, Radiation-thermal conversion of paraffinic oil, *Radiation Physics and Chemistry* 69 (2004) 229-238.
- [3] G.I. Zhuravlev, S.V. Voznesenskaya, I.V. Borisenko, L.A. Bilap, Radiothermal effect on heavy crude oil residues, *Khimiya Vysokih Energii* 25 (1) (1991) 27-31.
- [4] Y.A. Zaykin, R.F. Zaykina, G. Mirkin, On energetics of hydrocarbon chemical reactions by ionizing irradiation, *Radiation Physics and Chemistry* 67 (2003) 305-309.
- [5] Y.A. Zaykin, R.F. Zaykina, N.K. Nadirov, S.S. Sarsembinov, Patent of Republic of Kazakhstan No. 8142: Method and facility for used and residual oil mixes reprocessing (in Russian), (1997).
- [6] C. Smalley, Heavy oil and viscous oil, *Modern Petroleum Technology* 1 (2000) 409-435.
- [7] R.F. Meyer, World Heavy Crude Oil Resources, in: R.F. Meyer (ed.), 15th World Petroleum Congress, 1998, John Wiley & Sons, New York, 459-471.
- [8] C. Pauchon, Editorial, *Oil & Gas Science and Technology* 59 (4) (2004) 453-454.
- [9] World Energy Council, <http://www.worldenergy.org>, (2005).
- [10] R. Henderson, M. Rodwell, A. Harji, Consider modifying your refinery to handle heavy opportunity crude oils, *Hydrocarbon Processing* 84 (9) (2005) 47-54.
- [11] J.G. Speight, *Petroleum Refining Processes*, Marcel Dekker, Inc., New York 2002.
- [12] V. Simanzhenkov, R. Idem, *Crude Oil Chemistry*, Marcel Dekker, Inc., New York, 2003.

- [13] J.G. Speight, *The Chemistry and Technology of Petroleum*, Marcel Dekker, New York, 1999.
- [14] L. Schmerling, *Organic and Petroleum Chemistry for Nonchemists*, PennWell, Tulsa, 1981.
- [15] W.A. Gruse, D.R. Stevens, *The Chemical Technology of Petroleum*, McGraw-Hill, New York, 1960.
- [16] M.R. Gray, *Upgrading Petroleum Residues and Heavy Oils*, Marcell Dekker, New York, 1994.
- [17] T.Y. Yan, Upgrading of heavy oils - An overview, *Journal of Petroleum* 38 (4) (2002) 39-50.
- [18] S. Raseev, *Thermal and Catalytic Processes in Petroleum Refining*, Marcel Dekker, Inc., New York, 2003.
- [19] R.L. Dickenson, F.E. Biasca, Refiner options for converting and utilizing heavy fuel oil, *Hydrocarbon Processing* 76 (2) (1997) 57-61.
- [20] M.R. Gray, Tutorial on Upgrading of Oilsands Bitumen, <http://www.ualberta.ca/~gray/Library/Tutorials/Upgrading/>, (May 2006).
- [21] J.E. Turner, *Atoms, Radiation, and Radiation Protection*, Pergamon press, New York, 1986.
- [22] G. Foldiak, *Radiation Chemistry of Hydrocarbons*, Elsevier, Amsterdam, 1981.
- [23] R.J. Woods, A.K. Pikaev, *Applied Radiation Chemistry: Radiation Processing*, A Wiley-Interscience, New York, 1994.
- [24] G.F. Knoll, *Radiation Detection and Measurement*, John Wiley, New York, 2000.
- [25] International Atomic Energy Agency, <http://www.iaea.org>, (March 2006).
- [26] F.H. Attix, *Introduction to Radiological Physics and Radiation Dosimetry*, John Wiley & Sons, New York, 1986.
- [27] National Institute of Standards and Technology, <http://physics.nist.gov/PhysRefData/Star/Text/ESTAR.html>, (May 2006).
- [28] Wikipedia, the free encyclopedia, <http://en.wikipedia.org/>, (2006).

- [29] M.R. Cleland, Radiation processing: basic concepts and practical aspects, *Industrial Irradiation Technology* 1 (3) (1983) 191-218.
- [30] S. Lovell, *An Introduction to Radiation Dosimetry*, University Press, Cambridge, 1979.
- [31] G.G. Eichholz, J.W. Poston, *Principles of Nuclear Radiation Detection*, Ann Arbor Science Publisher Inc., Ann Arbor, 1979.
- [32] M.R. Cleland, High-voltage electron beam irradiation facilities, *Radiation Physics and Chemistry* 18 (1-2) (1981) 301-312.
- [33] J. Silverman, Radiation processing: the industrial applications of radiation chemistry, *Journal of Chemical Education* 58 (2) (1981) 168-173.
- [34] B.K. BhaskaraRao, *Modern Petroleum Refining Processes*, Oxford & IBH Publishing, New Delhi, 2001.
- [35] K.P. Lavrosky, *Catalytic, Thermal and Radiation-Chemical Conversion in Hydrocarbons* (Russian), Nauka, Moscow, 1976.
- [36] G. Foldiak (ed.), *Radiation Chemistry of Hydrocarbons*, Elsevier, Amsterdam, 1981.
- [37] Project #K-930: Bitumen radiation processing. International Science and Technology Center in Almaty, Kazakhstan (2005).
- [38] R.F. Zaykina, Y.A. Zaykin, G. Mirkin, N.K. Nadirov, Prospects for irradiation processing in the petroleum industry, *Radiation Physics and Chemistry* 63 (2002) 617-620.
- [39] Y.A. Zaykin, R.F. Zaykina, Bitumen radiation processing, *Radiation Physics and Chemistry* 71 (2004) 469-472.
- [40] A.M. Brodsky, N.V. Zvonov, K.P. Lavrosky, V.B. Titov, Radiation-thermal conversion in oil fractions, *Neftekhimiya* 1 (1961) 370-381.
- [41] R.F. Zaykina, Y.A. Zaykin, S.G. Yagudin, I.M. Fahrudinov, Specific approaches to radiation processing of high-sulfuric oil, *Radiation Physics and Chemistry* 71 (2004) 465-468.
- [42] R.F. Zaykina, Y.A. Zaykin, T.B. Mamonova, N.K. Nadirov, Radiation methods for demercaptanization and desulfurization of oil products, *Radiation Physics and Chemistry* 63 (2002) 621-624.

- [43] G.B. Skripchenko, V.I. Sekrieru, N.K. Larina, Z.S. Smutkina, O.K. Miesserova, V.A. Rudoi, Action of radiation on heavy petroleum and oil products, *Khimiya Tverdogo Topliva* 20 (4) (1986) 55-59.
- [44] F. Cataldo, Y. Keheyam, B. S., The effect of gamma-irradiation of anthracite coal and oil bitumen, *Journal of Radioanalytical and Nuclear Chemistry* 262 (2) (2004) 443-450.
- [45] V. Sorokin, Patent of Czech Republic WO0200811: Method for treatment of heavy hydrocarbon fraction and equipment thereto, (2002).
- [46] G. Pokacalov, Patent of Czech Republic WO9804653: Method of treating heavy hydrocarbon raw material, particularly heavy fractions of crude oil and apparatus for performing said method, (1998).
- [47] I. Mustafaev, N. Gulieva, The principles of radiation-chemical technology of refining the petroleum residues, *Radiation Physics and Chemistry* 46 (4-5) (1995) 1313-1316.
- [48] I. Mustafaev, L. Jabbarova, K. Yagubov, N. Gulieva, Radiation-thermal refining of oil-bituminous rocks, *Journal of Radioanalytical and Nuclear Chemistry* 262 (2) (2004) 509-511.
- [49] M.A. Bravo, J.G. Ibanez, Transformation of hydrocarbons under the action of radiation: an overview, *Reviews in Chemical Engineering* 14 (2) (1998) 89-108.
- [50] D.D. Danjou, R. Litman, Gamma-ray induced decomposition of oil shale, *Radiochem. Radioanal. Letters* 50 (1) (1981) 37-44.
- [51] H.J. Gomberg, United States Patent 4772379: Extraction and liquifaction of fossil fuels using gamma irradiation and solvents, (1988).
- [52] S. Humphries, *Principles of Charged Particle Acceleration*, John Wiley, New York, 1986.
- [53] E.J. Wilson, *Introduction to Particle Accelerators*, Oxford University Press, Oxford, 2001.
- [54] A. Chao, M. Tigner, *Handbook of Accelerator Physics and Engineering*, World Scientific Publishing Co., Hackensack, New Jersey, 1999.
- [55] H.D. Young, R.A. Freedman, *University Physics*, Addison-Wesley, New York, 1996.

- [56] G.J. Venturini, M. D.D., Simulation studies of steam-propane injection for the Hamaca heavy oil field, *Journal of Canadian Petroleum Technology* 43 (9) (2004) 40-46.
- [57] MCNP - A General Monte Carlo N-Particle Transport Code - Version 5, <http://mcnp-green.lanl.gov/>, (March 2005).
- [58] J. Kim, PhD candidate at department of Biological and Agricultural Engineering: MCNP calculations; Personal communication, (July 2005).
- [59] G.W. Gould, Wilkinson, V. M., *Food Irradiation: A Reference Guide*, Woodhead Pub Ltd, Cambridge, 1996.
- [60] V.L. Auslender, I.A. Baranov, V.N. Lazarev, V.V. Obnorskii, A.D. Panfilov, V.A. Polyakov, N.D. Romashko, S.M. Trofimenko, V.P. Shilov, V.P. Eismont, Multibeam accelerator for complex irradiations, *Soviet Atomic Energy* 51 (2) (1981) 525-527.
- [61] L. Braby, Beam current and beam power estimation; Personal communication, (May 2005).
- [62] J. Kim, PhD candidate at department of Biological and Agricultural Engineering: Absorbed dose distribution in a sample of Hamaca heavy oil; Personal communication, (July 2005).
- [63] NIST ESTAR stopping power and range for electrons, <http://physics.nist.gov/PhysRefData/Star/Text/ESTAR.html>, (2006).
- [64] L. Braby, Estimation of electron beam scattering with distance from exit beam window; Personal communication, (February 2006).
- [65] S. Korenev, I. Korenev, S. Rumege, L. Grossman, Real-time measurement and monitoring of absorbed dose for electron beams, *Radiation Physics and Chemistry* 71 (2004) 315-320.
- [66] Glassware joints, <http://www.ilpi.com/inorganic/glassware/joints.html>, (May, 2006).
- [67] Silicone rubber stoppers, <http://www.vwrsp.com>, (March, 2006).
- [68] M.R. Riazi, T.E. Daubert, Molecular weight of heavy-oil fractions from viscosity, *Oil & Gas Journal* Feb. 15 (1988) 40.

- [69] A. Danesh, PVT and Phase Behaviour of Petroleum Reservoir Fluids, Elsevier, Amsterdam, 1998.
- [70] W.R. Shu, A viscosity correlation for mixtures of heavy oil, bitumen, and petroleum fractions, Society of Petroleum Engineers Journal (June, 1984) 277-282.
- [71] L.E. Castro, Microemulsion systems applied to breakdown petroleum emulsions, Journal of Petroleum Science and Engineering 32 (2-4) (2001) 145.
- [72] A. Setiadarma, Rheological behavior of heavy oil and its mixtures at high pressures and high temperatures, Thesis, Texas A&M University, College Station, 2002.
- [73] M.R. Cleland, L.A. Parks, Medium and high-energy electron beam radiation processing equipment for commercial applications, Nuclear Instruments and Methods in Physics Research B 208 (2003) 74-89.
- [74] Inflation Calculator (consumer index), <http://www.westegg.com/inflation/>, (2006).
- [75] M.M. Todd, Emerging industrial applications of LINACS, in: M.M. Todd (ed.), XIX International Linear Accelerator Conference, 1998, Chicago, IL USA, Argonne National Laboratory 1036-1040.
- [76] R.E. Maples, Petroleum Refinery Process Economics, PennWell Books, Tulsa, 1993.
- [77] M.S. Peters, K.D. Timmerhaus, R.E. West, Plant Design and Economics for Chemical Engineers, McGraw-Hill, New York, 2003.
- [78] Producer price index inflation calculator, <http://www1.jsc.nasa.gov/bu2/inflation/ppi/inflatePPI.html>, (2006).
- [79] Energy Information Administration (EIA), <http://www.eia.doe.gov/>, (2006).
- [80] Information provider for the chemical and oil industry ICIS, <http://www.icispricing.com>, (2006).
- [81] R.F. Zaykina, Y.A. Zaykin, T.B. Mamonova, N.K. Nadirov, Radiation-thermal processing of high-viscous oil from Karazhanbas field, Radiation Physics and Chemistry 60 (2001) 211-221.

- [82] Webster's New Collegiate Dictionary, G.&C. Merriam Company, Springfield, 1976.
- [83] Brookfield digital Rheometer Model DV-III Operating instructions manual, M/91-210-I297, (1999), Brookfield Engineering Laboratories, Inc., Middleboro, MA.
- [84] OMB-Personal Daq USB Data Acquisition Modules User's Guide, OMB-491-0901 (2001), Omega Engineering, Inc., Stamford, CT.

APPENDIX A

CALIBRATION OF THE VISCOMETER

Calibration consists of determining the deviation from a known standard so as to ascertain the proper correction factors [82]. In other words, calibration of the radiation source is necessary to determine a firm scale of measurement based on meter readings and resulting in numerical multiplies of some appropriate unit. Two factors are important to get reliable radiation measurements: intrinsic consistency of the measurement procedure and accuracy of the measuring device.

The viscometer to measure the viscosity was a Brookfield LVDV-III. Temperature is maintained constant by a fluid circulating from a water bath with automated thermostat. This type of viscometer is generally used when only small sample volumes are available. The viscometer utilized in this project was a cone-and-plate spindle CPE-52 (cone angle 3.0°). The CPE-52 spindle is used to measure high viscosities in the range of 4.6–92,130 cP, and appropriate sample volume for it is 0.5 ml. The amount of sample is crucial for accurate viscosity measurement, because the size should be sufficient to cover the bottom of the cup. If the amount is too small it will result in low viscosity readings, or if it is too much and it covers the body of the spindle, readings will be too high [72]. The rheometer measures fluid parameters of shear stress and viscosity at given shear rates. The principle of operation is based on the measuring torque exerted on a calibrated spring immersed in the test fluid spindle. The viscous drag of the fluid against the spindle is measured by spring deflection. Spring deflection is measured by the rotary transducer. An appropriate selection will result in measurements made between 10 and 100 on the instrument % torque scale. In other words, to measure high viscosity, choose a slow speed of spindle rotation. If the chosen speed results in a reading above 100%, then the speed should be reduced. The cone spindle must rotate at least five times before a viscosity reading is taken. For example, if the speed is 1 RPM, at least 5 minutes should pass before recording a viscosity. Also, the viscosity reading should be verified that it is within the allowable 1% deviation. In this paper all viscosity

measurements are reported with corresponding fluctuation in readings. More detailed information about viscosity measurements with the Brookfield LVDV-III can be found in the operating instructions manual [83].

Calibration procedure 1

For first calibration we used a Canon viscosity standard S60 100% mineral oil. After turning on, the rheometer has to be auto zeroed. It is important to ensure proper gap between cone and plate, because either too small or too big a gap will lead to erroneous readings. To find the gap (0.013 mm) between the cone and plate, the procedure from viscometer manual was followed. The water bath was stabilized at 20.4°C and the temperature reading at the viscometer showed 20.0°C. A 0.5 ml of standard fluid was measured by syringe and placed in the sample cup. After oil attains thermal equilibrium with cup, it is attached to the rheometer. After each temperature increment sufficient time (around 15-20 minutes) should be allowed, for bath and cup with standard to reach thermal equilibrium. Table A-1 reports measured viscosity values with standard deviation of $\pm 0.43\%$ in average.

Table A- 1 Comparison with standard values

Measured Values		Standard Values	
Temperature (°C)	Viscosity (cP)	Temperature (°C)	Viscosity (cP)
20	142	20	141.2
25	107	25	103.8
37.8	54.9	37.78	51.89
40	51.2	40	46.59
50	32.1	50	29.69
90	7.1	98.89	6.381
-	-	100	6.223

In order to interpret calibration results and check whether the instrument is calibrated properly, calculations of total allowable error are needed:

1) From Appendix D [83] we found calibration parameters for LVDV-III: TK=0.09373, RPM=50 and SMC=9.83 (for CP-52).

Full Scale Viscosity Range is equal to:

$$\text{TK} \cdot \text{SMC} \cdot 10,000/\text{RPM} = 0.09373 \times 9.83 \times 10,000/50 = 184.3 \text{ cP.}$$

1% of this value is 1.843, thus deviation is $\pm 1.843 \text{ cP}$.

2) At 40 °C viscosity of the standard fluid is 46.59 cP. Its accuracy is $\pm 1\%$, thus $\pm 0.4659 \text{ cP}$.

3) Total allowable error is $(0.4659 + 1.843) \text{ cP}$ or $\pm 2.31 \text{ cP}$.

$$\text{“+”} = (46.59 + 2.31) \text{ cP} = 48.9 \text{ cP}$$

$$\text{“-”} = (46.59 - 2.31) \text{ cP} = 44.28 \text{ cP}$$

Since measured viscosity is 51.2 cP, it is out of this range (48.9 cP – 44.28 cP) and calibration is incorrect. Table A-2 summarizes calibration calculations for other temperatures.

Table A-2 Calibration 1 results

Temp, °C	μ_{STD} , cP	1)	2)	3)	“+”	“-”	μ , cP	Result
20	141.2	1.843	1.412	3.255	144.455	137.945	142	IN
25	103.8	1.843	1.038	2.881	106.681	100.919	107	OUT
37.8	51.89	1.843	0.5189	2.3619	54.2519	49.5281	54.9	OUT
40	46.59	1.843	0.4659	2.3089	48.8989	44.2811	51.2	OUT
50	29.69	1.843	0.2969	2.1399	31.8299	27.5501	32.1	OUT

Calibration procedure 2

Since results of the first calibration were not satisfactory, the second calibration was done with a higher viscosity standard. Note that it is not recommended to use silicone viscosity standards for viscosities above 5000 cP. For the second calibration we used a Brookfield viscosity standard S5000 pure silicon (high viscosity standard). At 25°C, viscosity of the standard fluid is supposed to be 4980 cP. Its accuracy is $\pm 1\%$, thus $\pm 49.80 \text{ cP}$; therefore, the total allowable error is $\pm 51.643 \text{ cP}$ and the measured viscosities should be in the range from 4928.357 to 5031.643 cP. Application of standard fluid with higher viscosity resulted in better calibration results.

APPENDIX B

DESCRIPTION OF THERMOCOUPLE

The thermocouple was purchased from Omega Engineering, Inc and has the following specifications: a pair of Iron-Constantan wires is capable to measure temperature in the range of 0-750°C with standard limits of error not greater than 2.2°C or 0.75%. It is made up of a stainless steel metal-sheathed thermocouple, 4 mm in diameter, which "transitions" to a lead wire via a slightly larger cylindrical barrel. The thermocouple is connected to a computer via USB data acquisition module OMB-DAQ 54 of Omega Engineering, Inc. In order to ensure correct data acquisition from the thermocouple, thermocouple wires have to be connected in differential mode to the digital channel of the module. Differential connection is made as follows:

- (a) the red wire connects to the channel's Low (L) connector.
- (b) the second white wire connects to the channel's High (H) connector [84].

To improve accuracy and repeatability of thermocouple readings, the thermocouple has to be centered in the top thermometer joint of the condenser. For this purpose we used a Chemglass CG-1048-A-01 Teflon adapter. It is designed for use with either 1/8"-in or 1/4"-in thermocouples and has an outer o-ring to form a grease-free, airtight seal between the adapter and the 10/18 outer joint. The compression nut works in conjunction with the o-ring to provide an airtight seal between the adapter and thermocouple. The tip of the thermocouple should be positioned as showed in Fig. B-1.

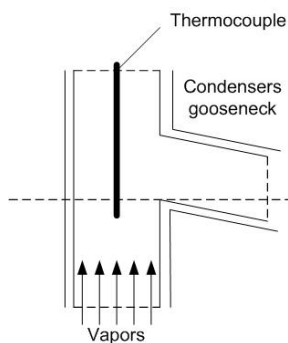


Fig. B-1 Position of thermocouple in the condenser

APPENDIX C

ELECTRONIC BALANCE SETTINGS

An XD-12K electronic balance from Denver Instrument Co is connected to the computer via a DB-9 connector cable. Standard DB-9 pin configuration should be modified according to the following scheme in order to ensure connectivity:

Table C-1 Cable connector pin configuration

COMPUTER	BALANCE
White wire goes to Pin 3 Black wire goes to Pin 5 Red wire goes to Pin 2 Shield is not used Jumper Pins 4 and 5	White wire goes to Pin 2 Black wire goes to Pin 7 Red wire goes to Pin 3 Shield goes to Pin 1 Jumper Pins 7 and 8

Once connected to the computer, HyperTerminal v.5.1 (Microsoft’s connectivity program) is used to start taking readings: COM1; 300 bits/sec; 8 data bits; none parity; 2 stop bits; hardware flow control. The procedure from the manual should be followed to set balance. Each parameter is entered through the keypad on the balance front panel. Settings of the balance are shown in Fig.C-1:

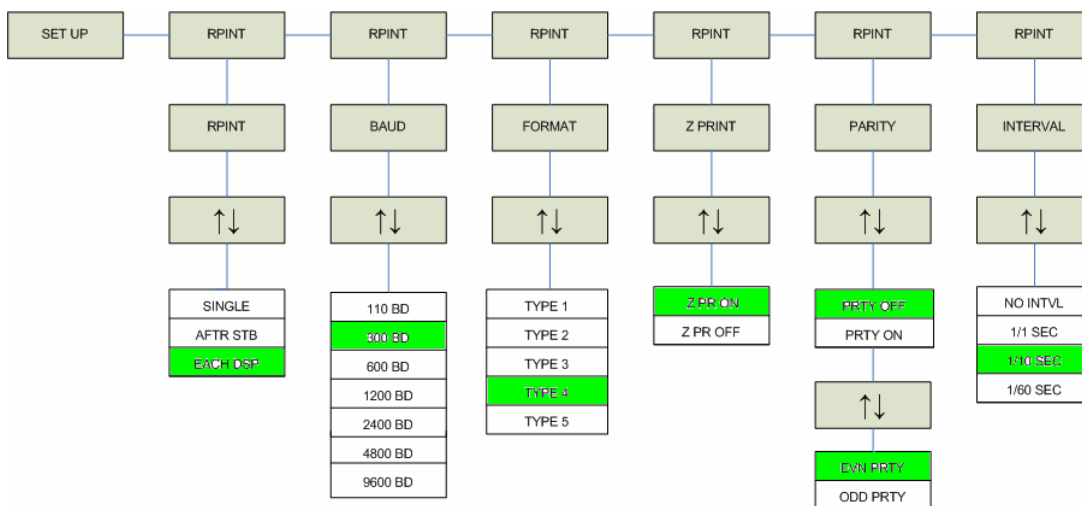


Fig. C-1 XD-12K balance settings

APPENDIX D

GAS CHROMATOGRAPHY ANALYSIS RESULTS

Table D- 1 GC results for RTC1

Component	MW (g/mol)	Flashed Oil	
		wt %	mole %
CO2	44.01	0.000	0.000
H2S	34.08	0.000	0.000
N2	28.01	0.000	0.000
C1	16.04	0.000	0.000
C2	30.07	0.000	0.000
C3	44.10	0.020	0.073
i-C4	58.12	0.007	0.021
n-C4	58.12	0.117	0.330
i-C5	72.15	0.153	0.348
n-C5	72.15	0.342	0.776
C6	84.00	1.363	2.659
Mycylo-C5	84.16	0.788	1.536
Benzene	78.11	0.073	0.154
Cyclo-C6	84.16	0.402	0.782
C7	96.00	3.577	6.109
Mycylo-C6	98.19	1.287	2.148
Toluene	92.14	0.306	0.544
C8	107.00	5.602	8.582
C2-Benzene	106.17	0.169	0.261
m&p-Xylene	106.17	0.426	0.658
o-Xylene	106.17	0.289	0.446
C9	121.00	5.809	7.871
C10	134.00	6.750	8.258
C11	147.00	6.777	7.558
C12	161.00	7.089	7.218
C13	175.00	8.950	8.384
C14	190.00	8.588	7.410
C15	206.00	8.624	6.863
C16	222.00	7.197	5.315
C17	237.00	6.527	4.515
C18	251.00	5.681	3.711
C19	263.00	4.219	2.630
C20	275.00	2.716	1.619
C21	291.00	1.952	1.100
C22	300.00	1.420	0.776
C23	312.00	0.899	0.472
C24	324.00	0.608	0.307
C25	337.00	0.407	0.198
C26	349.00	0.286	0.134
C27	360.00	0.199	0.091
C28	372.00	0.144	0.064
C29	382.00	0.099	0.042
C30+	580.00	0.139	0.039
MW			163.933
Mole %			0.000

Stock Tank Oil Properties at Standard Condition			C30+ Properties
	Measured	Calculated	
MW	164.120	163.930	580.000
Density (g/cc)	0.830	0.813	1.010

Single Stage Flash Data	
Original STO	
STO Density (g/cc)	0.830
STO API Gravity	38.982

Properties		Flashed Oil
Mole %		
C7+		93.32
C12+		50.89
C20+		4.84
C30+		0.04
Mass %		
C7+		96.74
C12+		65.74
C20+		8.87
C30+		0.14
Molar Mass		
C7+		169.93
C12+		211.80
C20+		300.23
C30+		580.00
Density (g/cc)		
C7+		0.8180
C12+		0.8419
C20+		0.8831
C30+		1.0100
Fluid Density at STP Condition (g/cc)		
		0.8300

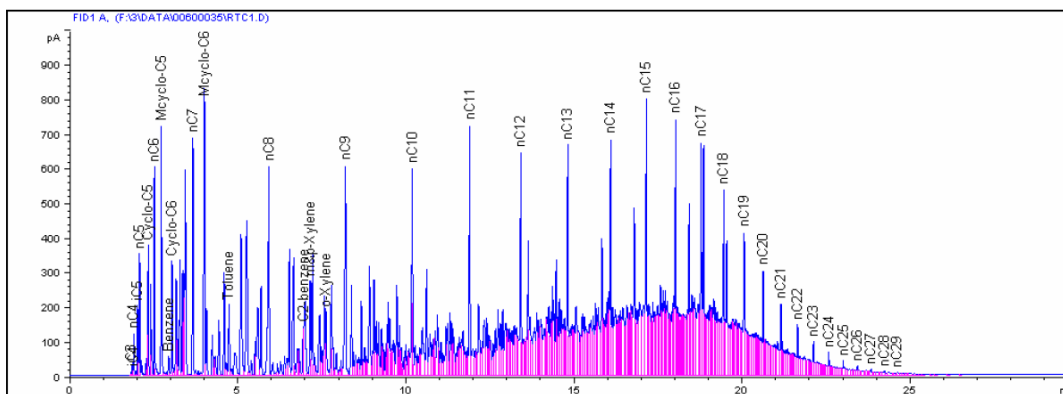


Table D- 2 GC results for RTC2

Component	MW (g/mol)	Flashed Oil	
		wt %	mole %
CO2	44.01	0.000	0.000
H2S	34.08	0.000	0.000
N2	28.01	0.000	0.000
C1	16.04	0.000	0.000
C2	30.07	0.000	0.000
C3	44.10	0.013	0.047
i-C4	58.12	0.007	0.018
n-C4	58.12	0.099	0.264
i-C5	72.15	0.187	0.401
n-C5	72.15	0.383	0.820
C6	84.00	1.686	3.105
Meyclo-C5	84.16	1.048	1.926
Benzene	78.11	0.075	0.148
Cyclo-C6	84.16	0.516	0.949
C7	96.00	4.397	7.085
Meyclo-C6	98.19	1.630	2.569
Toluene	92.14	0.375	0.629
C8	107.00	6.672	9.646
C2-Benzene	106.17	0.205	0.299
m&p-Xylene	106.17	0.485	0.707
o-Xylene	106.17	0.330	0.481
C9	121.00	6.764	8.648
C10	134.00	7.986	9.220
C11	147.00	7.605	8.003
C12	161.00	8.040	7.725
C13	175.00	9.762	8.629
C14	190.00	8.902	7.248
C15	206.00	8.342	6.265
C16	222.00	6.385	4.449
C17	237.00	5.331	3.480
C18	251.00	4.297	2.649
C19	263.00	2.948	1.734
C20	275.00	1.780	1.001
C21	291.00	1.223	0.650
C22	300.00	0.864	0.445
C23	312.00	0.536	0.266
C24	324.00	0.359	0.171
C25	337.00	0.243	0.112
C26	349.00	0.170	0.075
C27	360.00	0.124	0.053
C28	372.00	0.083	0.035
C29	382.00	0.065	0.026
C30+	580.00	0.084	0.023
MW			154.698
Mole %			0.000

Stock Tank Oil Properties at Standard Condition			C30+ Properties
MW	Measured 156.080	Calculated 154.700	580.000
Density (g/cc)	0.820	0.806	1.010

Single Stage Flash Data	
	Original STO
STO Density (g/cc)	0.820
STO API Gravity	41.019

Properties	Flashed Oil
Mole %	
C7+	92.32
C12+	45.04
C20+	2.86
C30+	0.02
Mass %	
C7+	95.99
C12+	59.54
C20+	5.53
C30+	0.08
Molar Mass	
C7+	160.84
C12+	204.51
C20+	299.44
C30+	580.00
Density (g/cc)	
C7+	0.8109
C12+	0.8375
C20+	0.8828
C30+	1.0100
Fluid Density at STP Condition (g/cc)	0.8202

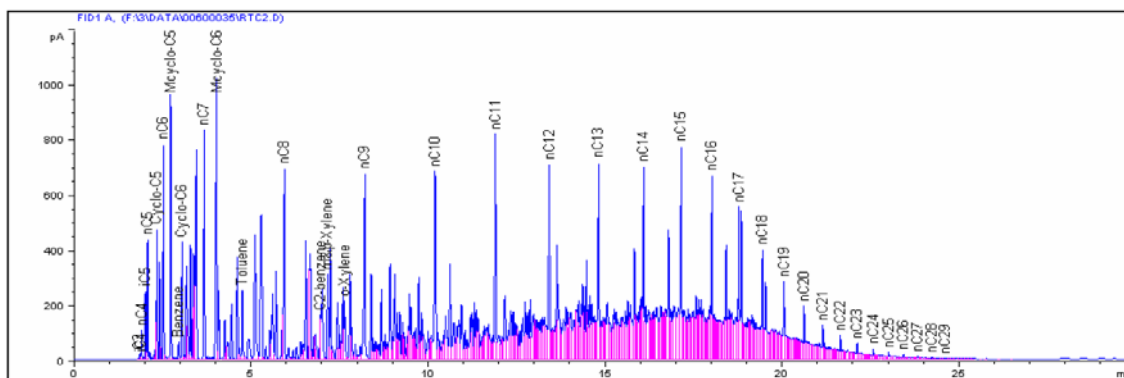


Table D- 3 GC results for RTC3

Component	MW (g/mol)	Flashed Oil	
		wt %	mole %
CO2	44.01	0.000	0.000
H2S	34.08	0.000	0.000
N2	28.01	0.000	0.000
C1	16.04	0.000	0.000
C2	30.07	0.000	0.000
C3	44.10	0.000	0.000
i-C4	58.12	0.002	0.004
n-C4	58.12	0.021	0.055
i-C5	72.15	0.128	0.266
n-C5	72.15	0.253	0.528
C6	84.00	1.610	2.879
Myclo-C5	84.16	1.126	2.011
Benzene	78.11	0.057	0.109
Cyclo-C6	84.16	0.559	0.999
C7	96.00	4.805	7.521
Myclo-C6	98.19	1.872	2.865
Toluene	92.14	0.413	0.673
C8	107.00	7.438	10.447
C2-Benzene	106.17	0.227	0.321
m&p-Xylene	106.17	0.523	0.740
o-Xylene	106.17	0.373	0.528
C9	121.00	7.590	9.426
C10	134.00	9.128	10.237
C11	147.00	8.703	8.897
C12	161.00	8.857	8.267
C13	175.00	10.172	8.734
C14	190.00	8.758	6.927
C15	206.00	7.705	5.620
C16	222.00	5.532	3.745
C17	237.00	4.416	2.800
C18	251.00	3.453	2.068
C19	263.00	2.312	1.321
C20	275.00	1.367	0.747
C21	291.00	0.919	0.474
C22	300.00	0.633	0.317
C23	312.00	0.374	0.180
C24	324.00	0.243	0.113
C25	337.00	0.158	0.070
C26	349.00	0.102	0.044
C27	360.00	0.069	0.029
C28	372.00	0.046	0.019
C29	382.00	0.032	0.013
C30+	580.00	0.026	0.007
MW			150.273
Mole %			0.000

Stock Tank Oil Properties at Standard Condition			C30+ Properties
MW	Measured	Calculated	580.000
Density (g/cc)	151.730	150.270	1.010
	0.815	0.802	

Single Stage Flash Data	
	Original STO
STO Density (g/cc)	0.815
STO API Gravity	42.035

Properties	Flashed Oil
Mole %	
C7+	93.15
C12+	41.49
C20+	2.01
C30+	0.01
Mass %	
C7+	96.24
C12+	55.17
C20+	3.97
C30+	0.03
Molar Mass	
C7+	155.27
C12+	199.81
C20+	296.34
C30+	580.00
Density (g/cc)	
C7+	0.8062
C12+	0.8345
C20+	0.8811
C30+	1.0100
Fluid Density at STP Condition (g/cc)	0.8154

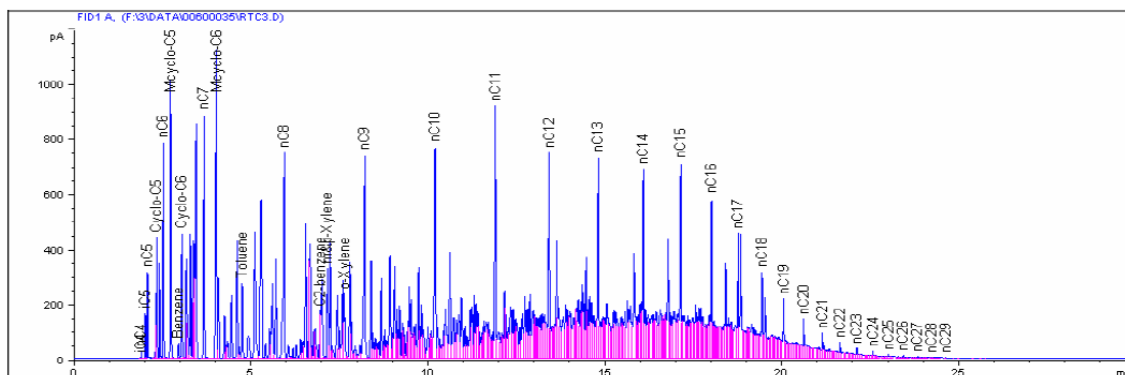


Table D- 4 GC results for RTC residue

Component	MW (g/mol)	Flashed Oil	
		wt %	mole %
CO2	44.01	0.000	0.000
H2S	34.08	0.000	0.000
N2	28.01	0.000	0.000
C1	16.04	0.000	0.000
C2	30.07	0.000	0.000
C3	44.10	0.002	0.017
i-C4	58.12	0.000	0.002
n-C4	58.12	0.003	0.026
i-C5	72.15	0.001	0.007
n-C5	72.15	0.003	0.021
C6	84.00	0.130	0.746
Myclo-C5	84.16	0.000	0.000
Benzene	78.11	0.013	0.078
Cyclo-C6	84.16	0.005	0.027
C7	96.00	0.093	0.464
Myclo-C6	98.19	0.000	0.000
Toluene	92.14	0.008	0.041
C8	107.00	0.067	0.301
C2-Benzene	106.17	0.001	0.003
m&p-Xylene	106.17	0.002	0.011
o-Xylene	106.17	0.003	0.014
C9	121.00	0.043	0.171
C10	134.00	0.053	0.192
C11	147.00	0.086	0.281
C12	161.00	0.134	0.399
C13	175.00	0.270	0.741
C14	190.00	0.406	1.026
C15	206.00	0.673	1.570
C16	222.00	0.978	2.117
C17	237.00	1.429	2.897
C18	251.00	2.037	3.898
C19	263.00	2.485	4.540
C20	275.00	2.674	4.671
C21	291.00	2.849	4.704
C22	300.00	2.951	4.727
C23	312.00	2.974	4.580
C24	324.00	2.746	4.071
C25	337.00	2.648	3.774
C26	349.00	2.440	3.359
C27	360.00	2.378	3.174
C28	372.00	2.294	2.963
C29	382.00	2.260	2.843
C30+	750.00	64.862	41.549
MW			480.429
Mole %			0.000

Stock Tank Oil Properties at Standard Condition			C30+ Properties
	Measured	Calculated	
MW	442.320	480.430	750.000
Density (g/cc)	0.981	0.959	1.010

Single Stage Flash Data	
	Original STO
STO Density (g/cc)	0.981
STO API Gravity	12.814

Properties	Flashed Oil
Mole %	
C7+	99.08
C12+	97.60
C20+	80.41
C30+	41.55
Mass %	
C7+	99.84
C12+	99.49
C20+	91.08
C30+	64.86
Molar Mass	
C7+	484.14
C12+	489.72
C20+	544.13
C30+	750.00
Density (g/cc)	
C7+	0.9601
C12+	0.9610
C20+	0.9723
C30+	1.0100
Fluid Density at STP Condition (g/cc)	
	0.9805

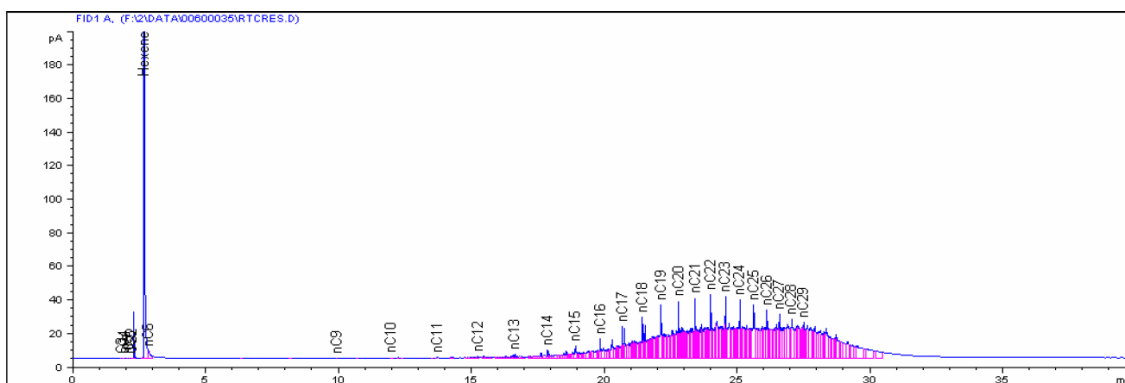


Table D- 5 GC results for TC1

Component	MW (g/mol)	Flashed Oil	
		wt %	mole %
CO2	44.01	0.000	0.000
H2S	34.08	0.000	0.000
N2	28.01	0.000	0.000
C1	16.04	0.000	0.000
C2	30.07	0.000	0.000
C3	44.10	0.008	0.028
i-C4	58.12	0.006	0.016
n-C4	58.12	0.068	0.186
i-C5	72.15	0.158	0.351
n-C5	72.15	0.307	0.681
C6	84.00	1.423	2.712
Mycylo-C5	84.16	0.892	1.697
Benzene	78.11	0.065	0.133
Cyclo-C6	84.16	0.444	0.845
C7	96.00	3.875	6.462
Mycylo-C6	98.19	1.438	2.344
Toluene	92.14	0.333	0.578
C8	107.00	6.046	9.048
C2-Benzene	106.17	0.181	0.273
m&p-Xylene	106.17	0.451	0.680
o-Xylene	106.17	0.311	0.470
C9	121.00	6.235	8.251
C10	134.00	7.256	8.671
C11	147.00	7.240	7.886
C12	161.00	7.526	7.485
C13	175.00	9.371	8.574
C14	190.00	8.861	7.468
C15	206.00	8.687	6.752
C16	222.00	6.988	5.040
C17	237.00	6.122	4.136
C18	251.00	5.144	3.282
C19	263.00	3.676	2.238
C20	275.00	2.277	1.326
C21	291.00	1.585	0.872
C22	300.00	1.117	0.596
C23	312.00	0.682	0.350
C24	324.00	0.444	0.219
C25	337.00	0.281	0.134
C26	349.00	0.191	0.088
C27	360.00	0.125	0.055
C28	372.00	0.081	0.035
C29	382.00	0.056	0.024
C30+	580.00	0.052	0.014
MW			160.121
Mole %			0.000

Stock Tank Oil Properties at Standard Condition			C30+ Properties
	Measured	Calculated	
MW	160.840	160.120	580.000
Density (g/cc)	0.826	0.810	1.010

Single Stage Flash Data		
	Original STO	De-Contaminated
STO Density (g/cc)	0.826	
STO API Gravity	39.849	

Properties	Flashed Oil
Mole %	
C7+	93.35
C12+	48.69
C20+	3.71
C30+	0.01
Mass %	
C7+	96.63
C12+	63.26
C20+	6.89
C30+	0.05
Molar Mass	
C7+	165.75
C12+	208.06
C20+	297.17
C30+	580.00
Density (g/cc)	
C7+	0.8147
C12+	0.8396
C20+	0.8815
C30+	1.0100
Fluid Density at STP Condition (g/cc)	0.8258

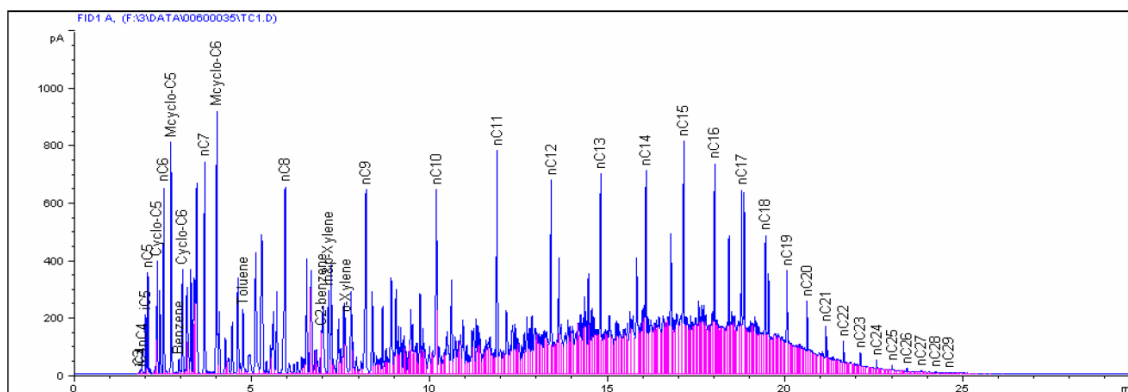


Table D- 6 GC results for TC2

Component	MW (g/mol)	Flashed Oil	
		wt %	mole %
CO2	44.01	0.000	0.000
H2S	34.08	0.000	0.000
N2	28.01	0.000	0.000
C1	16.04	0.000	0.000
C2	30.07	0.000	0.000
C3	44.10	0.008	0.026
i-C4	58.12	0.005	0.014
n-C4	58.12	0.062	0.160
i-C5	72.15	0.154	0.322
n-C5	72.15	0.300	0.628
C6	84.00	1.598	2.872
Myclo-C5	84.16	1.084	1.944
Benzene	78.11	0.063	0.121
Cyclo-C6	84.16	0.544	0.976
C7	96.00	4.720	7.423
Myclo-C6	98.19	1.824	2.804
Toluene	92.14	0.408	0.669
C8	107.00	7.338	10.353
C2-Benzene	106.17	0.224	0.318
m&p-Xylene	106.17	0.522	0.742
o-Xylene	106.17	0.364	0.518
C9	121.00	7.420	9.257
C10	134.00	8.780	9.891
C11	147.00	8.342	8.567
C12	161.00	8.676	8.135
C13	175.00	10.215	8.812
C14	190.00	8.971	7.128
C15	206.00	8.014	5.873
C16	222.00	5.807	3.949
C17	237.00	4.643	2.957
C18	251.00	3.611	2.172
C19	263.00	2.383	1.368
C20	275.00	1.390	0.763
C21	291.00	0.917	0.476
C22	300.00	0.619	0.312
C23	312.00	0.362	0.175
C24	324.00	0.229	0.107
C25	337.00	0.155	0.069
C26	349.00	0.087	0.038
C27	360.00	0.066	0.028
C28	372.00	0.043	0.017
C29	382.00	0.030	0.012
C30+	580.00	0.024	0.006
MW			150.962
Mole %			0.000

Stock Tank Oil Properties at Standard Condition			C30+ Properties
	Measured	Calculated	
MW	152.870	150.960	580.000
Density (g/cc)	0.816	0.803	1.010

Single Stage Flash Data

Original STO	
STO Density (g/cc)	0.816
STO API Gravity	41.822

Properties	Flashed Oil
Mole %	
C7+	92.94
C12+	42.40
C20+	2.00
C30+	0.01
Mass %	
C7+	96.18
C12+	56.24
C20+	3.92
C30+	0.02
Molar Mass	
C7+	156.23
C12+	200.26
C20+	295.70
C30+	580.00
Density (g/cc)	
C7+	0.8070
C12+	0.8348
C20+	0.8809
C30+	1.0100
Fluid Density at STP Condition (g/cc)	0.8164

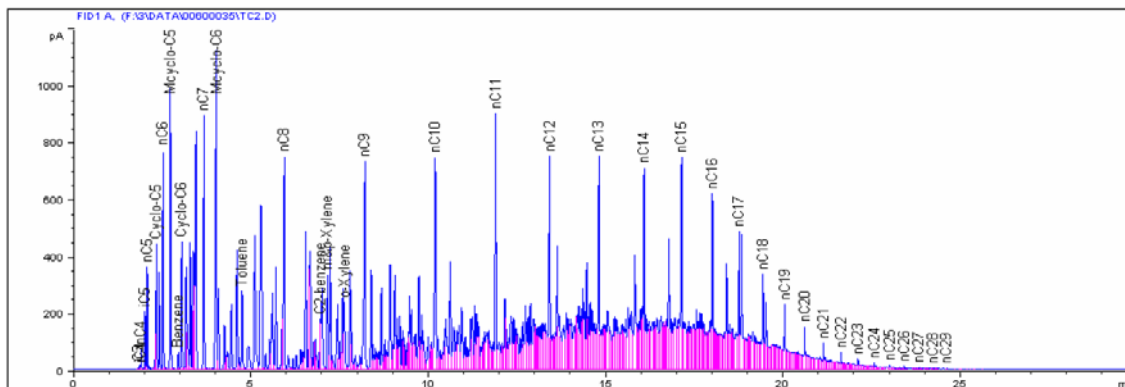


Table D- 7 GC results for TC3

Component	MW (g/mol)	Flashed Oil	
		wt %	mole %
CO2	44.01	0.000	0.000
H2S	34.08	0.000	0.000
N2	28.01	0.000	0.000
C1	16.04	0.000	0.000
C2	30.07	0.000	0.000
C3	44.10	0.004	0.013
i-C4	58.12	0.004	0.010
n-C4	58.12	0.042	0.105
i-C5	72.15	0.141	0.281
n-C5	72.15	0.275	0.548
C6	84.00	1.722	2.949
Meyclo-C5	84.16	1.234	2.110
Benzene	78.11	0.065	0.120
Cyclo-C6	84.16	0.628	1.073
C7	96.00	5.517	8.266
Meyclo-C6	98.19	2.174	3.185
Toluene	92.14	0.487	0.760
C8	107.00	8.687	11.679
C2-Benzene	106.17	0.269	0.365
m&p-Xylene	106.17	0.612	0.830
o-Xylene	106.17	0.430	0.582
C9	121.00	8.754	10.407
C10	134.00	10.308	11.066
C11	147.00	9.601	9.395
C12	161.00	9.461	8.453
C13	175.00	10.282	8.452
C14	190.00	8.236	6.236
C15	206.00	6.728	4.698
C16	222.00	4.476	2.900
C17	237.00	3.376	2.049
C18	251.00	2.473	1.418
C19	263.00	1.574	0.861
C20	275.00	0.882	0.462
C21	291.00	0.570	0.282
C22	300.00	0.383	0.184
C23	312.00	0.213	0.098
C24	324.00	0.143	0.064
C25	337.00	0.092	0.039
C26	349.00	0.060	0.025
C27	360.00	0.041	0.016
C28	372.00	0.026	0.010
C29	382.00	0.018	0.007
C30+	580.00	0.011	0.003
MW			143.853
Mole %			0.000

Stock Tank Oil Properties at Standard Condition			C30+ Properties
	Measured	Calculated	
MW	146.430	143.850	580.000
Density (g/cc)	0.808	0.796	1.010

Single Stage Flash Data

Original STO	
STO Density (g/cc)	0.808
STO API Gravity	43.667

Properties	Flashed Oil
Mole %	
C7+	92.79
C12+	36.26
C20+	1.19
C30+	0.00
Mass %	
C7+	95.88
C12+	49.05
C20+	2.44
C30+	0.01
Molar Mass	
C7+	148.65
C12+	194.60
C20+	295.24
C30+	580.00
Density (g/cc)	
C7+	0.8006
C12+	0.8311
C20+	0.8806
C30+	1.0100
Fluid Density at STP Condition (g/cc)	0.8078
Gas Gravity (Air=1)	
Dry Gross Heating Content (KJ/m ³)	
Wet Gross Heating Content (KJ/m ³)	

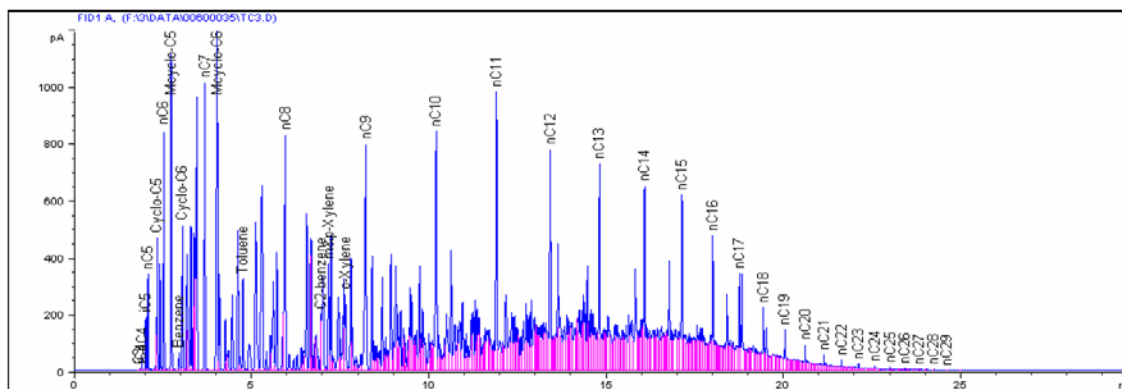


Table D- 8 GC results for TC residue

Component	MW (g/mol)	Flashed Oil	
		wt %	mole %
CO2	44.01	0.000	0.000
H2S	34.08	0.000	0.000
N2	28.01	0.000	0.000
C1	16.04	0.000	0.000
C2	30.07	0.000	0.000
C3	44.10	0.001	0.008
i-C4	58.12	0.000	0.001
n-C4	58.12	0.002	0.013
i-C5	72.15	0.001	0.006
n-C5	72.15	0.002	0.014
C6	84.00	0.057	0.329
Myclo-C5	84.16	0.000	0.000
Benzene	78.11	0.012	0.074
Cyclo-C6	84.16	0.000	0.000
C7	96.00	0.161	0.809
Myclo-C6	98.19	0.000	0.000
Toluene	92.14	0.000	0.000
C8	107.00	0.082	0.372
C2-Benzene	106.17	0.001	0.003
m&p-Xylene	106.17	0.001	0.006
o-Xylene	106.17	0.002	0.009
C9	121.00	0.036	0.145
C10	134.00	0.048	0.173
C11	147.00	0.076	0.249
C12	161.00	0.133	0.400
C13	175.00	0.304	0.839
C14	190.00	0.501	1.276
C15	206.00	0.956	2.245
C16	222.00	1.408	3.065
C17	237.00	1.771	3.612
C18	251.00	2.391	4.604
C19	263.00	2.578	4.738
C20	275.00	2.569	4.516
C21	291.00	2.573	4.274
C22	300.00	2.586	4.167
C23	312.00	2.516	3.899
C24	324.00	2.321	3.463
C25	337.00	2.174	3.119
C26	349.00	2.106	2.917
C27	360.00	2.003	2.690
C28	372.00	1.912	2.485
C29	382.00	1.904	2.410
C30+	750.00	66.815	43.070
MW			483.460
Mole %			0.000

Stock Tank Oil Properties at Standard Condition			C30+ Properties
	Measured	Calculated	
MW	443.460	483.460	750.000
Density (g/cc)	0.974	0.961	1.010

Single Stage Flash Data	
	Original STO
STO Density (g/cc)	0.974
STO API Gravity	13.792

Properties	Flashed Oil
Mole %	
C7+	99.55
C12+	97.79
C20+	77.01
C30+	43.07
Mass %	
C7+	99.93
C12+	99.52
C20+	89.48
C30+	66.81
Molar Mass	
C7+	485.26
C12+	492.02
C20+	561.74
C30+	750.00
Density (g/cc)	
C7+	0.9614
C12+	0.9624
C20+	0.9765
C30+	1.0100
Fluid Density at STP Condition (g/cc)	0.9739

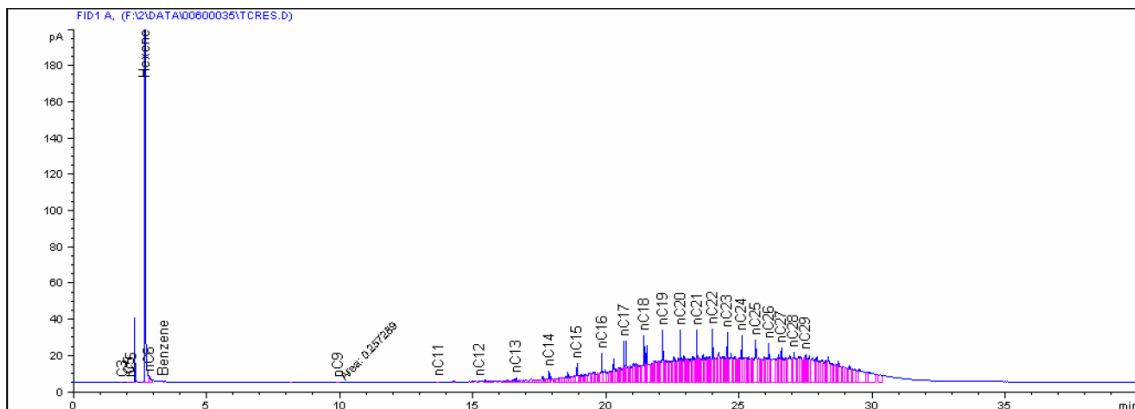


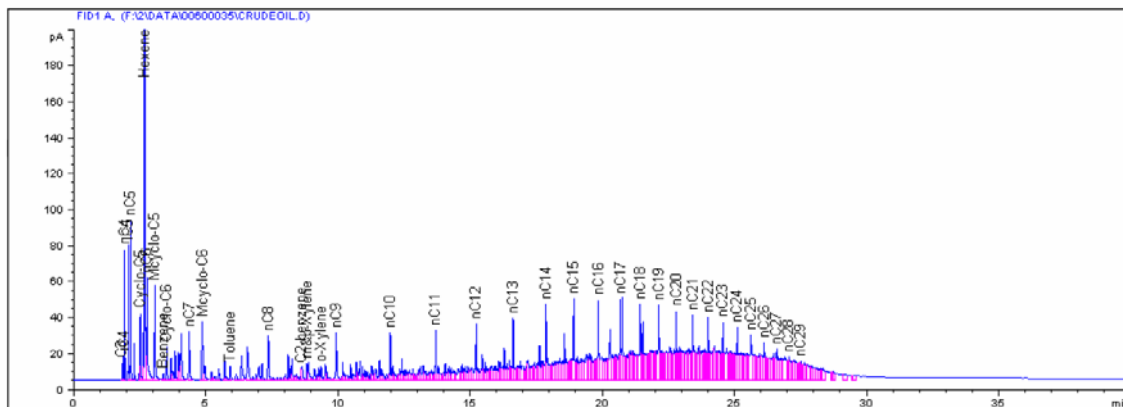
Table D- 9 GC results for Crude Oil

Component	MW (g/mol)	Flashed Oil	
		wt %	mole %
CO2	44.01	0.000	0.000
H2S	34.08	0.000	0.000
N2	28.01	0.000	0.000
C1	16.04	0.000	0.000
C2	30.07	0.000	0.000
C3	44.10	0.034	0.237
i-C4	58.12	0.049	0.254
n-C4	58.12	0.278	1.453
i-C5	72.15	0.319	1.344
n-C5	72.15	0.395	1.664
C6	84.00	1.061	3.837
Mecylo-C5	84.16	0.432	1.557
Benzene	78.11	0.027	0.105
Cyclo-C6	84.16	0.166	0.599
C7	96.00	1.178	3.726
Mecylo-C6	98.19	0.374	1.157
Toluene	92.14	0.093	0.307
C8	107.00	1.545	4.386
C2-Benzene	106.17	0.072	0.207
m&p-Xylene	106.17	0.081	0.232
o-Xylene	106.17	0.086	0.245
C9	121.00	1.483	3.722
C10	134.00	1.737	3.937
C11	147.00	1.773	3.664
C12	161.00	1.934	3.649
C13	175.00	2.482	4.307
C14	190.00	2.484	3.970
C15	206.00	2.808	4.139
C16	222.00	2.661	3.640
C17	237.00	2.544	3.260
C18	251.00	2.899	3.507
C19	263.00	2.711	3.131
C20	275.00	2.495	2.756
C21	291.00	2.371	2.474
C22	300.00	2.306	2.334
C23	312.00	2.151	2.093
C24	324.00	1.958	1.835
C25	337.00	1.783	1.607
C26	349.00	1.626	1.415
C27	360.00	1.428	1.205
C28	372.00	1.228	1.003
C29	382.00	1.054	0.838
C30+	750.00	49.894	20.204
MW			303.704
Mole %			0.000

Stock Tank Oil Properties at Standard Condition			C30+ Properties
	Measured	Calculated	
MW	323.190	303.700	750.000
Density (g/cc)	0.934	0.913	1.010

Single Stage Flash Data	
	Original STO
STO Density (g/cc)	0.934
STO API Gravity	20.048

Properties	Flashed Oil
Mole %	
C7+	88.95
C12+	67.37
C20+	37.76
C30+	20.20
Mass %	
C7+	97.24
C12+	88.82
C20+	68.29
C30+	49.89
Molar Mass	
C7+	332.00
C12+	400.40
C20+	549.23
C30+	750.00
Density (g/cc)	
C7+	0.9220
C12+	0.9396
C20+	0.9740
C30+	1.0100
Fluid Density at STP Condition (g/cc)	
	0.9337



VITA

Name: Daniyar Zhussupov

Born: May 31, 1979

Address: 223A-53 Valikhanova st., Shymkent,
Kazakhstan 486008

Email Address: zhussupov@gmail.com

Education: Kazakh State University,
Shymkent, Kazakhstan
B.S. Chemistry, 2001

Texas A&M University,
College Station, Texas, USA
M.S. Chemical Engineering, 2006